NEGATIVE DIELECTRIC CONSTANT OF PHOTO-CONDUCTING POLYMERS UPON CORONA-CHARGING

NEGATIVE DIELECTRIC CONSTANT OF PHOTO-CONDUCTING POLYMERS UPON CORONA-CHARGING

By

Han Yan, B. Eng., M.A.Sc.

A thesis

Submitted to the School of Graduate Studies

in Partial Fulfillment of the Requirements

for the Degree

Doctor of Philosophy

McMaster University © Copyright by Han Yan, April, 2013

Doctor of Philosophy (2013)

(Material Science and Engineering)

TITLE:	**Negative Dielectric Constant of Photo-conducting Polymers upon Corona-charging**
AUTHOR:	**Han Yan** **B. Eng. (McMaster University)** **M. A. Sc. (McMaster University)**
SUPERVISORS:	**Prof. Gu Xu; Dr. Richard Klenkler**
NUMBER OF PAGE:	**x, 119**

©Copyright by Han Yan, April 2013

Abstract

The phenomenon of image blurring on laser-printed or electro-photocopied paper has been discovered since the development of hard copy industry in the 1980s. In the 1990s, the problem was confirmed to be associated with the undesired surface conduction of charges along the unique photoconductive polymer surface during the photoconduction process. Other than this, little progress has been made in investigating this phenomenon, due to the limited experimental techniques that can be applied to the dielectric photoconductor.

In this thesis, the electrical properties of a commercially available photoconductor as a result of Corona charging were studied. Various techniques including vacuum deposition and step-function impedance spectroscopy were employed, to overcome the nature of the photoconductor that prevented the use of conventional techniques such as AC impedance spectroscopy. Negative dielectric constant (NDC) has been prevalently discovered at a broad range of frequencies (below 1Hz and up to 1 MHz) in this thesis and it was questioned in the form of a physically-impossible inductor. This precipitous sign switch of dielectric constant is found in various areas ranging from physics, chemistry, biology to electronics. The magnitude of the NDC decreased drastically with the decrease of electric field frequency. The system obeyed the proposed free-carrier plasma model with a resonance frequency at MHz level.

Commercially available polymeric photoconducting materials showing NDC at extremely low frequency are expected to provide unusual scattering to electromagnetic waves and therefore demonstrate profound implications with reduced cost. It has paved the way for many applications such as inductors in integrated chips without bulky coils and provides an insight into a possible revolution in electronics and photonics.

Acknowledgements

I wish to take this opportunity to thank all the people who helped me throughout the years of my PhD study.

Firstly, I would like to thank my supervisor Dr. Gu Xu, for his patient guidance and encouragement during my research. I would also like to thank my co-supervisor Dr. Richard Klenkler, from Xerox Research Center Canada (XRCC), who provided me with invaluable input on experimental steps, analysis and experimental results. I also gratefully acknowledge the help from Dr. Vlad Skorokhod, who is also from XRCC, for his instructions and discussions.

I also wish to express my thanks to my supervisory committee members, Dr. Adrian Kitai and Dr. Igor Zhitomirsky, for their constructive advices, inspiring discussions and faithful guidance.

I am also thankful to Dr. Kewei Wang, Miss Xinxin Zhao for their help on experimental details and theoretical discussions.

I would also like to thank Miss Lulu Deng and Mr. Yiqun Ma, for their suggestions and valuable discussions.

I want to acknowledge the invaluable help of Mr. Stephen Jones and Mr. David Rossouw, who have been constant consultants in my writing.

TABLE OF CONTENTS

LIST OF FIGURES

1. Introduction

Xerography, originally known as electrophotography, has been developed since its invention in 1938. It was invented by Chester Carlson and a following US patent was awarded in 1942. The name itself came from Greek roots: *"xeros"* stands for "dry" and *"graphia"* stands for "writing" [1]. This was used to distinguish this novel technology from other image reproduction methods at the time, where liquid chemicals were often involved [1]. As an example of a typical liquid-based chemical method at that age, Cyanotype was the one that we refer to as blueprints today. In this technique, equal volume of a potassium ferricyanide and ferric ammonium citrate solution was used to produce image. The key point of innovation Carlson introduced was to bring electrostatic charges into photography at dry state. After 18 years' of improvement, the first cylindrical drum, similar to that in a modern photocopier was invented. Before that, the process was manually done on several flat plates. This innovation marked the start of a new era of Xerography and kept its leading position ever since. The cylindrical drum laid a foundation for the design of today's Xerography process and it has since become the dominant method of reproducing images and printing data in photocopiers, laser printers and fax machines. The first Xerographic photocopier was introduced by Xerox in 1959 [1] and it soon replaced all other duplicating machines using photo-direct technology; it has truly revolutionized office procedures.

According to the premier provider of market intelligence of the information and consumer technology [2], in 2011, the overall world market for hardcopy including its peripherals was around 200 billon US dollars. In the peripheral market alone, the shipment approached 126 million units for the full year of 2011 and there had been a steady growth over the last 20 years; even during the financial crisis starting 2008. Among the overall hardcopy market, color laser printing and its peripherals posted the strongest growth of 17% in 2011 and over 8 million units were shipped that year. As color printing continues to infiltrate the overall hardcopy market, multi-functional devices that combine a printer, a fax machine and a photocopier within one unit continues to take over the market share previously occupied by single-functional printers.

1.1. Background: mechanism of Xerography and laser printing

The purpose of Xerography is to duplicate image composed of letters or figures onto the designated material by making use of electrostatic charges. Unlike the older copy technologies that relied on chemical means, the prevalent development of Xerography utilizes the electric field to attract and hold toner particles onto a medium. For the purpose of evaluating a high quality printer, the development process should be automatically controlled, easy to handle and economically feasible with reasonable quality. The quality of the printed image is assessed by accuracy, sharpness and durability. The mechanism for a photocopier using Xerography and a laser printer are identical in most steps; the only difference comes from the step of light exposure. There are seven basic steps in a Xerography process, they are schematically represented in figure 1.1 and listed below respectively:

1. Photoreceptor charging
2. Exposure with light/laser
3. Toner brought to drum
4. Toner transferred to paper
5. Toner fused in
6. Remaining toner removed
7. Photoreceptor discharging

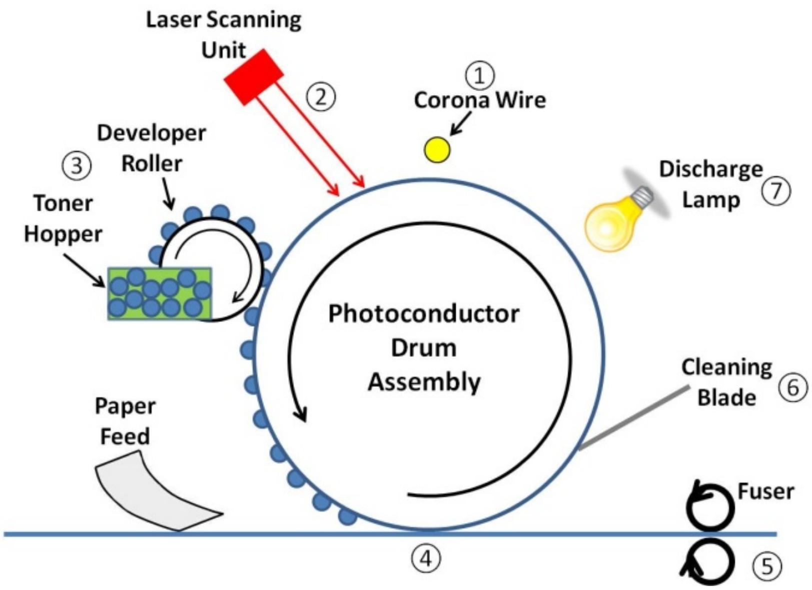

Figure 1. 1 Steps of Xerographic process around the photoreceptor drum

In step 1, charge is uniformly distributed onto the drum of photoreceptor surface by the Corona unit, which is located above the drum assembly. The uniformity is necessary to avoid non-uniformity in the developed image. The photoreceptor is made of photoconductive material that while in dark, exhibits the behavior of an insulator; resisting the flow of electrons or holes. Upon laser illumination, the energy of photon from laser liberates electrons or holes within the photoconductor and allows current flow through the material. In step 2, the photoreceptor is exposed to a laser in the pattern of the optical image to be produced. This selectively discharges the surface charge in the exposed region and this region is respectively the blank area on the printed sample. Laser light is controlled with high precision and therefore creates a high quality latent image in the form of an electrostatic charge pattern. The pattern of the image was obtained through a scanning step, which is omitted from figure 1.1. In a slightly different and more traditional case of a photocopier, where no laser unit is involved, the image to be copied is projected onto the photoreceptor through a lens. With a flash exposure, the entire image is reflected onto a photoreceptor. In both cases, the light energy is absorbed by the photoreceptor and creates electron-hole pairs in the bulk. The pairs are attracted and transported with respect to the electric field generated as a result of the latent charge on the photoreceptor surface and the conductive ground (metal core of the drum assembly). Generally, negative electrostatic charges are deposited onto the photoreceptor surface therefore the holes are generally attracted and transported upward through the bulk of the photoreceptor towards the charged surface. The surface charges exposed to laser are recombined with the holes travelling upward through the photoconductor. Good insulating qualities are important so that charge patterns can be retained for a period of time long enough to complete the development process. This process is slightly different in a photocopier where lenses and mirrors are used instead of laser; however the latent image is still formed on the charged photoreceptor. In step 3, electrostatically charged toner particles are brought into contact with the latent image. Many xerographic toners are made from copolymers of styrene and acrylic, with a small amount of carbon black pigment added [3]. The toner particles are transferred onto a piece of paper in step 4. The toner particles are loosely bounded to the paper surface and can easily be disturbed or rubbed off. Therefore, the paper and toner particles are fused in step 5; this is achieved by melting toner particles. On the photoreceptor side, the remaining toner particles are removed from its surface in step 6 by a blade. In step 7, the photoreceptor is uniformly exposed to light to remove any remaining surface charge, returning back to the original state before step 1. As mentioned previously, multi-functional laser units that reproduce images are taking place the traditional single-functional photocopier. The utilization of laser beam can eliminate the necessity to create an intermediate optical image thus speed up the reproducing process. There are three fundamental components in a laser unit: a computer that scans and transfers the electrical signal of the image, a laser whose output density is controlled and the Xerography that converts optical information onto the paper.

1.2. Problem statement: surface conduction caused by charging

In the continuous process of Xerography, latent image are established on the photoreceptor either optically through a lens or by using a laser beam. The establishment of homogenous electrostatic charge on the photoreceptor surface is as a result of the unique property of the photoreceptor. The photoreceptor is usually composed of several layers in difference thickness, serving different purposes, as illustrated in figure 1.2.

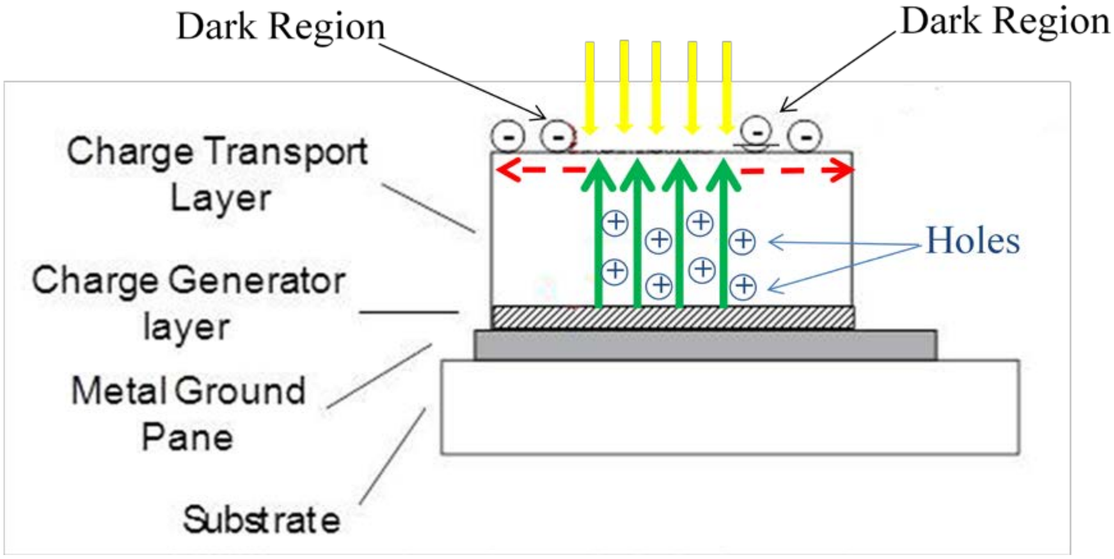

Figure 1.2 Cross section of a typical xerographic photoreceptor

The laser light passes through the transparent charge transport layer (CTL) and gets absorbed in the charge generation layer (CGL), creating detached electron-hole pairs, due to the electric field established between the electrostatic charge on the surface and the metal ground plane below. Holes are transported through the charge transport layer, towards the surface, where they annihilate the negative electrostatic charge. Charge transport layer made of photoconductor takes advantage of the photoconductivity which is the conversion of electromagnetic radiation into electrical current. Thus, photoconductors are materials which conduct electricity when illuminated by light of specific wavelengths but act as electrical insulators when kept in the dark. According to the type of xerographic machine, the photoconductor can be fabricated into drum, sheet or even flexible belt in photocopiers or laser printers. It is required that the photoconductor being: a good insulator in the dark, highly conductive in the light, mechanically stable and should be easily manufactured into photoreceptors. Organic photoreceptors gradually replaced inorganic photoconductors in the 1980s due to their major advantages such as non-toxicity for safer disposal, low cost, ease of manufacturing, flexibility, panchromaticity and high photosensitivity [4]. Performance stability of various photoconductors has been significantly improved since 1980s by adding organic additives as well as by the development and expansion of nanotechnology in last ten years. However, it has been found that the charge transporting ability of the charge transport layer is reduced with increasing exposure to negative charging emitted by the charging device in the Xerographic printer. It has been determined that this change in electrical properties is due to the interaction of the negative Corona with the charge transporting component of the transport layer. A change in the photoreceptor's electrical properties is undesirable since it alters the designated surface charge distribution after its exposure to laser. According to figure 1.2, the desired direction of conduction is perpendicular to the photoconductor surface as it will create a distinct edge of electrostatic charge pattern. Practically, observed result contradicts the ideal scenario by developing an unwanted parallel conduction along the photoconductor surface. This unwanted parallel conduction is graphically observed by the periphery of letter/figure being fuzzy and blurring after repeated use of the photoreceptor. Additionally, the problem aggravates with longer exposure to negative Corona charging.

Corona charging process is schematically plotted in figure 1.3. A wire is tightly stretched with one end isolated, and the other end biased to a high voltage of -5kV DC.

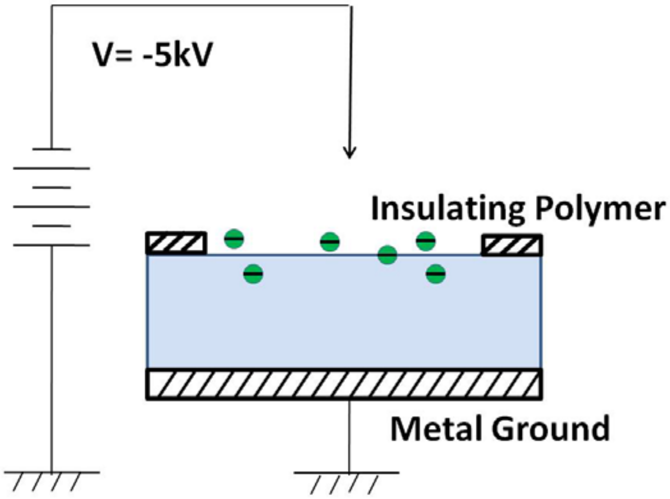

Figure 1.3 Photoconductor upon negative Corona charging

During Corona charging, high voltage applied to the wire is strong enough to ionize the air in the wire's immediate vicinity. Due to its attraction to the neutral surface, the ionized gas species is deposited onto the charge transport layer, which is still an insulator at this particular moment.

Corona discharge has a wide range of industry applications, such as charging the photosensitive layer and the toner particles in photocopying machines, modifying the wet-ability of plastic films, and conditioning the electrets for air filters [5]. Under negative Corona charging, which is commonly used in a photocopier, the ionized air species generated are electrons and other anions such as $NO_3^-(H_2O)_n$, $O_3^-(H_2O)_n$, $OH^-(H_2O)_n$, $O_2^-(H_2O)_n$ and $CO_3^-(H_2O)_n$. Although $NO_3^-(H_2O)_n$ is the predominant specie among others, it should be noted that the prevailing of it is dependent on numerous variable factors.

1.3. Significance of the research

1.3.1. Previous attempts to resolve the unwanted surface conduction.

In late 1980s, organic photoconductor had already taken up 40% of the market [6], organic photoconductors have since replaced the rest of the market due to the market demand and rapid research progress [7]. However, there are still outstanding problems in Xerographic printing, among which the unwanted parallel photoconductivity remains a long-standing yet unsolved problem.

As schematically in figure 1.3, the holes are generated in the CGL and travel upward upon illumination of the photoconductor. Unfortunately, the unwanted parallel conduction occurring near the photoconductor surface causes indistinctive edge of the printing sample. This problem is responsible for the rapid degradation of the drum/toner assembly [9] and causes replacement of the drum unit; increase the cost of laser printing or photocopying. Up to now, no systematic research has been carried out to explore the change brought to the photoconductor after repeated negative Corona charging.

In this thesis, Impedance Spectroscopy (IS) analysis of the surface has found pseudo-inductive behavior. An inductor is not only physically impossible, but also contradicts the generally accepted circuit analysis of insulating polymers. However, this non-physical inductor is also observed in other research areas.

1.3.2. Similar phenomenon from other research area (Corrosion)

In corrosion science, the pseudo-inductive behavior has been found since 1940s [10]. It remained controversial up till now, even though some researchers have proposed theories or explanations [11][12][13]. Unfortunately, the existence of the long-standing physically impossible inductor is still unclear, as many of the theories provided are easily rejected or dismissed [14][15] by other researchers in a slightly difference environment. The debate is continuing, although the corrosion systems mentioned are extensively studied over a great variety of applications.

1.3.3. Similar phenomenon from other research area (Conducting polymer system)

An unexplained inductive behavior has turned out to be an old yet unsolved and often ignored problem in ion conducting polymer research. Similar to the situation in corrosion science, various mechanisms have been proposed to explain the physically impossible inductor [16][17][18], but none of the theories is able to be applied into other examples [19][20][21]. In other words, no general answer is given for the manifestation of the inductor.

1.4. Research Objective

The purpose of the thesis is to find out the change that Corona charging brings to the photoconductor surface and its corresponding consequences. By determining the nature of this unwanted conduction caused by Corona charging, it will potentially increase the life time of the drum/toner assembly in a photocopier or a laser printer. In particular, the dielectric response of the photoconductor will be studied in terms of alternative current (AC) impedance spectrum via step-function direct current (DC) method. Further results will be discussed in details in “results and discussion”

1.5. Overview of the thesis

Extensive literature review on various topics will constitute the first part of the thesis, it will include but not limited to the basic physics of the insulating polymers, theories about Corona charging and dielectric properties of materials. After a preliminary experimental result, a more deliberate literature review is given: the theory and methodology of the measuring technique, detailed discussion of the physically-impossible inductor in literature, as well as a few alternative theories that could explain the existence of the physically unlikely inductor. This will be followed by results and discussion, and the proposed explanation of negative dielectric constant caused by Corona charging. This explanation is supported by a process of elimination of other alternative explanations. Furthermore, additional experimental results and evidence from literature will be discussed to show support for the proposed explanation.

2. Literature Review

2.1. Basics of photo-conducting material

2.1.1. History of photoconductor

In this section, a brief history of photoconductor is given. The transitions from inorganic to organic photoconductors and, from single layer structures to modern dual-layer structures are described. As mentioned in introduction, a photoreceptor in a xerographic printing system is composed of a photoconductor and a metal ground pane and/or substrate.

In Carlson's initial experiment [3], electrostatic charge was rubbed manually and a film of sulfur was used as the photoconductor. In the first commercial Xerox copier, a single layer of amorphous selenium was adopted as the photoconductor. Later the amorphous selenium was replaced by selenium alloys. According to current standards, these inorganic semiconductor materials are relatively poor photoconductors because they have relatively high dark conductivity (cause leak current) and low photosensitivity (cause fussy image). They also had barely little or even no photosensitivity with red light exposure which inevitably led to the problem of a copier being "blind" to a document containing reds. Furthermore, these semiconductors materials had a high dielectric constant and therefore high surface charge density was obtained for a given surface potential. Additionally, to be manufactured, these materials required high vacuum for deposition. As an example, the world's first visible-light sensitive photoconductor was a 10-50 μm layer of Selenium vacuum deposited onto an aluminum plate [22]. More practically, selenium based photoconductors were mechanically brittle therefore bared no possibility for drum or belts application. Last but not the least: they were environmentally unfriendly and expensive [7].

Even at the time when Selenium based photoconductor was economically successful, organic photoconductor research remained an active area. The search for better, cheaper and more environmentally friendly photoreceptors had been the topic ever since Carlson’s invention in the 1940s. Surprisingly, the configuration or the major components of a today’s laser printers are very similar to those in the 1950s but the material used for photoconductor has been advanced drastically [23].

It was in the 1970s, when the word “organic” was adopted in the generic sense to represent polymers: it was created from carbon-based starting materials. The first organic photoconductor used in commercial unit was based on a charge-transfer complex between poly(N-vinylcarbazole)(PVK) and 2,4,7-trinitro-9-fluorenone(TNF) at 1:1 ratio [24]. It was a single-layer of photoconductive material coated on a metalized polymer with low photosensitivity at wavelength < 800nm [25]. The first organic photoconductor, like many other first commercial products, was not a complete success due to its relatively short life time [23]. On the other hand, it demonstrated the feasibility of organic photoconductor in photocopy industry and later triggered the research for more appropriate organic photoconductors as well as its photoconduction mechanism. Shortly after that in 1978, another single-layer organic photoconductor based on a complex between a Pyryllium dye and Bisphenol-A-Carbonate was introduced by Kodak Company [26]. This material was in possession of high photosensitivity up to 700nm, which solved the problem mentioned for inorganic photoconductor: little or no sensitivity when exposed to red light. Afterwards, all organic photoconductors developed were able to work in the near-IR laser exposure. In the current market place, laser printers have exposure systems with either visible-light LED arrays or near-IR lasers and more essentially, all the photoconductors used are organic. The only exception is the amorphous silicon based photoreceptors which have a long lifetime but are expensive to manufacture.

The transition of photoconductors from inorganic to organic since 1980 seems to be evitable and so is the improved configuration of the photoreceptor. As mentioned in the last paragraph, both early examples were single-layer structured, the prototype inherited from the earlier inorganic photoconductor configuration.

In a single layer structure, the photoconductor is reasonable for quantum efficiency of photo-generation and high charge mobility across the device, for both electrons and holes. Quantum efficiency is defined as the ratio of the photons that eventually produce free charge carriers over photons hitting the device’s photo-reactive surface. It essentially measures the ability of the photoconductor to converting light energy into electric current. In other words, in single layer structure, photo-generation and transportation were carried on in the same material simultaneously, as schematically illustrated in figure 2.1.

Additionally, with the current design, the organic photoconductor was manufactured into the shape of drum or belt. As a consequence, it was required that the photoconductor itself maintained a certain level of mechanical strength. These requirements ruled out many polymer candidates as the two requirements were sometimes contradicting each other. As an example, due to the congenital deficiency that came by nature of their structure, the photoconductivity of early example of PVK/TNF was only one third of amorphous selenium [6].

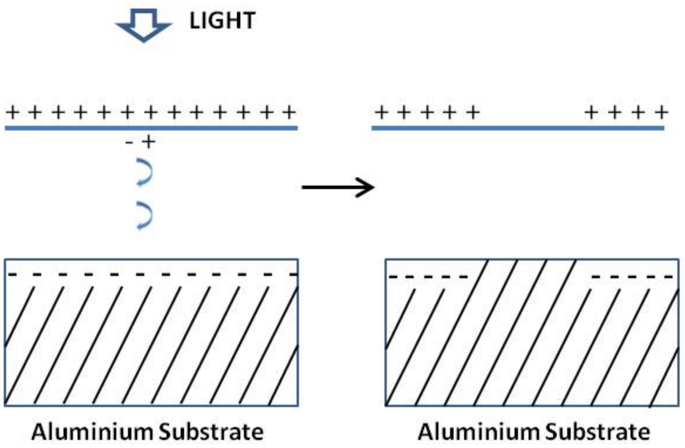

Figure 2.1 Configuration of single-layer photoconductor and its photodischarge process upon illumination

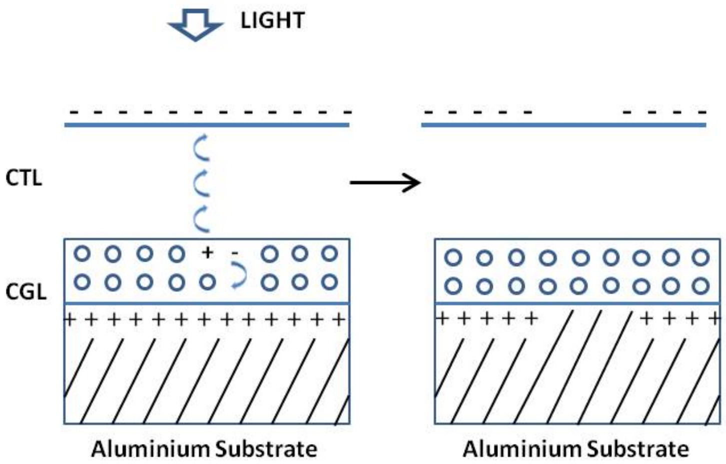

Figure 2.2 Configuration of dual-layer photoconductor and its photodischarging process upon illumination

To improve the quality of organic photoreceptors, a dual-layer configuration made of a thin charge generation layer (CGL) in continuous contact with a much thicker charge transport layer (CTL) was introduced, schematically in figure 2.2. The separated two layers played discrete roles in the photodischarging process. By design, most of the incoming light was absorbed by the CGL, whose thickness varied from 0.2 to 2 µm, depending on the concentration of the photoconductor in the layer. Above the CGL, the thicker CTL, in thickness ranging from 15 to 30 µm, not only had to transport the charges, but also served as a protective layer of the CGL and improved the mechanical property of the photoreceptor. As a matter of fact, the example of using electron transport material has been commercialized using the single layer structure only. Research based on dual-layer electron-transport CTL had been carried out but never commercialized. The electron reduction for electron-transport material is designed to be lower than of the photo-generated electron on the CGL. Only in this case, electrons are transferred into the CTL. It is believed that oxygen plays the role of electron trap so the reduction potential of the transport material must be lower than that required to reduce oxygen dissolved in the polymer [9]. Additionally, in general, the mobilities with electron-transport materials are much lower than for hole-transport materials. For this reason, dual layer structure is not used for electron-transport CTL and in most commercial laser printing systems, negative charge was applied onto the photoreceptor [27], which is shown in figure 2.2 as well. The CGL in majority of the commercial organic photoreceptors consisted of a dispersion of the photoconductive organic pigment in an electrically inert polymer matrix. As an example, by adopting the discrete structure with isolated functions, the photosensitivity was raised over ten times more than the PVK/TNF photoreceptors and it had taken up 40% of the world market of photoreceptors by 1988, a few years after its invention [6].

2.1.2. Organic photoconductors (OPC)

In this section, detailed characterization of different organic photoconductors is given. As of today, nearly all eletrophotographic machines are printers and a single-function photocopier is rarely seen on the market due to its limited function. The fundamental difference between the two, as described above, is the way how electrostatic charge pattern is imparted on the photoreceptor. In a printer, the image file stored in a computer is projected onto the photoreceptor using a laser-diode and rotating hologon scanner or an array of LEDs. It is also called a laser printer, even if the source of light in the system is from LEDs. For the purpose of faster photocopying, nowadays a photocopier employs the same mechanism as a laser printer by scanning the document onto a detector and stores the data in an image file. The subsequent data-rendering process converts the image file to half-tone, the technique used to simulate continuous tone image through the use of dots, varying either in size, shape or spacing.

The change from single-function photocopier to multi-function printer has been facilitated by the advancement of photoreceptors and compact light sources. More importantly, in terms of the wavelength, the photoreceptor didn’t have to be photosensitive to the white light wavelength, which is broad on the spectrum. Instead, it had to be only sensitive to the wavelength associated with laser diodes in the near infrared or LEDs (typically red) [28] .This change had caused the research of better photoconductor focused on a specific group of material with appropriate sensitivity. Another minor development as a result of the change from photocopier to laser printer was in the writing system. Most text-based documents are predominately “background”, meaning toners are not applied on the majority area of the page. In a machine that focused mostly on printing text with large background, the photodischarged area can receive toners. Exposing the text rather than the background significantly reduced the demand on the writing system.

2.1.3. Characterization of OPC

2.1.3.1. Operational criteria

The electrophotographic imaging begins by applying a Corona surface charge to the photoreceptor. The surface charge density is obtained:

$$\frac{Q}{A} = \frac{C}{A}V = \frac{\varepsilon\varepsilon_0}{L}V \qquad (2.1)$$

Where Q/A is the surface charge density, C/A is the capacitance per unit area, V is the surface potential, ε is the dielectric constant and ε_0 is the vacuum permittivity. For a typical organic photoconductor with L=40 μm, ε=3, V= -500 V, C/A ratio is 2E-10 F/cm^2. Assuming the surface is composed of molecules with an area of 10 nm^2 and only 1% of the atoms are associated with the surface charge, the applied field (V/L) is 1.25E5 V/cm.

In the next step of electrophotographic imaging, toners are attracted and they adhere to the designated area due to a difference in surface potential between the exposed and unexposed area. A potential difference of at least 300 V is desired and as a result, the bulk material of the photoconductor must be highly insulating or being a dielectric. Normally, the development process of applying and melting the toner requires no more than a second. As a result, a resistivity of 10E13 Ω.cm, which gives rise to a decay rate of nearly 200 V/s, at a field of 1.25E5 V/cm, is the minimum requirement. As an example, organic polymer such as polycarbonate has a resistivity of about 1E14-1E16 Ω.cm and it is the major component in organic photoconductors.

2.1.3.2. Formulation and basics

The basic formulation of a photoconductor is CGL and CTL. CGLs are often made in method of pigment dispersion. This methodology is based on milling of pigment and binder in its corresponding solvent. To characterize the CGL, one usually measures the ability of the pigment to absorb the imaging light and generates charge.

The CTL is always a solution of binder polymer and charge transport molecules. The charge transport polymer is usually 40-50% by weight of the CTL [6]. According to figure 2.1, CTL is at the top of the photoreceptor therefore in contact with ambient substance, such as toners and paper during development. During the investigation of polymers with proper anti-abrasion properties, researchers confirmed that it was strongly related to the polymer entanglement [29] of the binder polymer. As the content of binder molecule increases, the entanglement density increases therefore produces better wear resistance.

A smooth surface would benefit the development process and a trace amount of surfactant is applied on the surface to achieve this. Specific surfactant is selected and tested to ensure that it doesn't change the photoconductivity of the polymer. The organic photoconductor layers are coated on the substrate by dispersing the solution through a hopper on the moving substrate. Such coatings out of different organic solvent can have inhomogeneous surface roughness, due to the speed of coating or drying conditions.

During Corona charging, oxidant species are generated as a result of high voltage triggered species. These species are attracted onto the photoreceptor surface due to electric field. A final component, an antioxidant, is applied onto the photoconductor surface to suppress oxidation caused by Corona charging.

It is desired that, in a dual-layer photoconductor structure, the CGL is much thinner than the CTL. The reason is as follows: by considering all layers mentioned above, after light absorption and charge separation, the separated electrons and holes have to drift under the influence of the applied field to the opposite charged surface, in order to complete the photodischarge process. If the transport of either sign of charge is inefficient, photodischarge is incomplete and therefore hinders the entire process. In the charge generation material, hole transportation is much more effective than electron transportation. As a result, all commercialized photoconductor rely on the hole transport and it is for this reason, as described above, why negative Corona charging dominants laser printer market. Thus, in dual-layer organic photoconductor, the CGL is typically very thin (a few micros or sub-micro), compared to the CTL layer. As well as all above, CGL itself may also include charge transport species.

2.1.4. Considerations for fabrication

In this section, we will discuss the detailed mechanism of the materials and describe the charge generation and transport details as well as how these parameters affect the static charge based photocopy process.

Mixing of the components of the two layers (e.g., CGL and CTL) is important at the interface and there is an optimal concentration gradient. If there is no mixing at the interface, the layers will not adhere to each other. Conversely, the unique functionality of each component will diminish if the layers are mixed completely. Penetration of the coating fluid into a previously coated layer requires experience and repeated experiments to achieve empirical optimization. Altering the degree of layer mixing can cause dramatic change of the organic photoconductor performance, even though the overall composition stays unchanged.

Organic photoconductors are often configured as drums or belts. Drums, usually made of conductive aluminum metal, are usually in diameter of 1 to 10 inches. Belts are often made of poly(ethylene-terephthalate) or a similar polymer film, and a thin layer of metal, such as Ni, Al, Ti, is deposited on it as the electrode. In both situations, metal is served as a conductive substrate.

Fabrication of photoconductor in drums dominates the current laser printer market [30], therefore the fabrication process will be discussed. Fabrication of the belt bares the same principle but has a slightly different method due to the configuration. The organic photoconductor is fabricated by dip-coating or ring-coating of various layers. In both processes, the drum is dipped into a tank of solution or dispersion and slowly withdrawn to create the desired layer. In dip-coating, the layer thickness is a function of withdrawal speed and the physical characteristics (i.e., viscosity) of the solution. In ring-coating, the thickness on the drum is again a function of the geometry of an annulus where the drum is withdrawn through. Above is the overview of coating for a single layer, in the case of multi-layer coating, the drum is dip-coated for the subsequent layer after completely drying the surface. The previous solid layer will have contact with the subsequent liquid formulation during dipping; therefore the selection of solvent requires theoretical and empirical knowledge. Dip-coating formulations must be optimized for long life in the dip-coating tank [31]. As discussed above, only the proper interface between layers can facilitate effective charge transfer. In commercialized manufacturing, each layer of the photoconductors is coated separately in a batch process. As a real example in manufacturing, due to gravity, a liquid drop is formed right after dipping the drum in a batch and a thicker layer is formed at this position.

Since the photoreceptor surface is both in physical contact with toner particles (removing blade) and high field caused by static charging, the physical and electrical characteristics must be stable to these interactions throughout its life. Thanks to the following sub-layers and advanced scientific research, today the most durable OPCs can last as long as 100,000 imaging cycles [32]. Two commonly additional layers are the undercoat layer (UCL) and an overcoat layer (OCL), where the UCL is placed between the electrode and the CGL.

The UCL serves as the charge-injection blocking layer to prevent the unwanted dark-charge injection form the electrode into the bulk of the organic photoconductor. During Corona charging, a high field of up to 50 V/μm is produced, there might be significant charge injection from the substrate into the photoconductor. If, in the last step, it was negative Corona charging, then the injected holes would efficiently transport through the bulk of the photoconductor. This will result in an undesired high rate of dark discharge or small localized coating defects at a specific region. When the charged surface is exposed to toner during development, localized dark injection causes small toned area where it supposed to be no toner at all. This is called charge deficient spots and has to be reduced by the application of UCL. This layer, with respect to electron and hole transport, is with large resistivity. As a result, the thickness of the UCL should be as thin as possible (~ 1 μm) to reduce the residual surface potential. The UCL also helps smooth the aluminum substrate, which is usually rough when initially prepared. Lastly, the UCL may serve as an adhesive layer to ensure that the CGL and aluminum are properly adhered.

2.1.5. Charge transport mechanism

In the next section, we will discuss how charge transport is achieved within an organic photoconductor with charge transport material doped in polymer insulator binder. Up to now, it is a debated topic and various review papers have been initiated on it [33][34].

2.1.5.1. Models of charge transport

The CTL of a photoconductor is usually an amorphous solid solution of a charge transport active component in a polymer binder. This type of CTL is called molecularly doped polymers (MDP) and the transport active component of CTL is typically 40%-50% in weight percent. Although using a similar name, it is a completely different system than semiconductors, where dopant is typically introduced at a very low concentration to control the relative proportion of electron and holes in the conduction bands of a semiconductor crystal. Charge mobility in a doped semiconductor decreases geometrically with increasing temperature, due to the thermal scattering-perturbed motion of charge carriers. On the other hand, charge density in a doped semiconductor is a thermally activated process and this effect compensates the drop in mobility. As a result, conductivity in a doped semiconductor increased with temperature. Therefore, it is suggested that the conductivity in a doped semiconductor is thermally activated. Experimentally, at a fixed temperature, the drift mobility of extrinsic carriers decreases exponentially due to the increasing average intersite separation of the active molecule (in unit of length). As a result, the drift mobility of MDPs can be tuned over a broad range by adjusting concentration [35][36]. This property of tunability is important for application over a wide range of Xerographic speeds. Common hole transport material, *N*,*N′*-bis(3-methylphenyl)-*N*,*N′*-diphenyl-1,1′-biphenyl-4,4′-diamine (**TPD)** in, figure 2.3 is used to represent this property [37].

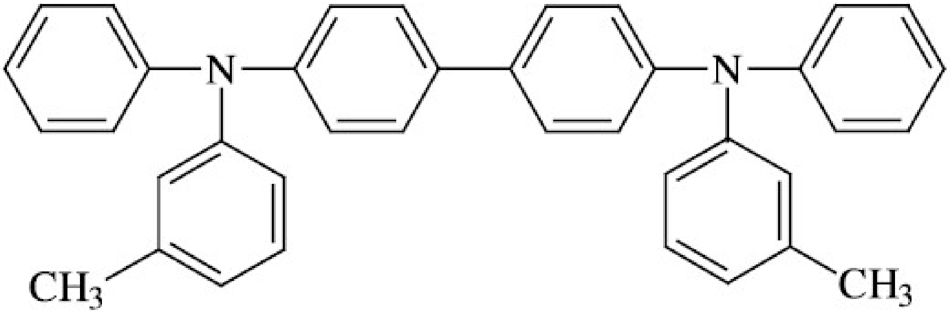

Figure 2.3 Schematic diagram of TPD structure

TPD contains phenyl rings linked by N atoms and side CH_3 groups. At 40-50 wt% doping, approximately 10000 “hops” are required for the hole to transit a 20 μm photoreceptor. The drift mobility of MDPs is always thermally activated. This theory is illustrated in Abkowitz’s work

[37]. Experimental data in Abkowitz's [37] is in conformity with a simple tunneling model for hole transport between transport active molecules. However, in a significant number of published literatures [9], the corresponding scaling is proportional to the square root of the inverse temperature; this is an indication of non-simple activation. The non-simple activation process is predicted and illustrated by Bassler et al. [38].

The experimental observation above, including the relation with intersite separation, temperature and high degree of disorder, is a clear indication that the electronic transport must involve the field-biased hopping of carriers on the transport active molecules. The properties of MDPs are well studied for the following reason: apart from its significance in photocopy using static charge, a number of key features in their transport behavior are also found in other systems with disordered molecular media [39]. The field and temperature dependent behavior are also observed in polymers with transport-active pendant groups like poly(N-vinylcar-bazole) [40], in which small-molecules clusters are incorporated in a main chain in sigma-conjugated polymers. Additionally, certain poly π-conjugated polymer systems, such as polytetraphenylbenzidine (PTPB), also exhibit field dependence of the hole drift mobility [37]. PTPB, as illustrated in figure 2.4, is an amorphous polymer in which TPD molecules (in dashed cubic) are covalently bonded into a main chain [41].

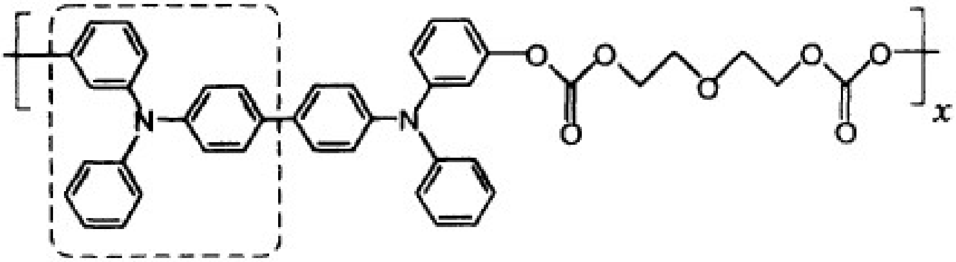

Figure 2.4 Schematic diagram of PTPB structure

It is shown in Abkowitz's work [37] that there is a linear relationship between the logarithm of mobility and the square root of the applied field. Additionally, the field dependence is also found as a function temperature and becomes stronger with decreasing temperature. Whole transport in PTPB is an Arrhenius process between 220K and 300K: a straight line is observed between mobility and square root of the applied field. On combining the drift mobility [42] and the data from spectroscopy [43], it is suggested that the transport in these sigma-conjugated polymers involves the hopping of holes among the main chain segments. As a result, its transport mechanism is similar to TPD in PTPB. Moreover, on π-conjugated systems, the hopping among discrete molecular sites with different energy level has been reported in time-of-flight experiments [44]. These combined results of the recurrent linear relationship found in systems with varying compositions suggest that a transport theory must be established on these commonly accepted characteristics. Although the theories stimulated by all the observations are intensive and too detailed to be illustrated, the principles and trends can be summarized. The temperature dependence appears to be universal to all these materials systems, because hopping-like behavior is found between sites with inequivalent energy levels. Polaron model typically predicts that the logarithm of mobility is linearly dependent on the applied field [45]. The disorder model, proposed by Bassler, is based on Monte-Carlo simulation of hopping on a finite lattice. This model can sufficiently account for a number of key experimental features in terms of a few set of disorder parameters [46][47]. Bassler's model is not an ideal model to simulate hole transport mobility as it could only model the observed field dependence over a very narrow range. In the recently proposed dipole disorder model [48][49], the slow site-to-site variation is accounted for treating them as fully random fluctuations. It was recognized that, under the effective electrostatic potential, this model could more accurately explain the field dependent behavior of mobility [50][51]. It is argued that the disorder model, based on a fully correlated disorder potential, is physically plausible. Later in the late 1990s, Young further considered the effect of group and net dipole moment due to the polymer binder or the transport material [52][53]. It is therefore concluded that the complete basis for mobility remains; no unified description of charge transport in MDPs has been adopted by all researchers [54][55] [56].

2.1.5.2. Miscellaneous considerations

While the charge transport mechanism is still under debate, there are other achieved realizations during the research of photoconductors. It is pointed out that hole transport is supported in MDPs when the neutral transport molecules is donor-like [57]. Similarly, for electron transport, the corresponding process is supported when the neutral transport molecules is acceptor-like. As a result, for the hole transport in CTL, it is ideal to make the transport molecules significantly more donor-like than any of the resident impurity species. All useful hole-transport materials are aromatic amines based with oxidation potentials between 0.6 and 1.2 eV (vs SCE). It is found that hole transport materials with oxidation potentials below 0.5 eV are easy to be oxidized in air by the oxidizing species from Corona charging. On the other hand, as long as the potential is higher than 1.2 eV, the huge potential gap makes hole injection from the charge generation material inefficient. Some typical molecules are listed in figure 2.5, they are namely Triarylamine (TPA), Hydrazone (DEH) and Butadiene.

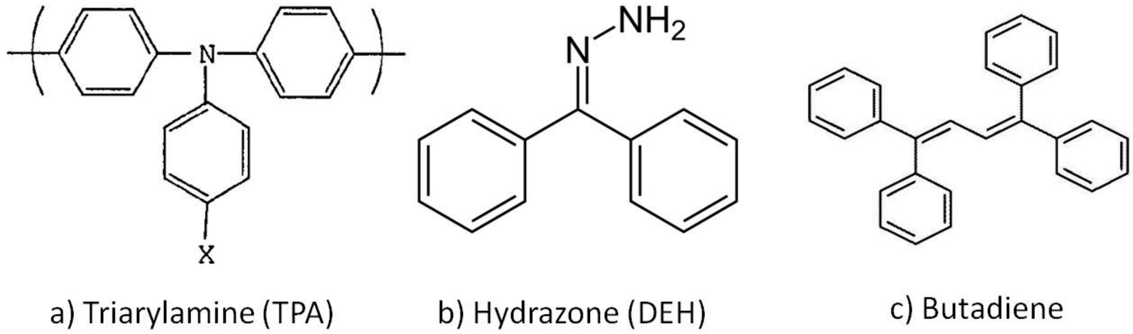

a) Triarylamine (TPA) b) Hydrazone (DEH) c) Butadiene

Figure 2.5 Molecular structures and commonly used molecular names of some typical hole-transport materials.

TPD, illustrated in figure 2.3, is another typical example of a strong donor in this collection of molecules. The advantage of the material used as CTL comes from its trap-free nature in hole transport, as there is no measured buildup of bulk space charge [58]. Calculation and measured results both demonstrate that the injecting metal contact is ohmic and the CTL is trap-free for holes [37]. Similar results have been found in other commonly used CTL with doped polymers such as TPD in bisphenol-a-polycarbonate and in films of poly (methylphenylsilylene). There has literally been thousands of hole-transport materials developed, but only a few of them are actually used commercially in OPC. The debate about the controversial models of hole-transport is still going. The realization of the transport model has not been very useful in the design of charge transport material with their superior characteristics. As a consequence, researchers have put more effort in studying those factors that might affect the charge transport materials such as mixing properties between layers, type of binder polymer, the polarizability of the CTL and oxidation potential. Some of them have been discussed above in connection with fabrication process or the comparison of transport models. The key property for a CTL is to transport charge without trapping over the time scale of the static charge based photocopy process. It is generally accepted that charge transport limitation comes partly from the increasing residual potential with repeated printing cycles. To date, commercially used photoconductor are still under active research and the hope for the combination of wear resistance and inexpensive synthesis with reasonable charge transport ability is being driven by the market demand for laser printing.

The use of organic photoconductor has been initiated since the 1970s; it enabled the development of eletrophotographic technologies into a multi-billion dollar business. As a commercial machine, organic photoconductor has facilitated the manufacturing of the printing unit with pixel resolution as small as 1200 dpi (dot per inch). The discussion in this section have included the device requirements and shown how organic photoconductors were developed to gradually meet these requirements. This was achieved through physical design and material fabrication. Organic photoconductor have to satisfy a wide range of requirements, in order to be successfully employed in commercial use. The diverged requirements come down to two categories: functional separation and material design for enhanced electrical and mechanical properties. The concept of functional separation, separation of charges upon illumination, is the fundamental property for organic photoconductor. As a result, with the abandon of the earlier single layer approach, where all the desirable characteristics are functioned in a single material, it is more productive to use isolated layers with their own enhanced functions and hence the multi-layer structure is superior.

2.2. Basics of Corona charging

2.2.1. Physical construction

Prior to the image exposure, it is necessary to establish an electrical field within the photoconductor film. In a static charge based photocopy machine or a laser printer, this charge distribution on the photoconductor surface is generated by absorbing ionized gas molecules that arise from an electrical Corona device. In electricity, Corona charging is the electric charge brought on by the ionization of a fluid either liquid or gas around an inductor. It only occurs when the potential gradient of the electric field around the conductor is high enough to form a conductive region in the fluid, but not too high as to cause electric breakdown. Figure 2.6 is a schematic of the Corona charging process where the inset shows an enlarged surface interaction between the Corona wire and the photoconductor surface.

The electrostatic charge is applied by passing a Corotron, a Corona emitting device, over the CTL. The Corotron is essentially a tightly stretched wire that is isolated at one end and biased to several thousand Volt DC at the other end. The wires, usually made of tungsten, employed in such devices are around 50 μm in diameter. These wires are placed about 0.5 cm over the photoconductor surface. The idea is that such a high voltage is applied to the wire that air in its immediate vicinity is ionized. The ionized gas species is deposited on the charge transport layer due to its attraction to the neutral surface.

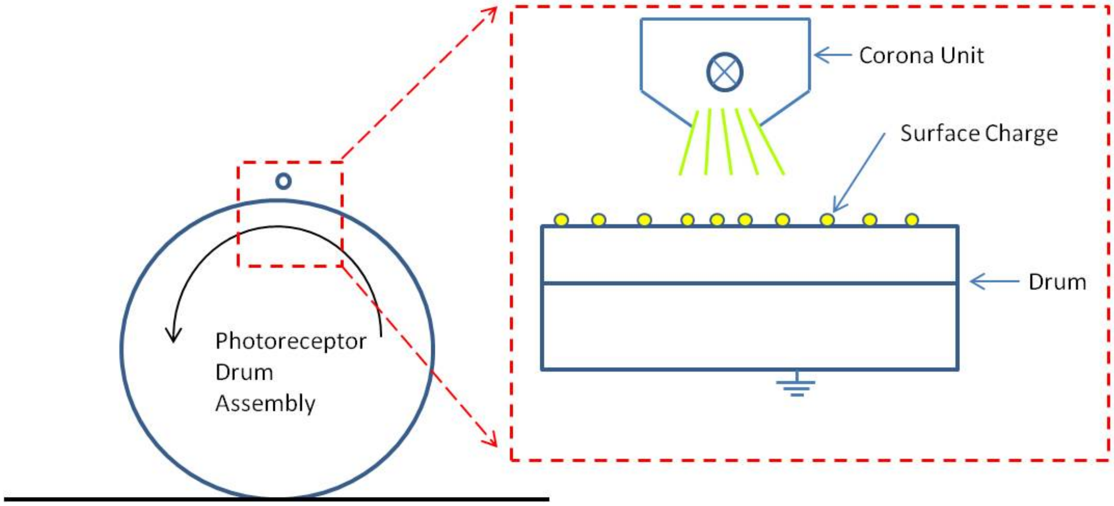

Figure 2.6 Schematic of the Corona charging process

The polarity of the Corona charging depends on various factors. For example, in the application of hole-transport photoconductor, holes instead of electrons are the charge carriers travelling upward through the layers. As a consequence, only negatively charged photoconductor surface is needed to attract the holes from the CGL. Additionally, other factors such as the dielectric strength under positive and negative Corona charging, the polarity of the charged toner particles may also have influence on the choice of polarity of Corotron. In order to utilize positive Corona charging as the charge source for static charge based photocopy, one could invert the configuration of the bi-layer by putting the CGL on top of CTL. This proposed alternative is not as practical because generally adopted CGL material have poor wear resistance.

2.2.2. Positive and negative Corona charging

From an energetic point view, negative Corona is superior to positive Corona charge and the reasons are explained here. The common phenomenon generated by both positive and negative Corona charging is the formation of an electron avalanche in the electric wire’s vicinity. The electrons naturally occurring in the air under a strong electric field is responsible for the formation of such avalanche. These free electrons gain kinetic energy through acceleration under the high electric field. They then collide with the neutral gas molecules in the air and cause ionization. Additional electrons are liberated during the collision and they collide with other gas molecules in the same way as they were liberated. As described, the number of free electrons in the vicinity of the Corona charging device grows exponentially and an avalanche rapidly builds up. In other words, a small amount of electrons are able to liberate and ionize the entire gas into plasma. Unlike positive Corona charging, in negative Corona, electrons ionized form the neutral gas molecules are of relatively little importance in sustaining a negative Corona since electrons generally move away from the negative electrode. In contrast, the dominant process for generating secondary electron in a negative Corona charging process is the photoelectric action of photons striking the surface of the negative electrode. Consequently, the energy required to liberate the electrons from the electrode surface is significantly lower than that to ionize air at room temperature than it is in positive Corona charging.

An ozone filter is usually installed to reduce the amount of ozone released to the ambient environment; ozone is another important byproduct in static charge based photocopy process. The charged species that are attracted towards the photoconductor under positive or negative Corona charging are namely hydrated protons $(H_2O)_nH^+$ for positive Corona charging and reaction product from O^- (mainly NO_3^- and $O3^-$) for negative Corona charging. In our area of interest of negative Corona charging, it is found that the vibrationally excited states of N_2 and NO_3^- are capable of injecting charge into the polymer. They are energy carriers to the polymer surface and effective injectors of charge in LDPE, PP and PTFE, where the surfaced traps lie to a depth of 0.5 μm and their lifetime can be as high as in the magnitude of 10^3 seconds [59]. In contrast, charge injection could not be detected in positive Corona charging and this may due to the relative concentration difference of excited species that formed after charging.

For the purpose of convenience, we will afterwards assume negative Corona charging throughout the discussion and it is consistent with the polarity used in results and discussion chapter. One may also find the nomenclature of "charge rollers" as the means to deposit charges onto photoreceptor in literature, to clarify its nature, it basically shares the same fundamental principle as Corona charging, except initially depositing charges on a separate roll.

2.2.3. Problems in OPC associated with Corona charging

Apart from the electrons liberated during Corona charging, it is discovered that ions are comprised of the following result from air species breakdown [60]:

- $NO_3^-(H_2O)_n$ (predominant)
- $O_3^-(H_2O)_n$
- $OH^-(H_2O)_n$
- $O_2^-(H_2O)_n$
- $CO_3^-(H_2O)_n$

By taking ozone into consideration, this mixture of the highly oxidizing chemicals change the surrounding air into a unipolar gaseous electrolyte, which have similar effect on the nearby objects as an aqueous nitrate electrolyte [61]. This is the reason why an anti-corrosion layer was employed in section 2.1. Furthermore, research for ozone reduction inside a static charge based photocopy machine becomes popular [62][63]. More specifically, detailed work on study of gas flow, type of the Corotron used, humidity and temperature are studied. It is found that in order to maintain a constant Corona charge flux, the applied voltage changes when the relative humidity changes in the positive Corona charge case. In the negative case, the applied voltage is changed by the temperature variation [64]. In other words, negative Corona charging is not affected by the level of humidity, which is an ideal property in terms of commercial application. It is much easier to control the temperature inside a laser printer than to control the humidity, a parameter largely influenced by the ambient environment. As a result of these developments, the Corona charging technology in high speed laser printers and earlier photocopiers has remained essentially unchanged over many years.

In term of the electrical properties and given the chemicals generated in an air Corona, it is not difficult to anticipate the unwanted ramifications on the photoconductor after repeated exposure to Corona charging. In addition, in the presence of high humidity, the OPC surface will become more conductive then it is supposed to be. The charges become less stable and thus cause failure of the latent image; as early as the first step for static charge based photocopy. The requirement of the printers decides the level of acceptable performance for OPC characteristics. For low-speed low volume printers, the chemical exposure may not be as serious; as the system is self-venting and is capable of removing most of the charge-generated species. As for high speed, large volume applications, it is necessary to reduce the chemical exposure by venting the charger and utilizing an anti-oxidation layer on the OPC. As explained before, the single layer structure that unifies CGL and CTL in a single polymer layer is unfavorable because the single layer is very sensitive to the gas species caused by Corona charging. In fact, all chemical substances including NO_X, HNO_X and ozone react with the CGL polymer material and the system will deteriorate rapidly after cycles. As for dual-layer structure, the problem of spreading image as a result of more conductive photoconductor remains less severe (image spreading only occur after many more cycles). It has been confirmed that exposing OPC to Corona gases results in an increased surface conductivity and spreading of the electrostatic latent image [65].

However, Kobayashi found that the exposure of dual-layer OPC with p-diethylaminobenzaldehyde-1,1-diphenyl hydrazone (DEH) as the charge transport material had no effect on spreading of latent image [66]. On solving the long-lasting problem of image spreading, another problem of decreased image resolution was observed after Corona charging cycles. They [66] suggested that the accumulation of nitrate salts and the DEH radical cations near the OPC surface was responsible for this behavior. The conductivity of the OPC increased by the radical and chemical alteration of the charge transport material and could lead to hole-transport limitations.

Yarmchuk and his colleague identified Corona contamination as the cause of image spreading and their conclusion were supported by the fact that wiping the surface with methanol could effectively eliminate the spreading [67][68]. However, another source for the image spreading was discovered not long after Yarmchuk's theory. In dual-layer OPC structure, the exposure related accumulation of positive charge carriers at a subsurface layer of the CGL and UCL interface was thought to cause image spreading. It was found that the CTL is damaged permanently, allowing positive charge injection into it. The charge characteristic of the CTLwas not restored after being annealed at 120 Celsius by abrasive wear of the CTL surface where charge injection occurred [69].

Since the search for the alternative CTL has proven unpopular, much of the research attention has been taken diverted to the use of stabilizing additives. The ultimate additive is one that can be added in sufficient amounts to stabilize the OPC while simultaneously have no deleterious effects on any OPC physical or electrical characteristics. Endo and co-workers found that, in a dual-layer OPC structure, the addition of antioxidants helped to maintain resolution of printed image [70]. Similarly, Kochelev and co-workers revealed that, among a large number of dual-layer OPC formulations, the addition of electron acceptors in both the CTL and CGL promoted the stability of OPCs after exposure to Corona charging [71]. As a result, it is concluded that the interaction between the OPC surface and Corona charging can lead to OPC fatigue, which is recognized by the blurring of the latent image, increased residual potential and decreased charge acceptance.

2.3. Introductory to dielectric polarization

2.3.1. Dielectric: definition and basics

As an indispensible aspect of the theory of impedance spectroscopy, it is vital to revisit the fundamentals of dielectrics. Dielectric relaxation, one of the most important concepts in dielectric properties, describes the motion of the host material subject to external field at molecular level. In order to understand dielectric relaxation, it is critical to first consider its physical counterpart: mechanical property of polymers such as anelastic relaxation or creep. When a polymeric filament is suspended by a weight, unlike metals, due to the molecular rearrangement in the polymer induced by the stress, the strain of the polymer will not be constant but rather will increase slowly with time. Similarly, on releasing the stress, the molecules slowly recover to its former spatial arrangement and the strain gradually returns to zero. The rearrangement of polymer chains can not only be perturbed by the mechanical stress, but also be influenced by the application of electric field. In fact one can use very similar arguments and models to develop equations for both mechanical and dielectric properties.

A dielectric is indeed an electric insulator that can be polarized under electric field. The more general term insulator is used to describe materials with low electric conductivity; the term dielectric narrows the category by confining the group of material with higher polarizability, which is discussed intensively as dielectric constant in the following sections. The name dielectric was firstly introduced by Michael Faraday, from the word “dia-electric” [72].

The application of a voltage across a conductor causes the movement of electrons and thus a flow of current. Metal is considered as a collection of nuclei indulged in a “sea of electron” but the situation is completely different in dielectric polymer. The electrons are tightly bounded to the central long chain and side groups through covalent bonding, which make them much more difficult for dielectric polymers to allow the movement of electrons.

2.3.2. Polarization

In classic model of materials, a material is made up of atoms. Each atom consists of a cloud of negative charged electrons and positive charged nuclei. The center of both electrons and nuclei overlap and cause no dipole, as displayed in figure 2.7(a). In the presence of an electric field, the cloud of electron is distorted as shown in figure 2.8(b). The resulting dipole moment, M, shown in figure 2.8(c) is represented by the product of the charge and distance between positive charge center and negative charge center.

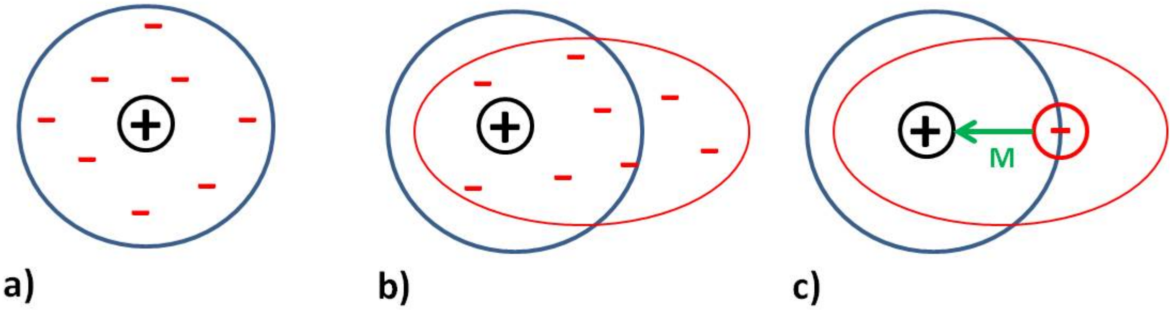

Figure 2.7 Classic model for polarization: a) without no external field; b) distortion of electrons as a result of external field; c) dipole moment caused by electron distortion

In the discussion of polarization, one may divide them into two categories: dipolar polarization and ionic polarization.

Ionic polarization is caused by relative displacement between positive and negative ions in ionic crystals. If there is more than one kind of atoms in the ionic crystal, for example, sodium ions and chloride ions in NaCl crystal, the distribution of positive and negative charge deviates from the center and therefore creates a dipole. Due to the fact that the topic of ionic polarization is less relevant to this study, we will put more emphasize on the topic of dipolar polarization.

Dipolar polarization is often divided into two separated groups. The first group of polarization comes from polar molecules that are in possession of permanent dipoles. For example, in a water molecule, the angle between the asymmetric bonds between oxygen and hydrogen atoms is 104.5°, the asymmetry of bonds retains polarization without the presence of electric field. However, water is neutral as dipoles in water are randomly orientated as a result of thermal agitation. The majority of polymers are made of molecules with dipoles and all examples listed section 2.1 have permanent dipoles.

When an external electric field in applied, the dipoles are reoriented so as to minimize the internal field, as illustrated in figure 2.8. The dipoles are aligned so that the heads and toes of individual dipoles are adjacent to each other and the surface of the dielectric is covered with partial charges. The direction of the local field or the field causes by dipole moments are the same as the external field.

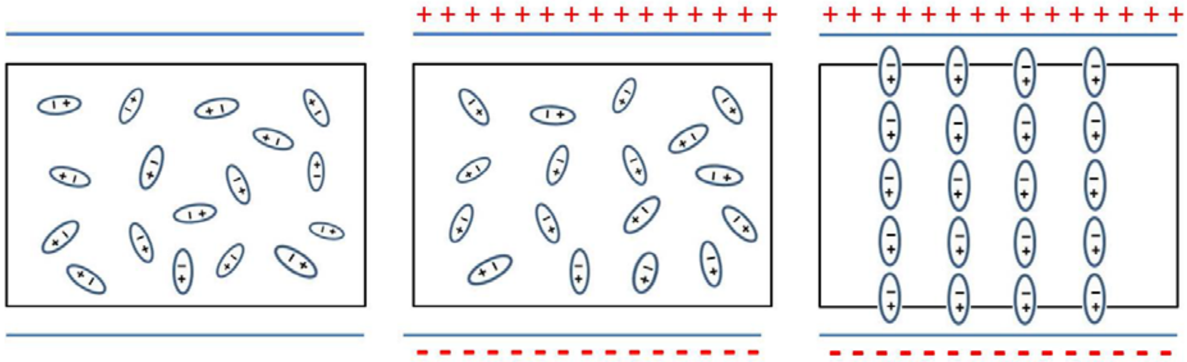

Figure 2.8 Dipole polarization as a result of external electric field

The reorientation doesn’t occur instantaneously, rather on a time scale that depends on the magnitude of the applied field, the torque and the surrounding local viscosity of molecules. As a result, the delayed response causes friction and therefore heat loss in the system.

2.3.3. Dielectric polarization

Free charges in a conductor will respond exactly to cancel the applied field. However, the charges in a dielectric will respond in such way that it cancel out the field partially within the polymer. As a matter of fact, the situation within a dielectric is much more complicated due to the presence of local field, caused by the response of the medium charges. These properties will be of great importance in the latter discussion of molecular polarization and the bulk polarization. In the following part, numerical model for dielectric polarization is discussed. To describe the dielectric properties in the absence of relaxation, we may consider two parallel metal plates in figure 2.9 of area “A” and a distance “d “between the plates.

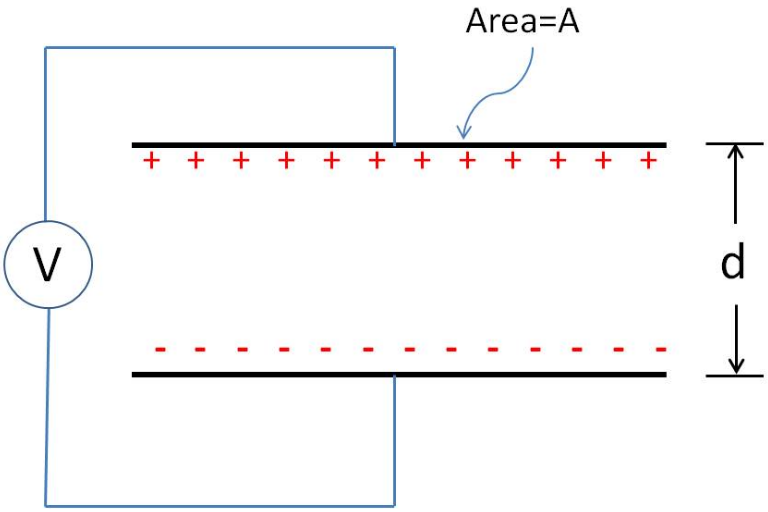

Figure 2.9 Charge separation between parallel under electric field

2.3.3.1. Time independent dielectric constant

If the two metal plates are identical and opposite charge of magnitude q_0, then a potential is established across the plates. The magnitude is given as:

$$V_0 = \frac{q_0}{C_0} \tag{2.2}$$

In (2.2), C_0 is used to represent the proportionality constant between voltage across the plates V_0 and real charge q_0. C_0 is also the capacitance of vacuum. If a piece of dielectric is inserted into the two plates and keep the charge q_0 constant. The voltage across the plate is reduced to V, instead of V_0. The ratio of the voltages, ε, defines the dielectric constant of the dielectric material:

$$\varepsilon = \frac{V_0}{V} = \frac{C}{C_0} \tag{2.3}$$

In the expression above, C is the capacitance of the plate with the presence of the dielectric and the voltage V across the capacitance with the dielectric inserted may be written as,

$$V = \frac{V_0}{\varepsilon} = \frac{q_0}{\varepsilon C_0} = \frac{q_1}{C_0} \tag{2.4}$$

Where

$$q_1 = \frac{q_0}{\varepsilon} = \frac{q_0 C_0}{C} \qquad (2.5)$$

In equation 2.4 and 2.5, q_0 is called the true charge because it represents the actual amount of charges that accumulated on the plate. q_1 is known as the free charge since it is the portion of the true charge which contributes to the voltage. The difference between the true charge and the free charge is the bound charge (q_0-q_1). The bound charge is also called polarized charge and it is the charge on the surface of the dielectric, as shown in figure 2.10.

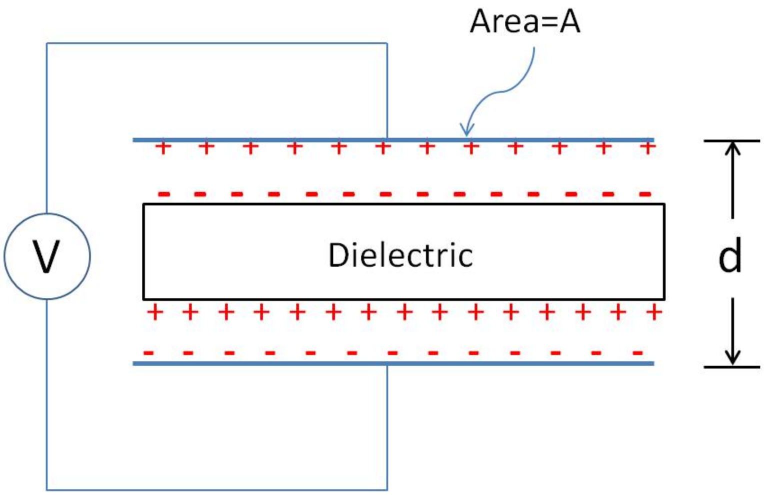

Figure 2.10 Charge separation on inserting the dielectric

As a matter of fact, the dielectric is in intimate contact with the metal plates and the dipoles are also aligned inside the dielectric, perpendicular to the surface, as shown in figure 2.8. However, for the purpose of addressing the charge accumulation elusively on the dielectric surface, the space between is exaggerated.

In the next step, the polarization, (P), of the dielectric is actually the surface density of the bound charge. Hence, by omitting the edge effect, we have:

$$P = \frac{1}{A}(q_0 - q_1) = \sigma_0 - \sigma_1 \qquad (2.6)$$

where σ_0 and σ_1 are the surface charge density on the metal plates of the true and free charges respectively and two charge densities define the electric displacement, D, and the electric field strength, E, by

$$D = \sigma_0 \tag{2.7}$$

$$E = \frac{\sigma_1}{\varepsilon_0} \tag{2.8}$$

The constant ε_0 is vacuum permittivity, in the value of 8.85E-12 F/m and therefore:

$$D = \varepsilon_0 E + P \tag{2.9}$$

By algebraic manipulation, it is shown that:

$$D = \varepsilon E \tag{2.10}$$

Equation (2.10) is an electric analogue of Young's modulus and P, D and E have been so far assumed to be independent of time. Physically speaking, equation (2.9) implies that the Polarization is entirely caused by the displacement of molecular electrons with respect to their nuclei and the entire process is time independent.

However, it is from general knowledge that these parameters may not be able to adequately describe real polymeric solids, as polymer molecules are extremely mobile: stretching a piece of polymer gives a time-dependant strain curve (creep). Consequently, as for electric property, a slow increase in the polarization is observed when a constant electric field is applied. In other words, a time dependant dielectric constant $\varepsilon(t)$ is obtained.

2.3.3.2. Time dependant polarization

In order to rationalize the process of time dependant dielectric constant, one may use two types of experiments. The first experiment is called step-function experiment and it measures the response of the material to a constant electric field as a function of time. The second is called dynamic experiment and it is the response to a sinusoidal electric field, as a function of time.

2.3.3.2.1. Step-function experiment

For polymer containing dipolar groups, dielectric relaxation effects are observed owing to the time required for the reorientation of the permanent dipoles. In a typical step-function measurement, a dielectric is placed between two metal plates and a constant DC potential, E is applied between time t=0 and t=t_0, as shown in figure 2.11.

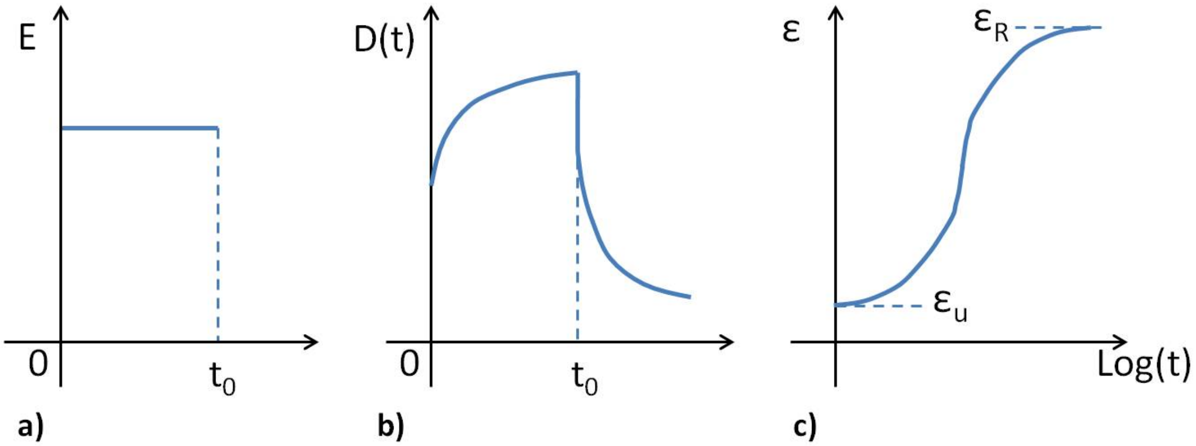

Figure 2.11 Step-function experiment for a dielectric material. a) Constant electric field strength (E) applied between t=0 and t=t0. b) Dielectric displacement (D) response under constant E. c) Dielectric constant of the measured dielectric material as a function

As a result, a changing and non-linear electric displacement is plotted as a function of time. It is obvious that there are four distinct regions of response. The first region is the instantaneous electronic response of D at t=0. The second region arises from paraelectric polarization due to the time dependent reorientation of dipoles and it is after region 1 and before t=t_0. The third region takes place right at t=t_0 where electric displacement reaches his maximum and it is the moment when the field E was removed. It is apparent that the magnitude of regions 1 and 3 are equal. The final region is an asymptotic recovery of the paraelectric polarization.

One important consideration here in the measurement is related to the reflection point in figure 2.11(c), which happens at the middle of the curve. If the reflection point occurs at a very short period, i.e., $<10^{-6}$ second, then the experiment becomes very difficult to perform due to the fact the total polarization appears almost instantaneously. It is therefore impossible to separate the instantaneous electric polarization from the time dependent paraelectric polarization. In this case, only a portion of the sigmoid curve in figure 2.11(c) is observed. In this case when the step-function observation is of little value, and the so-called dynamic experiment is of greater relevance.

2.3.3.2.2. Dynamic experiment.

If a sinusoidal stress is applied to a solid exhibiting relaxation, then the resulted strain response usually lags behind the applied force by some phase angle δ. The phase lag is the results of the time necessary for molecular rearrangement and it is consistent with time lags observed in step-function experiment.

As an analogous experiment to mechanical experiment, we expect similar phase lag in a dielectric experiment. On applying an alternating electric field, an alternating electric polarization is observed. In the case of a polar solid, electric displacement will lag behind the applied field by some phase angle δ and E and D are expressed as:

$$E^* = E_0 \exp\,(j\omega\mathrm{t}) \tag{2.11}$$

$$D^* = D_0 \exp\,(j\omega\mathrm{t} - \delta) \tag{2.12}$$

The angular frequency ω is proportional to the external AC frequency with the relationship such that ω =2πf. E_0 and D_0 are the field and displacement amplitude and the relationship between displacement and field can then be expressed as:

$$D^* = \varepsilon^* E^* = (\varepsilon' - j\varepsilon'')E^* \tag{2.13}$$

Euler’s rule states that;

$$\exp(j\theta) = cos\theta - jsin\theta \tag{2.14}$$

Therefore it follows that the dielectric constant can be expressed as:

$$\varepsilon' = |\varepsilon|cos\delta \tag{2.15}$$

$$\varepsilon'' = |\varepsilon|sin\delta \tag{2.16}$$

$$\frac{\varepsilon''}{\varepsilon'} = tan\delta \tag{2.17}$$

It is conventional to represent tanδ in equation 2.17 as loss tangent.

In the relaxation region in figure 2.12, the constant τ, is the relaxation time and represents the time needed for the relaxation of the molecular segments. It is obvious from the figure that ε’ decreases with ω from a value of ε_R to ε_U. The so-called term relaxed permittivity ε_R , represents the value of ε’ at the limit when ω→0 or the static DC voltage signal. The other one in figure 2.12, ε_U, represents the value of ε’ at the limit when ω→∞. This decrease is called the dispersion of the dielectric constant and the difference (ε_R - ε_U) is known as the magnitude of the relaxation and it is a measure of the orientation polarization.

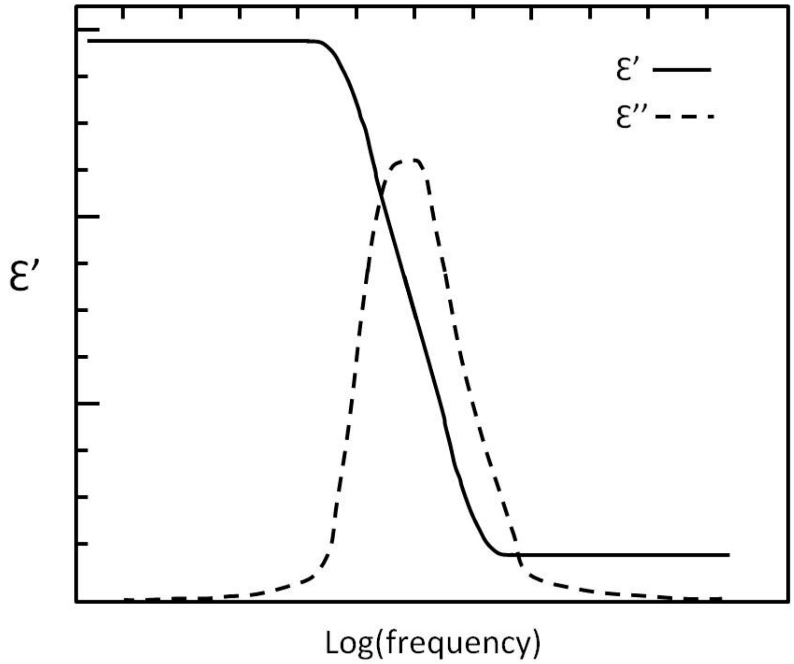

Figure 2.12 Relaxation of dielectric constants, real part and imaginary part

It is often found in polymeric material that (ε_R - ε_U) is much higher than 1. It is also realized that ε" reaches its maximum when ωτ=1. At the extremes of frequency, the value of ε" tends to be zero. Physically, the permittivity is completely real and thus no relaxation (tanδ=0) is occurring at extremely low and high frequencies. From the energy point of view, ε" is proportional to the rate of energy dissipation of the system.

2.3.3.2.3. Debye Equation

To take into account the result of a dynamic experiment, one only has to impose the criterion of an oscillating field. In the simplest case called Debye relaxation, [73] it gives:

$$\varepsilon^*(\omega) = \varepsilon_U + \frac{\varepsilon_R - \varepsilon_U}{1 + j\omega\tau} \tag{2.18}$$

$$\varepsilon'(\omega) = \varepsilon_U + \frac{\varepsilon_R - \varepsilon_U}{1 + \omega^2\tau^2} \tag{2.19}$$

$$\varepsilon''(\omega) = \frac{(\varepsilon_R - \varepsilon_U)\omega\tau}{1 + \omega^2\tau^2} \tag{2.20}$$

$$tan\delta = \frac{\varepsilon''}{\varepsilon'} = \frac{(\varepsilon_R - \varepsilon_U)\omega\tau}{\varepsilon_R + \varepsilon_U \omega^2 \tau^2} \tag{2.21}$$

This model was introduced and name after chemist Peter Debye. Similar to equations above, ε_R and ε_U represent relaxed permittivity and permittivity when frequency goes to infinity, respectively.

2.4. Impedance spectroscopy

Impedance spectroscopy (IS) is the measurement of linear electrical response as a result of small-signal AC perturbation and its corresponding analysis of the response, to elucidate desired information about the physicochemical properties of the system. As the key characteristic, IS is always carried out in frequency domain, although some of the analysis is done in time domain and then Fourier transformed into frequency domain. The concept of IS was initially introduced in 1880s by Oliver Heaviside. Vector diagram and complex representation, the form that is still actively adopted widely is introduced by Kennelly and Steinmetz [74]. Cole-cole plot, a plot utilizing real and imaginary axis to illustrate ε' and ε" was first introduced in 1941 by K. S. Cole and R. S. Cole [75] and it since then became the fundamental analytical technique that allows complete analysis of response.

2.4.1. Theory of impedance spectroscopy

There are two main categories of IS: electrochemical IS (EIS) and non-electrochemical IS. EIS focuses on analysis and measurement on system where ionic conduction dominates. Examples of EIS are ample, ranging from solid to liquid electrolytes and including ionically conducting glasses/polymers. In this particular thesis, however, much attention has been paid to the remaining category: IS study in dielectric materials. In these solid or liquid systems, the non-conductor involves dipolar rotation. Examples are insulating polymers, single-crystal or amorphous semiconductors. There is of course analysis based on the mixture of the two categories and a good example is the partly conducting dielectric material with some simultaneous ionic and electronic conductivity. Although EIS is the fastest growing branch in IS, non-electrochemical IS was developed first and still of great importance in various areas including the dielectric response of photoconductors.

The general process of IS is to apply an electrical stimulus, which is a known voltage or current, to the electrodes and observe the response, which is also a resulting current or voltage. It is the purpose of the IS to study the electric properties of systems, their interactions, and the dependences at controllable variable. These adjustable variables include but not limited to temperature, oxygen partial pressure, moisture level, and applied static voltage/current bias. During the application of the stimulus, a number of fundamental processes at microscopic level take place through the sample and lead to overall electrical response. In our study of dielectrics in particular, it includes the transport of electrons through the electronic conductors (metal electrodes, often coated on the dielectric to facilitate experiment) and the flow of charged atoms or atom agglomerates via the path. The flow rate of electrons depends on the overall impedance of the dielectric. More importantly, Impedance spectroscopy is a non-destructive technique and so can provide about ongoing processes such as corrosion or the discharge of batteries.

2.4.1.1. Step-function perturbation

There are three major types of distinguished stimuli in IS experimentation. First and the most fundamental one, it is a step function voltage in transient measurement, as illustrated in

(2.22) and (2.23) and figure 2.13. It may be applied at time t=0, to the system and the resulting current response i(t) in time domain is measured.

$$V(t) = V_0 \text{ for } t > 0 \tag{2.22}$$

$$V(t) = 0 \text{ for } t < 0 \tag{2.23}$$

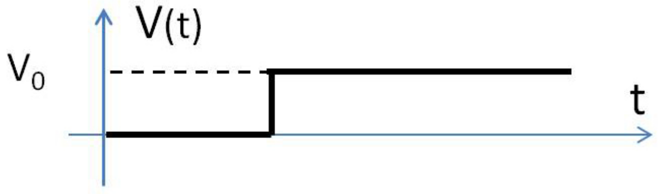

Figure 2.13 Step-function signal for impedance spectroscopy

The ratio of V_0/i(t) in the case of step function, is called the indicial impedance or the time-varying resistance. It measures only the impedance resulting from the step function voltage perturbation at the electrochemical interface. This quantity, although easily obtained, bears little useful information and therefore is usually conducted as part of IS measurements. Instead, these time-varying results are generally Fourier-transformed into the frequency domain and yields result in frequency domain. This method is theoretically simple yet requires several additional conditions. It is only valid when the electric response is sufficiently small so that the system response can be treated as linear, as illustrated in figure 2.14.

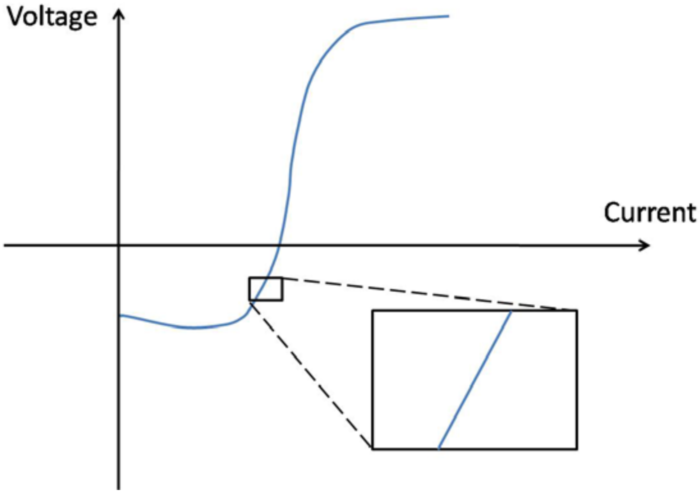

Figure 2.14 Small voltage signal yields linear current response

The advantage of this approach is obvious: it is experimentally easy to accomplish. Similarly, the voltage of the perturbation signal, which is an independent variable, is able to control the electrochemical reaction rate at the interface. Unlike the AC impedance method whose magnitude for perturbation is in the range of several volts, the magnitude of the step-function can be as high as several hundred volts. This significantly increases the perturbation signal and yields response that is more discernible for sample with high resistivity. In a usual case, the response current can be as low as Femto (1E-12) Ampere, which is beyond the range of effective measurement for existing experimental equipment. The disadvantages of the step-function method include the need to make Fourier transform, which is not always easily accomplished. Additionally, unlike the nature of the tunable sweeping frequency in AC IS, the frequency spectrum of step-function IS is not controlled directly. Instead, the corresponding frequency is Fourier transformed, as illustrated in figure 2.15. Consequently, the impedance may not be well determined over all desired frequencies.

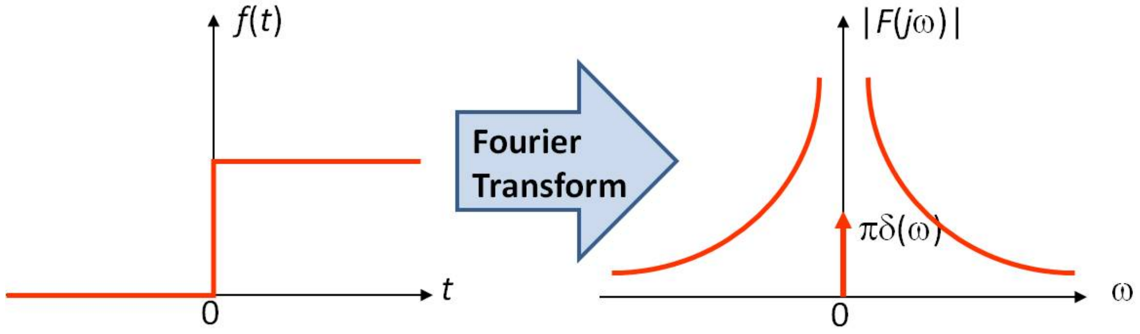

Figure 2.15 Fourier transformed step-function signal

It is important to notice that the rising edge sharpness of the step-function signal is of paramount importance when measuring impedance. Mathematically, the high frequency end of the transformed image in figure 2.15 is derived from the data point near t=0 before transform (figure on the left). It is mathematically proved that the product of the width of the rising edge before transform and highest frequency it reaches after Fourier transform is unity. As an example, in the situation where high frequency (i.e., 1 kHz) response is desired, one should employ equipment that is able to generate voltage signal rise within a short period of time (1ms).

2.4.1.2. Random noise perturbation

The second type of stimuli is to apply a signal that consists of random noise to the interface and probe the current response. Similar to the step-function method, the current is Fourier transformed into frequency domain. This approach provides easier data collection as only one signal is applied to the system at one time. However, its disadvantage is more obvious. Similar to any other impedance spectroscopy method, signals have to be transformed into frequency domain and the transform of a random signal is a computationally complex process. In addition to this, the random signal is usually generated digitally with a digital signal processor or microprocessor. Both techniques rely on the feeding of a stream of random numbers to a digital-to-analog converter. The random signal generated from a computer is calculated based on a specific algorithms and the number generated is indeed only pseudorandom. This method is employed in limited areas such as neurological intensive study on stroke patients [76] or to non-invasively obtain image of the internal conductivity distribution of the human body [77].

2.4.1.3. AC signal perturbation

The third method possible is alternating current (AC) impedance spectroscopy and it is the most widely adopted method. Due to its wide application, it has become the standard impedance method and sometimes can be referred as impedance spectroscopy directly. It measures impedance response directly in the frequency domain by applying a single-frequency voltage to the test sample. The key quantities to be measured are phase shift of the perturbation signal as well as its amplitude. The system undergoes sweeping frequencies from as low as 1 µHz to as high as MHz. Commercial instruments are readily available and one can sweep across the frequency domain that he prefers, depending on the system to be studied. AC perturbation signal is capable of applying impedance measurement in a broad range of research areas, including electrochemistry that focuses on interface, corrosion analysis, batteries, fuel cells and electrodeposition. When a sinusoidal potential excitation is applied to the system, the response is also a sinusoidal AC current signal, which contains the excitation frequency and its harmonics. Similar to the first two methods, this current signal can be analyzed as a sum of sinusoidal functions or a Fourier series. As a non-destructive method, AC impedance spectroscopy is capable of using only small excitation signal. This gives rise to a pseudo-linear response of the system. The excitation signal, expressed as a function of time, has the form of:

$$E(t) = E_0 \cos(\omega t) \tag{2.24}$$

Where E is potential applied at time t and E_0 is the amplitude of the potential. The angular frequency ω in the unit of radians/sec is the product of a constant (2π) and the sweeping frequency in the unit of Hertz, as in equation 2.25:

$$\omega = 2\pi f \tag{2.25}$$

The impedance of the system at any frequency ω_0 is a complex number because the resulting current δI(ω), as a result of small signal δV(ω) perturbation, contains not only phase information, but also magnitude information. It is indeed the complex ratio between voltage perturbation and current signal, as in 2.26:

$$Z(\omega, V_0) = \frac{\delta V(\omega)}{\delta I(\omega)} \tag{2.25}$$

The AC current measured may have a phase lag φ with respect to AC voltage, if we apply

$$V = V_0 + |\delta V|\cos(\omega t) \tag{2.26}$$

And measure current

$$I = I_0 + |\delta I|\cos(\omega t - \varphi) \tag{2.27}$$

Then the resulting impedance is:

$$Z(\omega, V_0) = \left|\frac{\delta V}{\delta I}\right| \{\cos(\varphi) + jsin(\varphi)\} \tag{2.28}$$

Where j^2=1.

Using Euler's relationship,

$$\exp(j\varphi) = \cos\varphi + jsin(\varphi) \tag{2.29}$$

It is mathematically applicable to express the impedance as a complex function in exponential form and equation 2.28 can be rewritten as:

$$Z(\omega, V_0) = \left|\frac{\delta V}{\delta I}\right| \exp\,(j\varphi) \tag{2.30}$$

In time domain analysis, if we plot the applied sinusoidal signal v(t) on the X-axis of a graph and the sinusoidal response signal I(t) on the Y-axis, an oval is plotted. This oval is known as a "Lissajous figure". Analysis of Lissajous figures is the accepted method of impedance measurement prior to frequency response analysis, as schematically illustrated in figure 2.16:

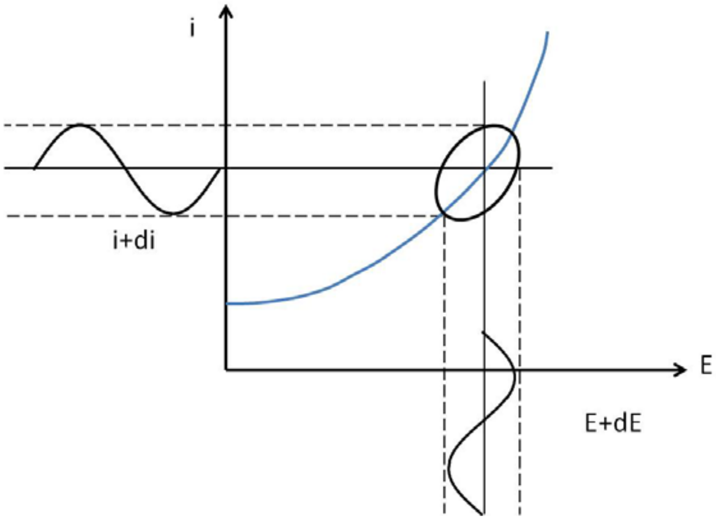

Figure 2.16 Time domain Lissajous figure

More often and perhaps the reason why electric response analysis is always carried out in the frequency domain, is because the time domain signal is always full of noises that cannot be separated easily using time domain analysis. Unless applying pure sinusoidal signal on an ideal circuit element (i.e., capacitor with no dissipation energy loss), a real signal obtained from experiment is made up of many frequencies. Frequency domain analysis helps to differentiate which frequencies a signal consists of and their corresponding amplitude. In other words, Fourier transform or Laplace transform, depending on specific example, is a tool to decompose signal into its various frequency components.

A linear system is the one that possess superposition principle: if the input composed of the weighted sum of several signals, then the output is simply the weighted sum of the responses of the system to each of the signals. In a linear system we may conduct impedance analysis in frequency domain. However, for many electrochemical systems, they are not linear. In other words, only systems with linear response or pseudo-linear response are to be studied using impedance spectroscopy. Consequently, only a small signal, often from 10 mV to ~1V is applied to the system. A small amplitude perturbation is specific enough to confine the system to a pseudo-linear segment on the current-voltage curve and this is the situation in figure 2.14.

Overall, it is useful to summarize the importance of IS by its many research applications. Based on a relatively simple electrical measurement, IS has become a popular analytical tool to investigate many complex material variables or processes including mass transport, corrosion, dielectric properties, microstructures of the interface. IS is even capable of investigating membrane behavior in a running cell with transient electrochemical process taking place.

Once the impedance of the system or process is obtained, its equivalent circuit can be derived based on impedance representation of various ideal electrical elements. The evolution and interpretation of elements will be discussed in the next section.

2.4.2. Basics of the Nyquist plot and the four-quadrants

Impedance is defined as a complex quantity and it is dependent on frequency. When a monochromatic signal

$$v(t) = V_m \sin(\omega t) \tag{2.31}$$

is applied to a system with the single frequency at

$$f = \frac{\omega}{2\pi} \tag{2.32}$$

The resulting current response is measured:

$$i(t) = I_m \sin(\omega t + \theta) \tag{2.33}$$

and θ is the phase difference between the voltage and current. For a pure resistive system, this phase shift is zero. It can be easily seen that in the frequency domain, based on Ohm's law, the complex quantity Z(ω) is defined as the impedance function and its value at a particular frequency is called its impedance:

$$Z(\omega) = \mathcal{F}\{v(t)\}/\mathcal{F}\{i(t)\} \tag{2.34}$$

In the above expression, $\mathcal{F}$ {} is used to denote a Fourier transform. This operator is only valid when the system is linear or at least pseudo-linear in the region to be analyzed. Mathematically, impedance Z(ω) can be expressed in the complex form of a+bj where j is square root of -1 or:

$$j = \sqrt{-1} = \exp\left(\frac{j\pi}{2}\right) \tag{2.35}$$

In detail, j in complex plane represents an anticlockwise rotation with respect to the real axis, such as the one in figure 2.17. Consequently, real and imaginary part of the impedance takes up the real and imaginary axis accordingly. The vector Z(ω)=Z'+jZ" is plotted in figure 2.17.

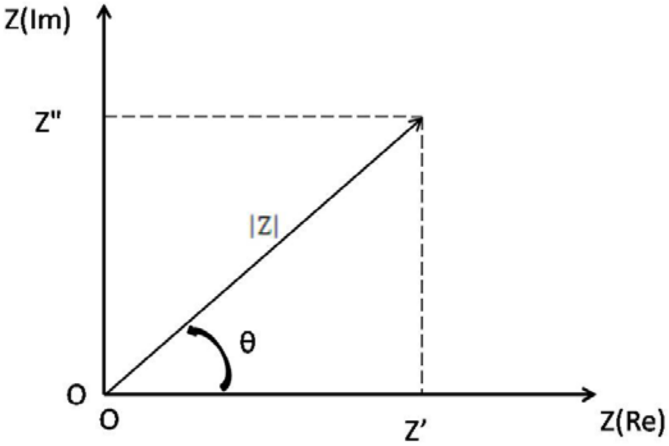

Figure 2.17 Impedance plot in vector form

It is readily obtained that the real part and imaginary part of the coordinates are:

$$\mathrm{Z(Re)} = \mathrm{Z'} = |\mathrm{Z}|\cos\theta \tag{2.36}$$

$$\mathrm{Z(Im)} = \mathrm{Z''} = |\mathrm{Z}|\sin\theta \tag{2.37}$$

With the phase angle:

$$\theta = \tan^{-1}(\mathrm{Z''}/\mathrm{Z'}) \tag{2.38}$$

These three relationships define the real and imaginary axis in Cole-cole plot, which will be discussed in next section. It is also important to note that the relationship of 2.34 is valid as long as such overall material system response is electrically linear. The linearity is discussed in each system individually and most equipments that carry impedance spectroscopy measurement take this point into consideration. As an example, in the particular systems for dielectric measurement, typical impedance measurement device, (i.e., Parstat 2273 advanced electrochemical system, Gamry 600 Potentiostat Operator), the amplitude of the perturbation voltage can be adjusted as low as 10 mV. Such low amplitude only presents such a small portion on the I-V characteristic curve that it can be treated as linear.

Impedance by name stands for complex impedance measurement in frequency domain and it is only a real number when frequency is zero, which describes pure resistance behavior. This is evident from equations 2.36 and 2.37 as Z=R when θ is zero. As a matter of fact, there are other measured or derived quantities used in impedance analysis. The Reciprocal of impedance is called admittance where:

$$Y = \frac{1}{Z} = Y' + jY'' \tag{2.39}$$

Admittance is mathematically more convenient when dealing with systems that are complicated using impedance. In this particular case, we may rewrite current (i) and voltage (V) relation as:

$$i = Yv \tag{2.40}$$

Armed with the relation above, we may further express impedance and admittance in terms of resistivity and capacitance:

$$Z = R_s(\omega) - jX_s(\omega) \tag{2.41}$$

$$Y = G_p(\omega) + jB_p(\omega) \tag{2.42}$$

In 2.41 and 2.42, X, reactance and B susceptance are expressed by capacitance C:

$$X_s = \frac{1}{\omega C_s(\omega)} \tag{2.43}$$

$$B_p = \omega C_p(\omega) \tag{2.44}$$

The subscripts s and p stand for “series” and “parallel”.

Similar to the relationship between impedance and admittance, Modulus M and dielectric constant ε are also defined:

$$\mathrm{M} = \mathrm{j}\omega \mathrm{C}_0 \mathrm{Z} = \mathrm{M}' + \mathrm{jM}'' \tag{2.45}$$

$$\varepsilon = \frac{1}{\mathrm{M}} = \frac{1}{\mathrm{j}\omega \mathrm{C}_0} = \varepsilon' - \mathrm{j}\varepsilon'' \tag{2.46}$$

C_0 in 2.45 and 2.46 are vacuum capacitance in the unit of Farad/m, with the expression:

$$\mathrm{C}_0 = \varepsilon_0 \frac{\mathrm{A}}{\mathrm{d}} \tag{2.47}$$

A is the area the electrode and d is the distance between of separation between electrode. The vacuum dielectric constant or permittivity of free space ε_0 is a constant with value of 8.85E-12 F/m. Therefore, the four immittance functions are namely impedance (Z), admittance (Y), modulus (M) and dielectric constant (ε). The use of complex dielectric constant dated back to the 1950s and became popularized by Cole and Cole [75], who first plotted dielectric constant in the complex plane and the plot is now called a Cole-cole plot. The emphasis on dielectric constant is important in polymer or ceramic applications; it is an ordinary quantity containing information of energy loss during application of an electric field.

Impedance spectroscopy takes advantages of the four immittances by plotting them in the complex plane. The plot is very effective in analyzing the small signal response of the material. The point of interpreting such complex plots is to fit the plot using ideal circuit elements such as resistors, capacitors and inductors. Experimentally obtained impedance data can be analyzed using an exact mathematical model that predicts theoretical impedance or by a relative empirical model based on the system’s similarity to other well-developed systems. In either case, the parameters can be estimated using data fitting. Analyses of charge transport or dielectric polarization process in a physical model often suggest an equivalent circuit of ideal resistors and capacitors. This is due to the nature of charge separation and the flow of charge carriers; they both fundamentally reflect capacitive and resistive behavior respectively in the system. In other words, we already have a proposed equivalent circuit established for this system. However, for a new system, the equivalent circuit can be only established after evaluating its physical model based on theory and corresponding mathematical model. Ideally, the following curve fitting produces identical results based on the empirical data and the expected physical simulations.

The Cole-cole plot, originally was only used to plot complex dielectric behavior. It has been expanded to express other immittances, especially impedance. The impedance complex plot are sometimes called Nyquist plot. The two plots are generally identically except for the fact that Nyquist plot was originally only designated for measurements involving multiples terminals. It is now in general, identical to Cole-cole plot at present. Although not as distinctive as it used to be, the name of Cole-cole plot was confined in the area of electrochemical impedance analysis where ionic conduction predominates, instead of Nyquist plot, whose name can be seen in both electrochemical analysis and dielectric measurement. As a convention as well as adopting the dielectric system of this thesis, the name of Nyquist plot is used.

For the purpose of developing impedance representations on the Nyquist plot, one may start from the simplest electrical elements. It is obvious from 2.36 that a pure resistor is a single point on the real axis of Nyquist plot, as in figure 2.18(a). An ideal capacitor, as in figure 2.18(b), is a straight line on the negative side of the imaginary axis. It approaches zero with increasing sweeping frequency. An inductor, however, is asymmetric to a capacitor, as in figure 2.18(c). It’s also a straight line, but on the positive side, it moves upward with increasing frequency. The figures are consistent with their impedance presentations:

$$\mathrm{Z_R = R} \tag{2.48}$$

$$\mathrm{Z_C = \frac{1}{j\omega C}} \tag{2.49}$$

$$Z_L = j\omega L \tag{2.50}$$

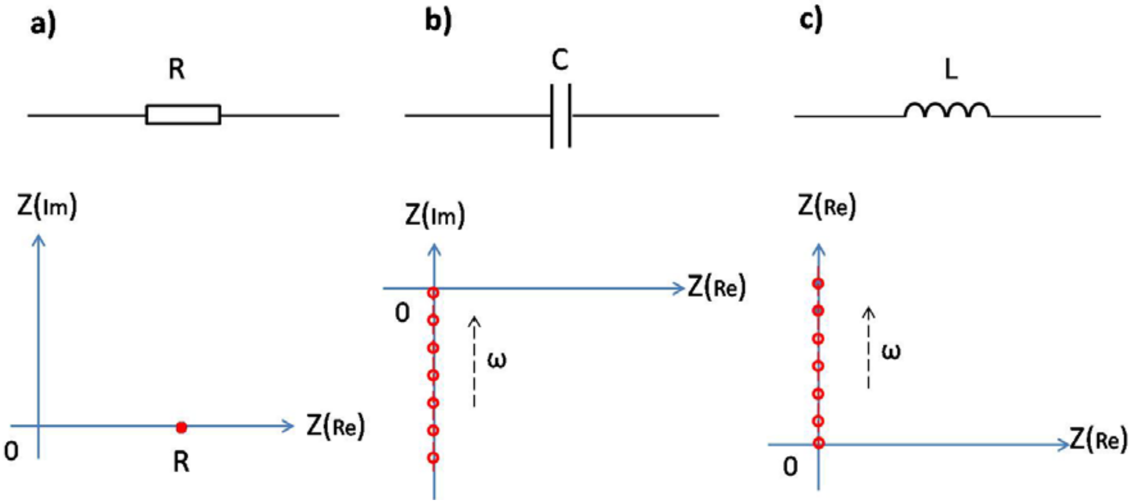

Figure 2.18 Impedance representations of resistor, capacitor and inductor

The relationships in 2.49 and 2.50 can be derived using the definition of both circuit elements. Suppose an alternating voltage wave is applied on a capacitor C,

$$v(t) = V_m \exp(j\omega t) \tag{2.51}$$

By definition, the current going through an ideal capacitor C is calculated as:

$$\mathrm{i(t)} = \mathrm{C}\frac{\mathrm{dv}}{\mathrm{dt}} \tag{2.52}$$

A current is solved by differentiating 2.51:

$$i(t) = j\omega C V_m \exp\,(j\omega t) \tag{2.53}$$

The resulting impedance Z_c is:

$$Z_C = \frac{\mathrm{V(t)}}{\mathrm{i(t)}} = \frac{V_m \exp(j\omega t)}{j\omega C V_m \exp\,(j\omega t)} = \frac{1}{j\omega C} \tag{2.54}$$

The same deductive method applies to an inductor. By definition, the voltage across an inductor L is defined:

$$\mathrm{v(t)} = \mathrm{L}\frac{\mathrm{di}}{\mathrm{dt}} \tag{2.55}$$

Suppose an alternating current signal is travelling through an ideal inductor L:

$$i(t) = I_m \exp(j\omega t) \tag{2.56}$$

The voltage is solved by differentiating 2.56:

$$v(t) = j\omega L I_m \exp\,(j\omega t) \tag{2.57}$$

The resulting impedance Z_L is given by:

$$\mathrm{Z_L} = \frac{\mathrm{V(t)}}{\mathrm{i(t)}} = \frac{j\omega L I_m \exp\,(j\omega t)}{I_m \exp(j\omega t)} = \mathrm{j\omega L} \tag{2.58}$$

Expression 2.54 and 2.58 not only explain the shape of impedance representation in complex plain as in figure 2.18, but also points out the direction they move with increasing sweeping frequency. For example, capacitor takes up the negative side of the imaginary plain and could only propagate upward with increasing frequency and it confines itself into a single point when the frequency goes to infinity.

Situation becomes complicated when elements are placed together, either in parallel or in series. For the purpose of clarity, inductor will be ignored for a while and the impedance between resistor and capacitor will be discussed.

Once a resistor and a capacitor are placed in series, it is natural to end up with an impedance calculation as:

$$\mathrm{Z_{tot}} = \mathrm{Z_R} + \mathrm{Z_C} \tag{2.59}$$

The impedance representation is naturally:

$$\mathrm{Z_{tot}} = \mathrm{R} + \frac{1}{\mathrm{j\omega C}} \tag{2.60}$$

and its corresponding impedance representation in figure 2.19(a):

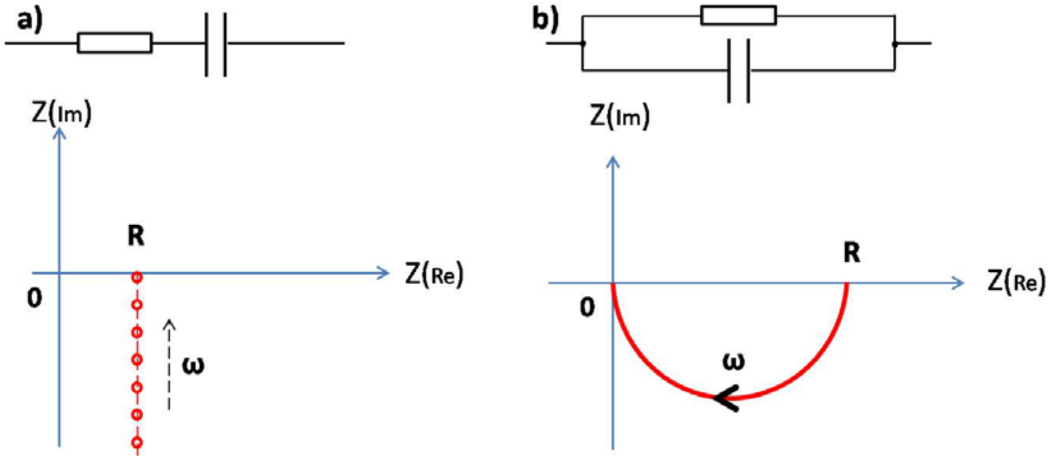

Figure 2.19 Impedance representations for the combination of resistor and capacitor

When they are placed in parallel, one can easily from the basics of impedance spectroscopy that only admittance of the two elements can be added directly. The expression is in 2.61 and equivalently presentenced in 2.62 as:

$$\mathrm{Y_{tot}} = \mathrm{Y_R} + \mathrm{Y_C} \tag{2.61}$$

$$\frac{1}{\mathrm{Z_{tot}}} = \frac{1}{\mathrm{Z_R}} + \frac{1}{\mathrm{Z_C}} \tag{2.62}$$

Therefore, the total impedance is calculated as:

$$Z = \left(\frac{1}{R} + j\omega C\right)^{-1} = R\left[\frac{1}{1+(\omega RC)^2}\right] - jR\left[\frac{\omega RC}{1+(\omega RC)^2}\right] \tag{2.63}$$

The expression in 2.63 was obtained by separating real part and imaginary part of the impedance. The product of RC is called time constant and it is usually written in letter τ=RC. The expression shows the same denominator for both real and imaginary part. After some math manipulation, it is readily found that:

$$\left(Z' - \frac{R}{2}\right)^2 + Z"^2 = \left(\frac{R}{2}\right)^2 \tag{2.64}$$

This is, as in figure 2.19(b), a semi-circle below the real axis, as Z” can only be found in the negative side of the imaginary axis. The imaginary part reaches its minimum when it is equivalent to the magnitude of the real part. At this particular point, the sweeping frequency is such that ωτ=1.

A similar situation can be found for the combination of inductor and resistor in parallel, as in figure 2.20.

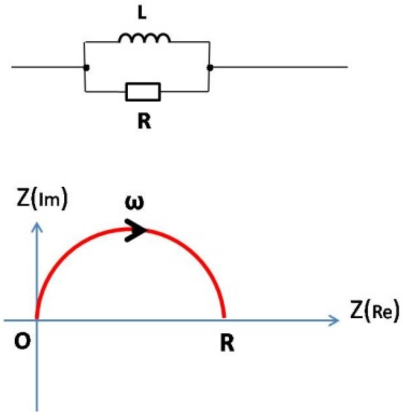

Figure 2.20 Impedance representations for the combination of inductor and resistor

By taking advantage of 2.26, the express of the total impedance in figure 2.20 is:

$$Z = (\frac{1}{R} + \frac{1}{j\omega L})^{-1} = \left(\frac{j\omega L + R}{Rj\omega L}\right)^{-1} = \frac{R\left(\omega\frac{L}{R}\right)^2 + j\omega L}{1+\left(\omega\frac{L}{R}\right)^2} = R\left[\frac{1}{1+\left(\omega\frac{L}{R}\right)^2}\right] + iR\left[\frac{\omega\frac{L}{R}}{1+\left(\omega\frac{L}{R}\right)^2}\right] \qquad (2.65)$$

Here, time constant τ becomes L/R and the minus sign in 2.63 has been replaced by a plus sign and this change manifests a semicircle above the real axis, where 2.64 still holds. Similarly, at the frequency when ωτ=1, Z(Im) reaches its maximum and it is equal to the value of Z(Re).

A possible ambiguity during the equivalent circuit analysis is that ordinary ideal circuit elements, such as the ones above, can only present ideal lumped-constant properties. In real cases, all electrolytic cells are distributed in space and their microscopic properties may be also independently distributed [78]. Consequently, ideal elements may not be able to adequately explain the electrical response. As a result, the real impedance obtained from Nyquist plot, cannot well approximated by the equivalent circuit involving only a finite number of ordinary lumped-constant elements. In this case, the use of distributed impedance elements is inevitable and the constant phase element (CPEs) is an example of one such system.

In addition to this concern, there is another serious potential issue regarding the equivalent circuit. An equivalent circuit involving multiple elements is commonly seen: a simple interface may involve as many as 10 elements at a time in real experiment. These elements can be rearranged in several ways resulting in the same impedance representation. The elements themselves that contributed to different systems undergo different physical processes and therefore at most only one of these models is correct. More specifically, there are circuits where the overall impedance or a section of it, Z_i, is arbitrary and may be composed of either ideal elements, distributed elements, or a combination of both types. The ultimate goal is to limit the number of possible combinations based on the physicochemical process of the system under study. In all, impedance spectroscopy is an experimental method that requires preliminary physical and experimentational understanding of the system.

3. Experimental Details

For the purpose of exploring the unknown surface conduction that is parallel to the polymer surface, various techniques were employed. In this part of thesis, experimental details will be included. It starts with how the testing sample is prepared and continues onto the Corona charging process. Following that, the details of measurement for the step-function impedance method is introduced, based on the theory developed in the literature review.

3.1. Sample preparation for impedance measurement

Each manufacturer of laser printer uses slightly different materials for the photoconductor, as discussed in literature. No matter what material they use, the systems of all photoconductors are similar: a solid solution of charge transporting material distributed in polymer matrix that provides mechanical strength. In this thesis, a commercially available example was adopted: a solid solution of polycarbonate (PC) and small molecule diphenylbenzidine (TPD) with 1:1 mass ratio. The chemical structure of TPD is in figure 3.1. The sample was physically transparent to light and it had a thickness of ~60 μm. The sample was washed by water and isopropyl alcohol (IPA) to remove any contaminate on the sample surface before use. It served the role of charge transport layer in the entire photoconductor system.

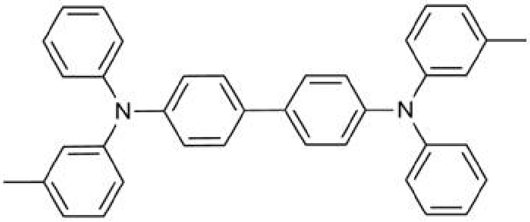

Figure 3.1 Chemical structure of TPD

In the preparation procedure, gold metal electrode was vacuum coated onto the photoconductor. The coating rate of at about 10 Angstrom per second was used to ensure proper adhesion. An interdigitated circuit was used to maximize the effective area of electrode. As seen in figure 3.2, the thickness of the electrode as well as the spacing between the electrodes was 1mm. The coated interdigitated circuit was used to increase the effective area between electrodes.

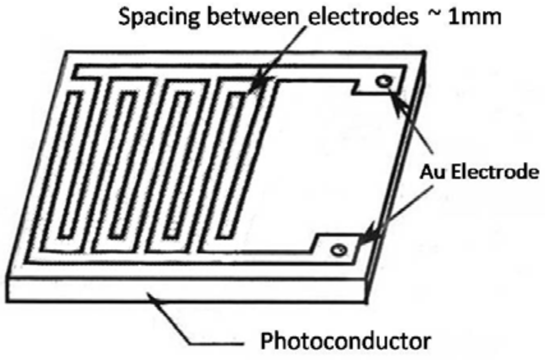

Figure 3.2 Metal electrode coated on the photoconductor

3.2. Corona charge set-up

As part of the Xerographic experimental process, negative electrostatic charge was deposited onto the photoconductor surface via Corona charging in a sealed box. The photoconductor was placed 1cm under the stretched metal for 30 minutes. The wire voltage and current were -5000 DC volt and 0.5 Ampere respectively via a HV power supply, as illustrated in figure 3.3.

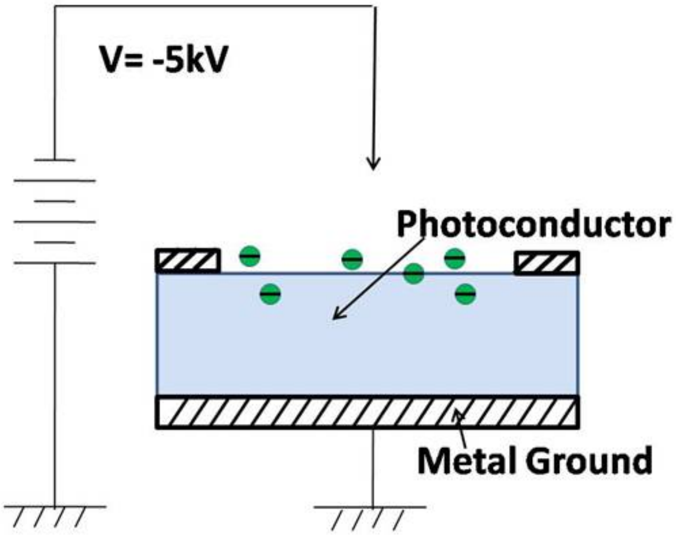

Figure 3.3 Corona charging of the photoconductor

3.3. AC impedance spectroscopy using DC step-function perturbation

Literature review shows that step-function perturbation signal is one type of the impedance spectroscopy. One may naturally question whether a step-function is theoretically identical to the well-known AC impedance spectroscopy. The following section will explore its similarity in theory and mathematically exam the perturbation signal and resulting electric response both in time and frequency domain to find out if it is the same as AC impedance spectroscopy.

3.3.1. Theoretical argument

Usually the i(t) relationship for any circuit is complicated. In other words, the diminishing current response gives divergent impedance in time domain and leaves no possibility to mathematically convert impedance into frequency domain. More precisely, the current signal in time domain reflects the history of the circuit, instead of the instantaneous response at infinitely small time interval. As a result, impedance cannot be obtained via integration of the response equations.

On the other hand, for a single frequency harmonic oscillation, both I(t) and V(t) will have to follow exp(iωt) in the steady state, where ω is angular sweeping frequency. At any frequency ω_0, the complex impedance $Z(\omega_0)$ can be obtained by $Z(\omega_0)= V(\omega_0)/I(\omega_0)$, without involving integration. By scanning the entire frequency spectrum, an impedance spectrum, Z(ω) is obtained for collective frequencies and gives accurate description of the unknown impedance. V(t) and I(t) can be treated as the sum of innumerable simple harmonic oscillations at variable angular frequencies. Thus V(t) will be decomposed into components at variable frequencies. Since a simple harmonic oscillatory voltage produces a simple harmonic current in the steady state, I(t) will be decomposed into variable frequency components as well. By using Fourier transform, V(t) and I(t) can be mathematically converted into V(ω) and I(ω), the variable frequency components. The impedance is finally solved by V(ω)/ I(ω).

3.3.2. Model construction

In order to test the equivalence between step-function impedance spectroscopy and AC impedance spectroscopy, a model consists of various circuit elements is established. Take the simplest case for example in figure 3.4, where an ideal capacitor and an ideal resistor are connected in series.

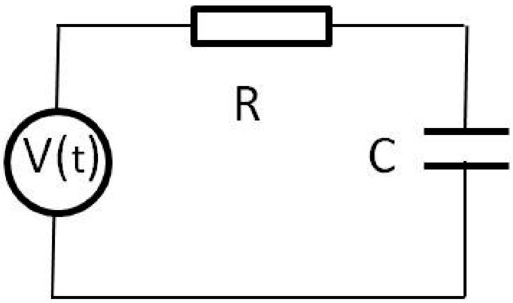

Figure 3. 4 Testing circuit for step-function impedance spectroscopy

The voltage source V(t) is used to simulate the step function perturbation therefore it has the form of:

$$V(t) = 0, t < 0; \tag{3.2}$$

$$V(t) = U, t \geq 0. \tag{3.3}$$

Due to the fact that the current going through each element is equal at all time, by applying Kirchhoff's current law, one can obtain:

$$C\frac{dV_C}{dt} = \frac{U - V_C}{R} = I \tag{3.4}$$

Where V_C denotes the voltage across the capacitor and I denotes current. By separating variables and solving the differential equation, the current is expressed:

$$I(t) = \frac{U}{R}\exp\left(\frac{-t}{RC}\right) \tag{3.5}$$

3.3.3. Fourier transform

Now that current and voltage are expressed in time domain, the next step is to transform them into frequency domain using Fourier transform. Fourier transform is by definition [80]:

$$F(\omega) = \mathcal{F}[f(t)] = \int_{-\infty}^{\infty} f(t)\exp(-j\omega t)\,dt \tag{3.6}$$

The symbol $\mathcal{F}$ in 3.6 denotes Fourier transform and ω denotes angular frequency. Therefore, perturbation voltage signal after t=0 becomes:

$$U(\omega) = \int_0^{\infty} U exp(-j\omega t)\, dt \tag{3.7}$$

The function exp(-jωt) is a periodic function that shows no convergence when time approaches infinity, therefore integration becomes impossible. However, by employing an infinitely small term δ into the expression, the problem is solved.

$$U(\omega) = U \int_0^{\infty} \lim_{\delta\to 0} \exp[(-j\omega - \delta)t]\, dt \tag{3.8}$$

We may take the limit outside the integration:

$$U(\omega) = U \lim_{\delta\to 0} \int_0^{\infty} \exp\,[(-j\,\omega - \delta)t] dt \tag{3.9}$$

$$U(\omega) = U \lim_{\delta\to 0} \frac{1}{-j\omega-\delta} \exp[(-j\omega - \delta)t]\,|_{t=0}^{t=\infty} \tag{3.10}$$

Finally, since δ is infinitely small,

$$U(\omega) = U \lim_{\delta\to 0} \frac{-1}{-j\omega-\delta} = \frac{U}{j\omega} \tag{3.11}$$

On the other side, current in time domain can be integrated using the same method:

$$I(\omega) = \int_0^{\infty} I(t) \exp(-j\omega t)\, dt = \int_0^{\infty} \frac{U}{R} \exp\,(\frac{-t}{RC} - j\omega t) dt \tag{3.12}$$

Following 3.12, one may change the differentiate element dt into d(-t/RC-jωt):

$$I(\omega) = \int_0^{\infty} \frac{U}{R\left(\frac{-1}{RC}-j\omega\right)} \exp\left(\frac{-t}{RC} - j\omega t\right) d(\frac{-t}{RC} - j\omega t) \tag{3.13}$$

The integration over changed variable ends up with:

$$I(\omega) = \frac{U}{R\left(\frac{-1}{RC}-j\omega\right)} \exp\left(\frac{-t}{RC} - j\omega t\right) |_{t=0}^{t=\infty} = \frac{U}{R\left(\frac{1}{RC}+j\omega\right)} \tag{3.14}$$

Now that we have the Fourier transformed result for both current and voltage in 3.14 and 3.11 respectively, their complex ratio gives the impedance in frequency domain as:

$$Z(\omega) = \frac{U(\omega)}{I(\omega)} = \frac{\frac{U}{j\omega}}{\frac{U}{R\left(\frac{1}{RC}+j\omega\right)}} = R + \frac{1}{j\omega C} \tag{3.15}$$

Recall from section 2.4.2 in literature that this expression is the same the impedance representation directly obtained from the circuit above. This equivalence comes from the physical process instead of a coincidence and the equivalence can be expanded to more complicated system if necessary.

As a preliminary conclusion, the step-function perturbation impedance spectroscopy is theoretically identical to AC impedance spectroscopy but only more convenient in some circumstances. Step-function impedance can be employed in the experiment process if needed, to replace AC impedance spectroscopy. More specifically, for dielectric material measurement, the system's impedance can be as high as several hundred GΩ. In this case, the predominant small amplitude AC signal coming from a commercial impedance machine may reveal very weak signal, too small (in the range of Femto Ampere) to be distinguished from background noise. The huge resistance as a result of dielectric material also gives rise to large time constant, AC impedance is not capable of revealing true impedance result as it requires a long time to sweep the entire frequency spectrum.

3.4. DC step-function perturbation design

The electrode coated on the surface, as in figure 3.5, is used to measure the surface conduction signal, instead of bulk reaction.

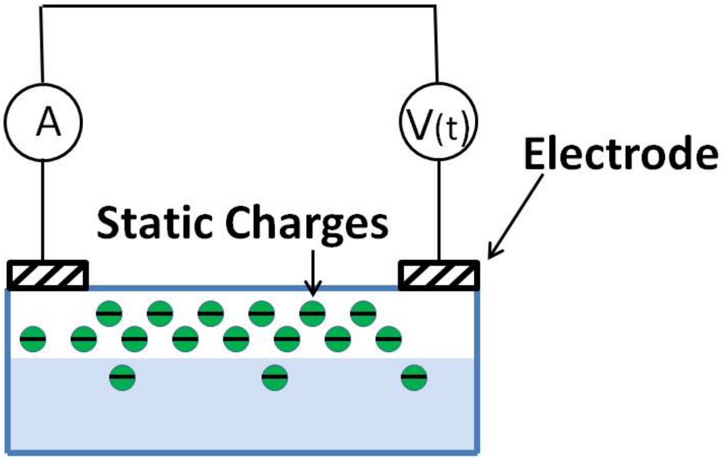

Figure 3. 5 Step-function perturbation measurements

The measurement is done in dark after removing the surface electrons. The sample was placed in high vacuum (2E-6 Torr), so as to vaporize any solid contaminant. The current signal was collected using DSA7000/B digital signal analyzer (Tektronix, USA).

The voltage perturbation signal is schematically as follows in figure 3.6:

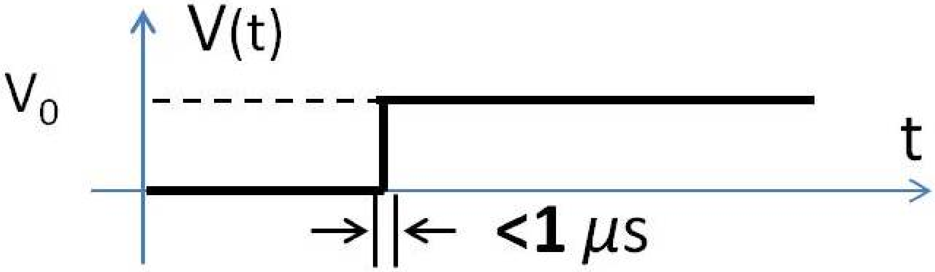

Figure 3. 6 Schematic of the step-function perturbation signal

The value of V_0 is set to be 400 Volts, for the purpose of magnifying the electric response signal from the dielectric material. The rising edge of the voltage source is so sharp that it is below 1 μs. It is not difficult to observe the relationship between the highest sweeping frequency and the lowest time step in the derivation from 3.7 to 3.11. The product of the rising edge sharpness and the highest frequency is unity and these two terms are closely interrelated by the

Fourier transform. A sharp rising edge results in a broader range on the frequency spectrum, which is desired for the experiment.

4. Results and Discussion

4.1. Problem of the unwanted surface conduction Confirmed

Few decades after the invention of photoconductor based photocopiers, many engineering and scientific issues have been solved step by step, based on the work devoted by engineers and deeper understanding of science behind photoconductors. In the 1980s, on the rapid growth of photocopier or laser printer market and fast pace in the research development, the long standing problem of image blurring became non-trivial: basically no progress had been made on the subject even though great research efforts have been invested. As a matter of fact, as of the late 80s, scientists had positively identified that the image blurring indeed came from the parallel movement of charge carrier near the bulk surface of charge transport layer (CTL). Yarmchuck in 1989 [67] and Keefe in 1991 [68] both confirmed this discovery. Afterwards, the research in this particularly area became stagnant, primarily due to the lack of investigative techniques. Only recently in 2007, Tokarski and his colleague [69] [79] confirmed that the parallel conduction is as a result of Corona charging by abrasion test.

4.1.1. Charge transport measurement

Charge transport behavior of the photoconductor was tested by sandwiching the polymer between two metal electrodes, as described by Tokarski [79]. The so-called time-of-flight (TOF) charge transport measurement is essentially the comparison of arbitrary photocurrent flow composed of electrons or holes. TOF is a well established technique that measures the time it takes for an electromagnetic particle or other wave to travel a distance through a specific medium. It is for the purpose of measuring velocity or path length through the given medium or to learn information about the particle/wave or medium itself. It is used in the industry of image reproduction as a technique to measure carrier motility in insulating materials. The photoconductor is sandwiched between two electrodes. The electrode on one side is a semi-transparent electrode and it is an ordinary metal electrode on the other side. A laser pulse bombards on the material through the semitransparent contact and creates a thin sheet of electron–hole pairs. Holes driven by the electric field move towards the other end of the photoconductor and create a photocurrent.

Increasing exposure in Tokarski's work [69][79] was found to give rise to decreasing transit time for photocurrent flowing through the CTL. This result suggested that the effect starts at the surface and penetrates into the bulk with increasing duration of exposure. This revealed the effect of Corona charging was similar to a diffusion process: as if some particles were diffusing into the layer and disrupting hole transport in CTL.

Further experiment showed that if the Corona charged CTL were rested in room temperature for as long as a week, the CTL regained its ability to transport holes as if it was a virgin sample. During the course of the week, the transport ability recovered gradually as if the substance that impeded hole transport had diffused out slowly into the atmosphere. It was also suggested to be a thermally activated process as the rate of recovery could be dramatically accelerated with a mild heat treatment at 50 to 70 Celsius. No further heat treatment was implemented as a temperature close to the glass transition temperature of the CTL T_g could cause complication to the measured results.

4.1.2. Corona affected surface of photoconductor

In the last step, Tokarski confirmed that negative Corona charging had altered the hole conduction in the CTL and its charge transport ability as a function of time exposure. In this particular case, one may ask whether the charge transport was altered in the bulk of the photoconductor or on the exposed surface only. Tokarski [69][79] compared the samples exposed to negative Corona with a successive abrasion test.

A similar TOF technique was adopted for charge transport measurement in this test. The normalized transit time indicates how long it took the current to travel through one miron (μm) of the CTL, in the direction perpendicular to the Corona charged surface. It was clear that when only a thin layer of CTL was removed, normalized transit time recovered for only a small amount, comparing with the fully charged sample. Furthermore, once the entire surface bulk (up to 6 micron) was abraded away, the transit time as a function of thickness returned to that of the virgin state. This gave evidence that the negative Corona not only affected the surface of the CTL, as predicted by theory in literature, but also influenced the top bulk region of the CTL (the abraded volume).

4.2. Nyquist plot of extra current due to the Corona charging

Results indicating extra current due to negative Corona charging will be illustrated in this section both in time domain, and in frequency domain after Fourier transform.

4.2.1. Extra current in time domain

A sample with and without negative Corona charging was measured, using the voltage step method described chapter 3. The current response is, as expected, recorded in time domain in figure 4.1.

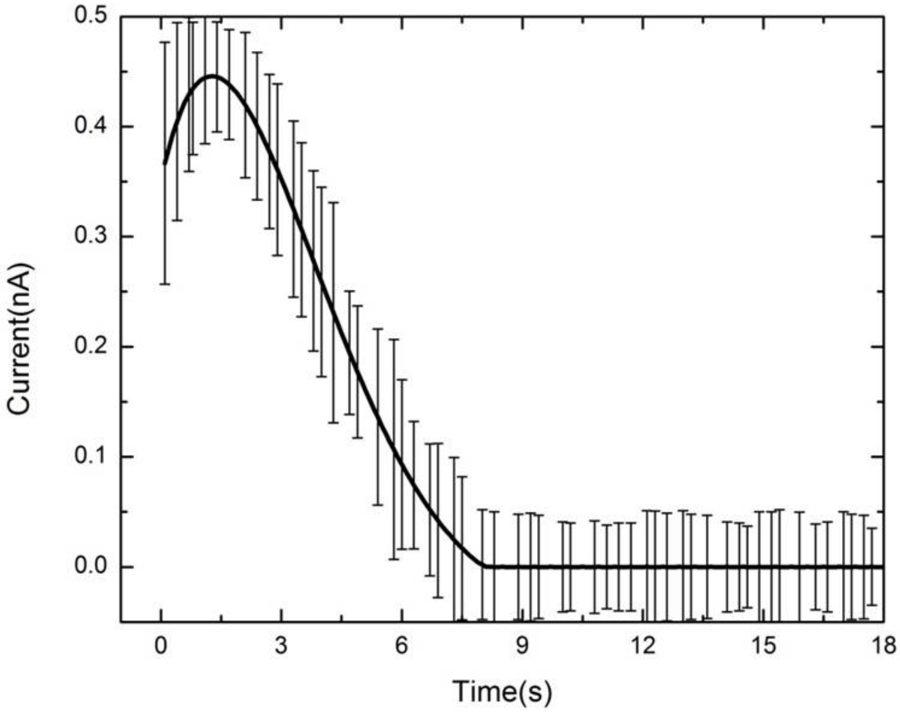

Figure 4. 1 Current response as a result of Corona Charging

The smoothed line in figure 4.1 represents the mean value of the measured data, and the error bar is to represent the overall distribution of the data. The seemingly large error is due to the fact that the current response is quite weak. The sub-nano Ampere signal is on the fringe of the effective range of the data-collecting device. Therefore, a large sample rate or more points taken in a period of time is ideal. The computer aided measurement is able to collect data point for every 0.002 second or 500 points/sec equivalently.

4.2.2. Fourier transformed result

The mean value of the measured data or the smoothed line is obtained as I(t) from figure 4.1 and the voltage signal, recall from chapter 3, is

$$V(t) = 0, t < 0; \tag{4.1}$$

$$V(t) = U, t \geq 0. \tag{4.2}$$

After Fourier transform, both voltage and current in time domain are converted into frequency domain:

$$U(\omega) = \int_0^\infty U(t) exp(-i\omega t)\, dt \tag{4.3}$$

$$I(\omega) = \int_0^\infty I(t) \exp(-i\omega t)\, dt \tag{4.4}$$

The resulting impedance, as a result of extra current caused by negative Corona charging is given as the complex ratio of 4.3 and 4.4:

$$Z(\omega) = \frac{U(\omega)}{I(\omega)} \tag{4.5}$$

The Nyquist plot of the extra impedance is given in figure 4.2

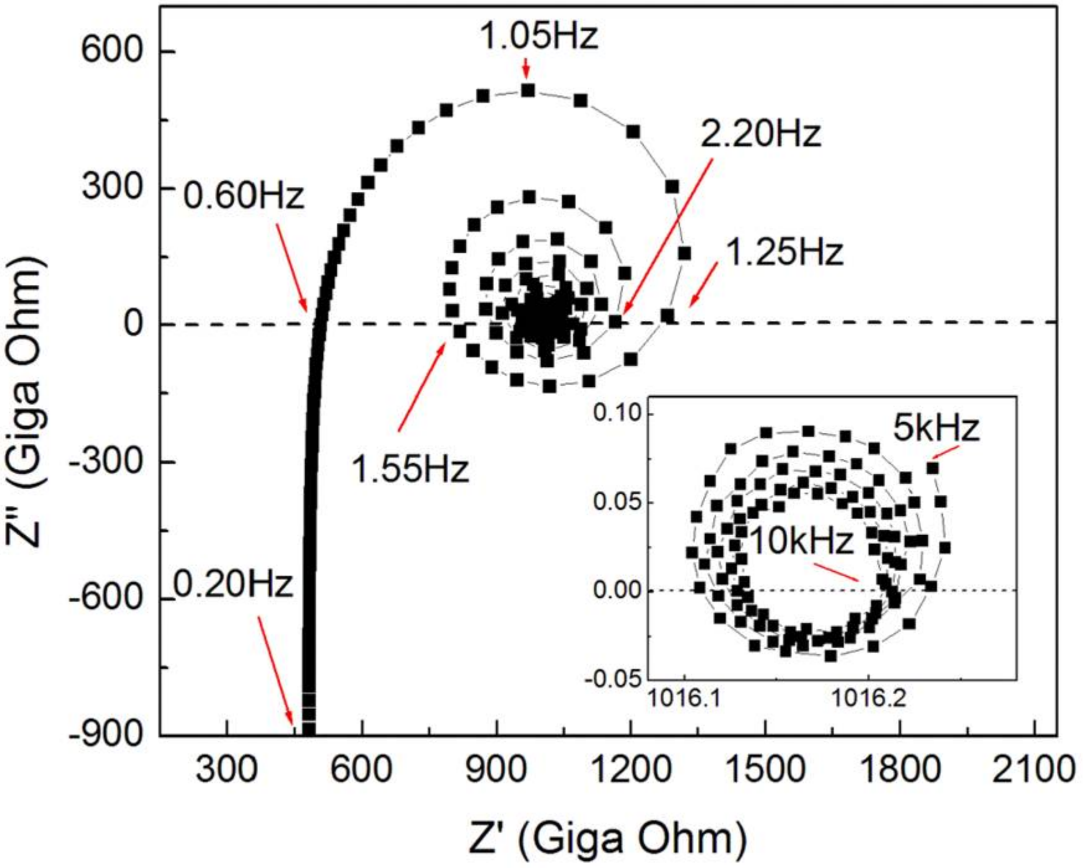

Figure 4. 2 Nyquist plot as a result of Corona Charging

It is clear from the Nyquist plot that, below the frequency of 0.6 Hz, it appears to be a pure capacitor: a straight line moving up with increasing frequency. The situation becomes complicated starting at 0.6 Hz and above. It shows a spiral with multiple turns. The figure moves above and below the real axis and gradually diminishes on the real axis at a point of about 950 GΩ. The spiral is indeed composed of diminishing semi-circles with various diameters on the real axis. The semi-circles revolve in both the upper and lower halves of the complex plane. This observation is surprising as in a Nyquist plot, only inductors can form semi-circle with the presence of resistors on the positive side of the imaginary plane.

4.3. Mysterious inductor-physically impossible

An inductor is a circuit element that stores energy in its magnetic field. It is usually made of metal wire wound into a coil. When the current flow through an inductor varies, the rate of current change is proportional to the time-varying magnetic field created inside the coil. According to Faraday’s law of electromagnetic induction, the current induced magnetic field always opposes the change in current.

4.3.1. Equivalent circuit analysis

The given Nyquist plot requires information in an equivalent circuit to understand the physics behind it. Adopted from figure 2.19b and 2.20, a resistor in parallel with a capacitor or inductor can form a semi-circle, respectively below and above the real axis. When these two circumstances are combined, namely if a capacitor, an inductor and a resistor are in parallel with each other, the following impedance plot is obtained in figure 4.3.

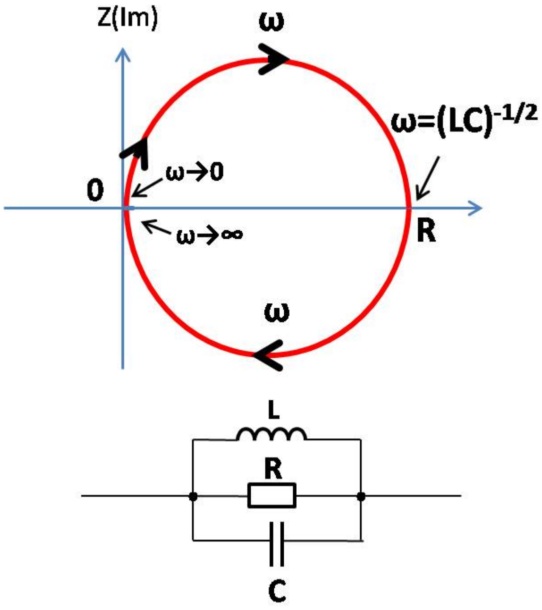

Figure 4. 3 Impedance representation of R, C and L

A complete circle is obtained on the right hand side of the imaginary axis. Starting from the origin at zero Hertz, the circle moves clock-wise with increasing frequency and returns to the origin as frequency goes to infinity. At the half of the journey, more specifically when the circle intercepts with the real axis away from the origin, the imaginary parts of the inductor and capacitor cancel each other and the real part of the impedance reaches the maximum. The total admittance and impedance of circuit in 4.7 are written as:

$$\mathrm{Y_{tot}} = \mathrm{Y_R} + \mathrm{Y_C} + \mathrm{Y_L} \tag{4.6}$$

$$\frac{1}{\mathrm{Z_{tot}}} = \frac{1}{\mathrm{Z_R}} + \frac{1}{\mathrm{Z_C}} + \frac{1}{\mathrm{Z_L}} \tag{4.7}$$

By expressing inductor and capacitor individually:

$$\frac{1}{\mathrm{Z_{tot}}} = \frac{1}{\mathrm{R}} + \mathrm{j\omega C} + \frac{1}{\mathrm{j\omega L}} \tag{4.8}$$

$\mathrm{Z_{tot}}$ is therefore a function of ω, it shows pure resistive behavior when:

$$\mathrm{j\omega C} = -\frac{1}{\mathrm{j\omega L}} \tag{4.9}$$

or:

$$\omega = \frac{1}{\sqrt{\mathrm{LC}}} \tag{4.10}$$

This is called the resonance frequency, defined as the frequency at which the impedance is purely real. Energy in this circuit is stored either in an electric field as the capacitor is charged or in the magnetic field as the current flows through the inductor. More specifically, energy is transferred from one form to another. The mechanical analogy of such a resonator is a suspended gravity pendulum. Without friction or air drag, it will oscillate about the equilibrium position and swing back and forth at constant amplitude. Energy is stored at equilibrium position as kinetic energy completely transferred into potential energy when it swings to the highest point.

As seen in figure 4.4, it is clear that the inductor dominates the overall impedance at low frequency while capacitor dominates the overall impedance at high frequency. Similar to a single resistor-capacitor or resistor-inductor system, when the imaginary part of the impedance reaches a minimum or maximum, the characteristic frequency relationship such that $\omega\tau=1$ is still valid. The moment Z_{Im} reaches its maximum, its corresponding angular frequency becomes:

$$\omega_L = \frac{R}{L} \tag{4.11}$$

Equivalently, the moment Z_{Im} reaches its minimum, its corresponding angular frequency becomes:

$$\omega_C = \frac{1}{RC} \tag{4.12}$$

The complete circle in figure 4.3 resembles a single turn in the measured Nyquist plot, if the lower semicircle has a smaller diameter. Experimentally, if another resistor is inserted in series with the capacitor, a smaller semicircle is obtained below the real axis. The two distinguished semicircles constitute a single turn in a spiral, as in figure 4.4.

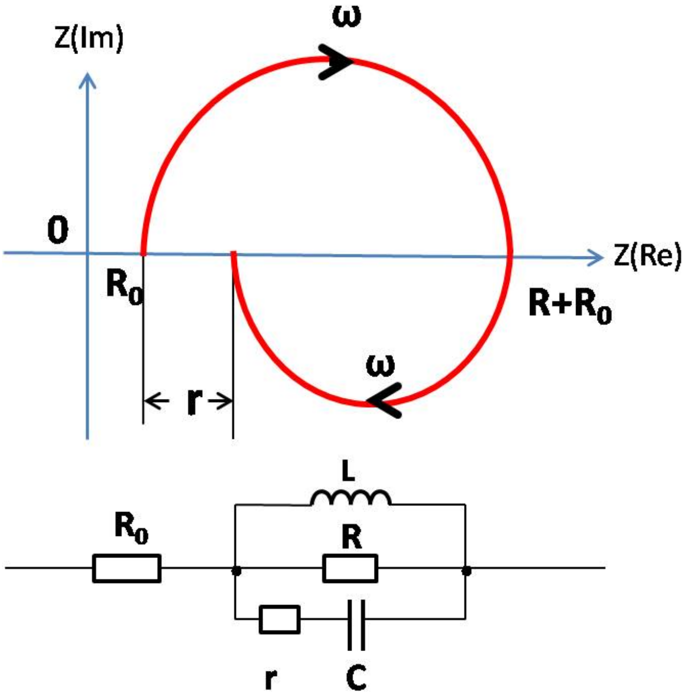

Figure 4. 4 Impedance representation for a single term in a spiral

Initiating from point (R_0, 0), the curve in figure 4.4 revolves clock-wise and hits the real axis again at the point $R+R_0$. Physically, the equivalent circuit of the dielectric polymer is based on a resistor and a capacitor in parallel where the capacitor represents the charge accumulation process as a dielectric material and the resistor represents dielectric loss.

In the case of the repeated units of such combinations from figure 4.4, figure 4.5 is obtained. Apart from the inductors in the equivalent circuit, the circuit itself seems to provide a reasonable physical picture for a photoconductor. It is likely that there are distributed units of resistor-capacitor within the bulk of the dielectric.

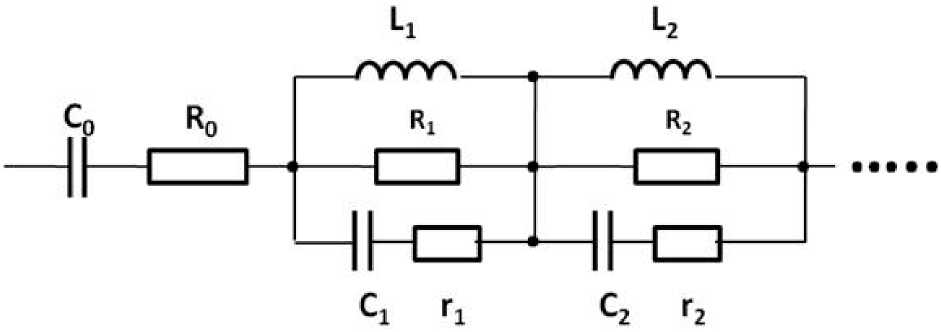

Figure 4. 5 Equivalent circuit that constitutes spiral

Due to the nature of a series circuit, when swept under various frequencies, each R-L-C-r unit is “excited” when reaching its own characteristic resonance frequency, and therefore produces a spiral for the overall impedance. The spiral can then be obtained by many resonant R-L-C-r loops connected in series, where the impedance of each loop peaks at its resonant frequency. At all frequencies other than its resonance frequencies, each of the R-L-C loops may be regarded as a short cut.

The only odd situation comes from the presence of the inductors, a circuit element often made of a metal coil, which are impossible to exist in a piece of thin dielectric polymer. This is to conclude qualitatively that the traditional inductor is physically unlikely in the equivalent circuit of dielectric materials.

Qualitatively, following figure 4.4, each element in the circuit can be found through data fitting. The values are listed in table 4.1 below for the first two R-L-C-r units:

R_o	488 GΩ	L_1	**715 GH**	L_2	**19.8 GH**
		R_1	1200 GΩ	R_2	590 GΩ
C_o	21.9 pF	C_1	0.94 pF	C_2	0.112 pF
		r_1	332 GΩ	r_2	190 GΩ

Table 4. 1 Values of each element obtained through data fitting

The values of resistors and capacitors are within one's expectation for a regular dielectric material, huge resistance as well as tiny capacitance. The numbers in bold are surprising, since there is certainly no magnetic coil here, not to mention the incredible large unit of hundreds of Giga Henry.

4.3.2. Working mechanism of an inductor

An inductor is capable of not only storing energy in its magnetic field, but also changing the shape of current/voltage wave, due to its ability to delay and reshape AC current. The typical current voltage response is plotted in figure 4.6.

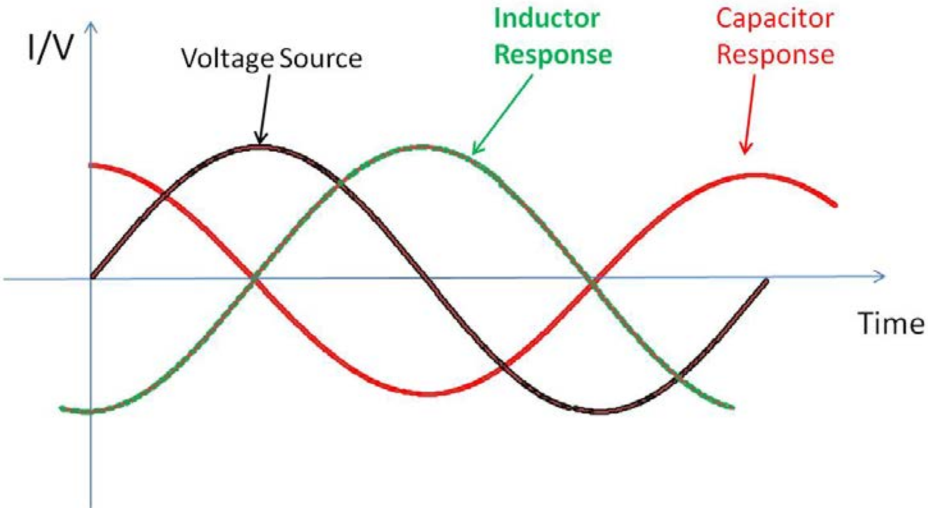

Figure 4. 6 Characteristic response of inductor and capacitor

The inductor response is always behind the voltage source signal by a phase difference of π/4. The unlikely inductor found in the equivalent circuit of figure 4.5 lags the sweeping signal also by π/4, otherwise no semicircle above the real axis is in the Nyquist plot. The lag mathematically corresponds to the imaginary unit j in its impedance expression of Z_L=jωL.

In the opposite case for a capacitor, its current response always leads the voltage signal by π/4 and that is verified by the imaginary unit j in the denominator of Z_C=1/jωC.

The resonance frequencies of the measured result take place at 1.25Hz and 2.2 Hz for the first two R-L-C-r units respectively. Huge inductors must be present to fulfill such low resonance frequencies. Geometrically, it is again concluded that the inductor suggested on the Nyquist plot is not real.

4.4. Similar inductor found in other areas –A long-standing problem

It is not the first time that this mysterious inductor is found or questioned. Even in the fundamental book written by Barsoukov and Macdonald [78], inductance behaviors were also observed. They admitted that a low frequency inductive response was of considerable theoretical and experimental interest as fourth quadrant behavior was observed experimentally. They took the example from Keddam et al. [81] such that, on increasing the potential through an active-to-passive transition, an inductive semi-circle was formed. They believed that the origin of the inductive behavior was due to an adsorbed intermediate caused by the potential increase. Epelboin et al. [82] had a different view and believed it was caused by the coupling between mass transfer and a surface reaction. In this fundamental book, Gohr's [83] theory of relaxation impedance was also mentioned where it was used to describe the surface relaxation of the interface. The theory of relaxation impedance itself was too weak to be applied to other systems that eliminated the presence of interface relaxation. One such example was provided by Muller [84], who also showed the so-called “pseudoinductive behavior” in the low frequency range. Last but not least, the book introduced another example of Liu’s study [85] on a Pt-Ru anode, where an inductive loop in the low frequency range was also found. Various points of view had been given in the book with no critical judgment provided. Each theory can more or less explain the existence of an inductive behavior or “pseudo-inductor” by introducing surface adsorption or a transient effect associated with mass transfer (such as diffusion). Nevertheless, no universal solution has been proposed or discussed.

The examples above rely mainly on the theory of impedance spectroscopy while experimental examples below will put more weight on individual electrochemical processes.

4.4.1. Inductive loop found in corrosion science

Impedance spectroscopy is widely used to study the interface behavior during corrosion therefore inductance behavior can be often found in this area. As an example, Bechet et al. [86] in 1977 studied the anodic dissolution of iron in acidic medium by measuring the interface impedance at various current densities or the pH. The impedance was found to be inductive at lower current density and at low frequencies. Bechet believed that it was related to the mechanism of $(FeOH)_{ads}$ adsorption occurring on the electrode. This paper didn’t provide too much information on explaining the origin of the inductance.

Bessone et al. in 1992 [87] studied the formation of Aluminum passive film at low frequency range using IS method. The diffusion controlled process within the oxide film was responsible for the EIS spectra observed and an inductive arc was observed at low frequencies. Bessone believed that it could be ascribed to surface area modulation or salt film property modulations, for example associated with changes in density, ionic conductivity or thickness. Coincidently, he also raised the possibility of another cause: relaxation of an adsorbed intermediate species. He admitted, in agreement with colleagues in this area, that the origin of the inductive loop needed further study.

Baril et al. in 2007 [14] studied the corrosion of Magnesium in sodium sulphate solutions with a rotating disc electrode. The anodic dissolution behavior of Magnesium was measured using impedance spectroscopy. The resulting impedance diagram was characterized by two well defined capacitive loops at high and medium frequencies. Unexpectedly, an inductive loop was found in the low frequency range (less than 1 Hz). On discussing the origin of the inductor, he agreed with Bechet's [86] idea and suggested it may be due to the existence of relaxation process of adsorbed species on the electrode surface.

Above are a few examples in corrosion study, most studies treated the inductive behavior as a side effect and didn't put much emphasis on it in their discussion. The majority of the explanation was based on surface absorption, but no detailed mechanism or proof was given. As a preliminary conclusion for the inductive behavior in corrosion study, no conclusive answer has been proposed.

4.4.2. Inductive loop found in conducting polymer research

Ionic conduction in conductive film is usually studied using impedance spectroscopy. As an example in 2001, Chen et al. [16] investigated the inductive behavior found on a Polyaniline (PANI) film electrodeposited in HCl medium. The author asserted that the Redox reaction involving unstable intermediate species coupled with electrochemical reaction in PANI caused a competing reaction sequence. This can result in an inductive behavior. The author for the first time proposed an inductor in the equivalent circuit of PANI film and suggested that the inductor’s presence was probably due to the contribution of the faradaic pseudocapacitance of the polymer film. His argument was based on the fact that PANI behaves close to a capacitor in the highly positive potential range. The paper provided an insight on a complicated polymer system under various sweeping frequencies based on sufficient experimental experience. Still, the proposed answer couldn’t explain how the proposed reaction could possibly resemble inductive behavior.

As another example, the characteristic impedance response of a Nafion membrane in an operating polymer electrolyte fuel cell was investigated by Schneider et al. in 2008 [18]. Not surprisingly, the inductive loop was found again at low frequency region. Schneider proposed it was as a result of water hydration and dehydration. He believed that at quasi-steady state, namely sweep frequency ω is close 0, the hydration state is virtually identical to that at equilibrium state. However, towards higher frequencies, the hydration of the ionomer gradually couldn’t keep pace with AC current. The delayed hydration/dehydration of the ionomer induced an additional phase shift, which is responsible for the lag of current with respect to voltage. The argument provided a molecular image of the polymer chain at low frequency even though no other proof was given. As a matter of fact, water hydration and dehydration is not a necessary condition to trigger an inductive loop because they are found in other similar systems with no water. This attempt provided an insight for discovering the origin of the inductor but didn’t receive favorable comments in subsequent literature [88].

Similar to the discussion in corrosion science, results based on inductive behavior in conductive polymer also treated the physically unlikely phenomenon as a side effect. However, more recently in 2011, Nanda and his colleague [19] observed change of ion conductivity of a solid electrolyte exposed to Gamma radiation and found the inductive loop as a new feature. The author did a quick review on the comments of the inductive feature provided by other scientists. Gray [88] suspected that the inductive feature may be due to the peculiarities of the set-up or transient effects. Neyertz et al. [89] and Thomson et al. [90] suggested that the spirally coiled or zigzag polymer molecules may affect the path of charge carriers and induce a winding motion, which showed up as an inductor in the Nyquist plot. Nanda finally suggested that the complicated motion paths for charge carriers in the sample, associated with rough porous surface may have caused the inductor behavior.

In conclusion, no quantitative analysis has been done, relating the details of microstructure to the inductance observed. Researchers have provided various scenarios ranging from Redox reaction to water hydration. Nevertheless, some of them are able to explain the inductive behavior in their own systems, the debate is still continuing.

4.5. Possible explanation

The observation of an equivalent inductor in a Nyquist plot cannot be dismissed as an artifact as the phenomenon is found in multiple systems over a long period of time. When proposing the explanation for the physically impossible inductors, there are several necessary conditions to meet. Firstly, according to figure 4.2, the origin of the inductive behavior is associated with resonance behavior. In other words, energy in one form has to be transferred into another form back and forth continuously. Secondly, microstructure of the photoconductor polymer must have been affected so that the charge carrier motion has been altered. Thirdly, a delayed motion must be found in the explanation so as to mimic an inductive loop in a Nyquist plot.

4.5.1. Why quartz crystal resonator is not the explanation

Due to the structure and nature of the photoconductor system, metal coils are not present. A model for similar inductive behavior in a small size comparable to the one in our experiment is desired. The quartz crystal resonator becomes an ideal candidate as it is usually a very small, thin piece or wafer of cut quartz with the two parallel surfaces. Its geometrical resemblance as well as its characteristic resonance frequency makes it a possible explanation.

The resonator takes advantage of piezoelectric quartz crystal. When a voltage is applied to a thin piece of the quartz crystal, it begins to change shape, producing a characteristic known as the piezoelectric effect. When the field is removed, the crystal generates an electric field as it goes back to its original shape. As a consequence, the quartz crystal behaves as an element with an equivalent circuit that composed of an inductor, capacitor and resistor in figure 4.7.

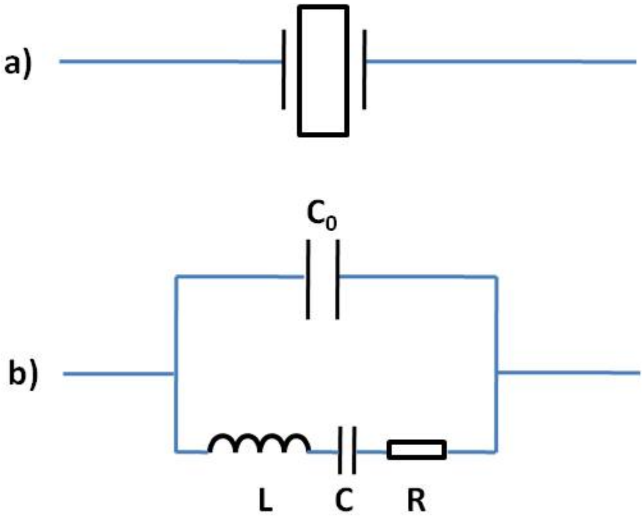

Figure 4. 7 Circuit representation and equivalent circuit for quartz resonator

Figure 4.7 a) illustrates the circuit presentation of a quartz resonator and part b) illustrates the equivalent circuit: a typical RLC series circuit. The RCL circuit is used to represent the mechanical vibration of the crystal, in parallel with C_0, which represents self capacitance of the crystal. The capacitor C in series with the inductor L and resistor R, physically indicates inertia, friction and stiffness of crystal. More often in real cases, C_0 is much larger than C so that only one resonance frequency is considered.

One of the most useful features from the crystal resonator is its frequency stability. It can provide a constant and accurate frequency output under varying loading conditions. The impedance of the circuit in figure 4.7 is given by:

$$\frac{1}{\mathrm{Ztot}} = (\mathrm{R} + \mathrm{j}\omega\mathrm{L} + \frac{1}{\mathrm{J}\omega\mathrm{C}})^{-1} + \mathrm{j}\omega\mathrm{C}_0 \tag{4.13}$$

Since C_0 is significantly larger than C, we may drop the term of $j\omega C_0$ and 4.13 become:

$$\mathrm{Z_{tot}} = \mathrm{R} + \mathrm{j}\omega\mathrm{L} + \frac{1}{\mathrm{j}\omega\mathrm{C}} \tag{4.14}$$

Z_{tot} is therefore a function of ω and shows pure resistive behavior when:

$$\mathrm{j}\omega\mathrm{C} = -\frac{1}{\mathrm{j}\omega\mathrm{L}} \tag{4.15}$$

or:

$$\omega = \frac{1}{\sqrt{\mathrm{LC}}} \tag{4.16}$$

At the resonance frequency, the impedance reaches its minimum below or above this frequency, energy is transformed back and forth between mechanical energy and electrical energy.

A typical quartz crystal resonator in the size of about 1 cm is in possession of a resonance frequency in Mega Hertz range, which is much higher than the resonance frequencies measured in figure 4.2. In a mechanical resonance such as the quartz crystal resonator, the frequency is proportional to the square root of the mass of the system [91]. Therefore, for the purpose of getting a resonance frequency at the range of 1 Hz, the mass of the quartz resonator is 10E12 times higher than the 1 cm resonator. Geometrically, the size of the resonator is in the range of 100 meter, which is physically impossible.

The quartz crystal resonator, whose equivalent circuit contains a non-physical inductor, provides a qualitative possibility to explain the origin of the huge inductor found in the photoconductor. However, after a quantitative estimation, it appears to be highly improbable.

4.6. Negative dielectric constant

As discussed in 4.3, capacitors are often found in the equivalent circuit of dielectric materials, for the purpose of simulating ideal capacitance using dielectric material. An ideal capacitor can be expressed as:

$$C = \varepsilon\frac{A}{d} = \varepsilon_0\varepsilon_r\frac{A}{d} \tag{4.17}$$

In 4,17, ε is used to denote dielectric constant or permittivity, it is the product of vacuum permittivity, ε_0 and relative dielectric constant ε_r. ε_0, also called vacuum dielectric constant, is a constant in the value of 8.85E-12 (Farad/m). It is the value of a capacitor with vacuum between its metal plates. The relative dielectric constant has no unit and it describes how many times of charge a capacitor can store relative to a vacuum capacitor, if a specific dielectric material is placed between metal plates. Letter A in 4.17 is the area of capacitor and d represents the spacing between metal plates. If the geometry for a capacitor is fixed, its capacitor value is only proportional to the relative dielectric constant, as all other terms are constants.

Additionally, the impedance representation, taken from equation 2.48, can be written as:

$$Z_C = \frac{1}{j\omega C} = \frac{j}{j * j\omega C} = (-1) * i * \frac{1}{\omega C} \tag{4.18}$$

Recall equation 2.50 where $Z_L = j\omega L$. Comparing it with 4.18 indicates that the only essential difference between an inductor and a capacitor in impedance representation is the negative sign, when frequency is fixed.

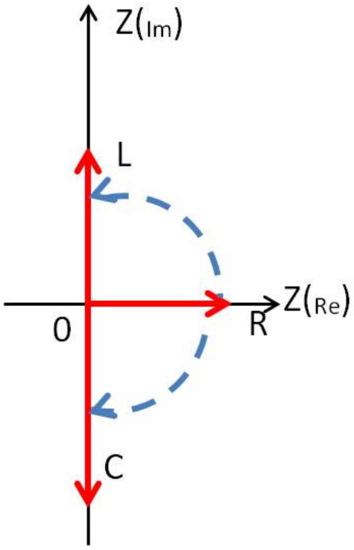

Figure 4. 8 Simplified impedance representation

This is consistent with impedance representation on the complex plane, as in figure 4.8. Capacitors alone take up the negative side of the imaginary axis while inductors are 180 degrees away. Mathematically, the imaginary unit j indicates a 90 degree rotation counter clock-wise on the complex plain since:

$$j = \exp\,(j * \frac{\pi}{2}) \tag{4.19}$$

If the relative dielectric constant is negative, a capacitor inserted with this special dielectric show the same impedance representation as an inductor. The change of sign eliminates the negative sign in equation 4.18, the only essential difference between an inductor and a capacitor.

The above argument is a qualitative estimate. Under quantitative consideration, the problem associated with the inductor is often found at low frequencies with huge value (Giga Henry magnitude measured from figure 4.2). If the previous argument about negative dielectric constant is valid, at low sweeping frequency, a capacitor in nano F with a negative dielectric constant will be able to explain the incredible magnitude. Now the question comes down to the mechanism of how the dielectric constant in a regular photoconductor dielectric material could possibly turn negative.

4.6.1. Previous work on negative dielectric constant

Negative dielectric constant has already been found in metal and plasma under certain conditions.

Plasma is a fourth fundamental state other than solid, liquid or gas. It can be achieved by either heating the gas or by strong electromagnetic field. Molecular bonds within the gas are dissociated and form a gas of charge particles, where both positive charge particles and negative particles are found. The presence of charged particles makes plasma a conductive medium so that it responds strongly to electromagnetic fields.

The model to derive negative dielectric constant is called Drude [92] model and it is usually derived based on metallic systems. Metal is considered to behave as a free gas of electrons interspersed with heavy positive nuclei. An important assumption is that electron-electron and electron-nuclei interactions are neglected, with the exception of random electron collisions with the nuclei. The model is a classical approach and electrons are treated as free and independent particles. We take advantage of Newton’s second law of motion such that:

$$ma = F \tag{4.20}$$

When applying the equation onto a single electron:

$$m_e \frac{d^2x}{dt^2} + m_e\gamma \frac{dx}{dt} = -eE(t) \tag{4.21}$$

The second derivative of distance "x" travelled with respect to time represents acceleration of an electron. Similarly, damping factor γ denotes the number of collisions per second between electrons and positive nuclei in the metal, in the unit of 1/s. The product of variation of position x, damping factor and mass of electron is also in the unit of Newton. On the right hand side of 4.21, the product of incident electric field E and basic charge e gives rise to the external force that facilitates electron motion. If the field is monochromatic, we have field and distance variation as:

$$m_e \frac{d^2x}{dt^2} + m_e\gamma \frac{dx}{dt} = -eE_0 \exp{(i\omega t)} \tag{4.22}$$

$$x(t) = x_0 \exp{(j\omega t)} \tag{4.23}$$

Using 4.23, 4.22 is solved by substitution:

$$x(t) = \frac{eE(t)}{m_e(\omega^2 - j\omega\gamma)} \tag{4.24}$$

The metal itself macroscopically maintain electrical neutrality and the displacement of electron x(t) may be considered as a dipole of charge e and length x(t). The overall polarization per unit volume caused by all diploes is:

$$P(t) = -Nex(t) \tag{4.25}$$

In 4.25, N is the number of electrons per unit volume and with the unit of 1/m^3.Similar to the relationship of electric displacement D, electric field E and total polarization P in a simple dielectric; one may use this definition to derive relative dielectric constant ε_r:

$$D(t) = \varepsilon_0 E(t) + P(t) = \varepsilon_0 E(t) - \frac{Ne^2}{m_e(\omega^2 - j\omega\gamma)} E(t) = \varepsilon_0 E(t)\varepsilon_r \tag{4.26}$$

$$\varepsilon_r(\omega) = 1 - \frac{\mathrm{Ne}^2}{\mathrm{m_e}\varepsilon_0(\omega^2 - j\omega\gamma)} = 1 - \frac{\omega_\mathrm{p}^2}{\omega^2 - j\omega\gamma} \tag{4.27}$$

Now the relative dielectric constant is a function of frequency and the so-called plasma frequency is defined:

$$\omega_p = \left(\frac{\mathrm{Ne}^2}{\mathrm{m_e}\varepsilon_0}\right)^{1/2} \tag{4.28}$$

On substituting electron mass, electron charge as well as electron density in metals, it is found that the plasma frequency for metal is very high, usually in the optical-UV range.

In a similar derivation for plasma system, the only difference is the absence of the damping factor. Therefore, the dielectric constant expression becomes:

$$\varepsilon_r(\omega) = \frac{\mathrm{Ne}^2}{\mathrm{m_e}\varepsilon_0\omega^2} = 1 - \frac{\omega_\mathrm{p}^2}{\omega^2} \tag{4.29}$$

For a plasma sample that with no imaginary part of the dielectric constant, plotting the equation 4.27 or 4.29 yields figure 4.9.

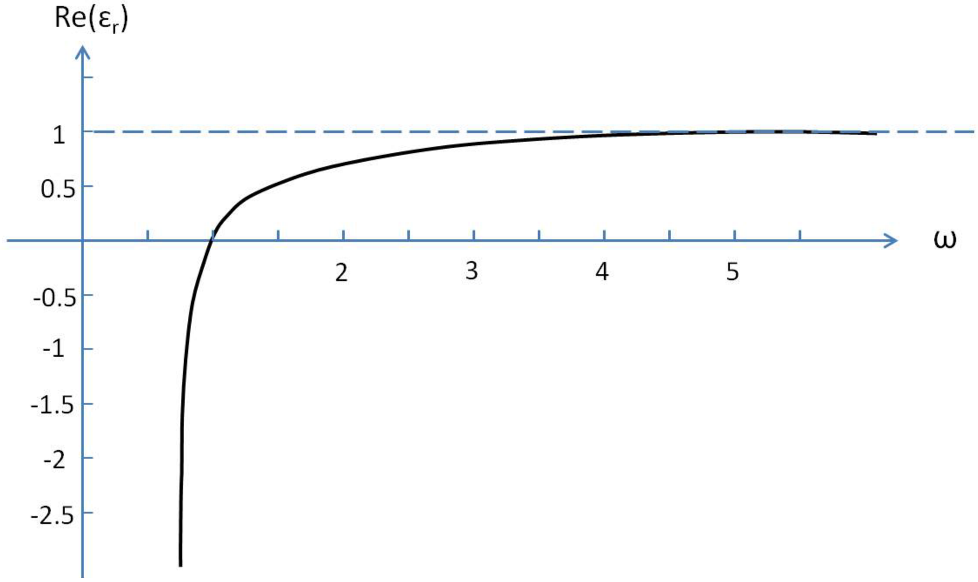

Figure 4. 9 Dielectric function as a function of normalized frequency

The frequency in figure 4.9 has been normalized to plasma frequency, for the purpose of making the x-intercept more intuitive. It is obvious from the figure that below the plasma frequency, the dielectric constant becomes negative.

When the applied alternating field is below the plasma frequency, the electron gas in the metal is displaced slightly with respect to the arrangement of positive ion. In this case, the so-called plasma oscillation or “Plasmon” takes place. The displaced electron gas produces a field that is opposite to the external field and thus a restoring force. The polarization caused by these displaced electrons is opposite to the direction of the electric field and corresponds to a negative relative dielectric constant. They oscillate back and forth at the plasma frequency until energy is consumed by damping. Plasmons are a quantization of such oscillation.

4.6.2. Modified polymeric structure with negative dielectric constant

Research interest has been paid to plasma systems due to their potentially revolutionary impact in energy research [93]. Negative dielectric constant research has also been expanded to other fields due to their possible revolutionary impact on electronics [94]. Much work has been done to address the fact that plasma frequencies for metal or plasma are too high for many desired applications. If negative dielectric constant can be achieved at low even zero frequency, electrons would be attracted to each other, offering new opportunities in physics and electronics.

Recently, scientists have focused on new and complex material systems and the examples of progress are illustrated here.

It has been proved that [95] the metal wire mesh structure is able to obtain negative dielectric with a plasma frequency near the microwave range. This significantly decreased plasma frequency and provided a possible route to achieve low frequency negative dielectric material.

In 2000, Smith et al.'s periodic array [96] of conducting split ring and continuous wires exhibited negative dielectric constant in microwave regime. Li et al. [97] in 2009 showed negative dielectric constant, based on polymer nanocomposites in the megahertz range. Wang et al. [98] in 2008 observed negative dielectric constant in the megahertz range based on $La_{0.8}Sr_{0.2}MnO_3$ /Nb-doped $SrTiO_3$ heterojunctions. Rahman et al. [99] found negative dielectric constant conducting polymer nanowires near the kilohertz range.

However, all systems above involve complicated material structure, sophisticated treatment or nano-structures. Negative dielectrics have been achieved by their special designed structure, rather than their compositions.

4.7. Model that shows negative dielectric constant in our system.

Ramakrishna [95] predicted that negative dielectric constant could be found in more ordinary systems then those listed above. Specifically he predicted the occurrence in dielectric media with bound charges. He also suggested in the predicted system, that the Drude form of plasma could be obtained, as a result of the bound electrons' restoring force.

With this in mind, by revisiting the treatment of the photoconductor discussed earlier in this chapter, a description of the process is obtained.

Under high voltage up to 5KV, Corona charging can ionized the air in its vicinity. Anions and electrons are accelerated by the electric field towards the photoconductor surface. Electrons have much higher charge/mass ratio and so are accelerated to a higher velocity than the ions. As a result, electrons can penetrate deeper into the bulk surface as has been verified by successive abrasion testing. The charges left over are those that penetrate deep (6 um for the deepest) into the photoconductor and become static charges. At this stage, the so-called electro-neutrality is not necessarily maintained and static charges in the bulk are found stable for several weeks, long enough for the following steps. The inductive behavior of the Nyquist plot is unexpected and the photoconductor shows no such inductor before Corona charging. Therefore the only possible origin of the inductor has to be the static charge "planted" during high voltage charging.

The static charges behave like plasma electrons in response to an oscillating electric field or the step-function perturbation signal. The static charge responds to the external field and oscillates at the position where it stays, similar to that in plasma or metal. The long-lasting static charges embedded in the dielectric are not often observed in other systems as they require a high voltage to "diffuse" into the photoconductor. Inside a laser printer, the dry and isolated environment helps to stabilize the electrons within the surface bulk of the photoconductor. Otherwise they are easily annihilated by humid air or by the high ambient temperature. Compared to the Drude model for negative dielectric constant of a plasma system, the static charge carriers are similar to the free electrons in plasma, but much lower density.

In a quantitative picture, recall plasma frequency $\omega_p=(Ne^2/m\varepsilon_0)^{-0.5}$ from 4.26 and from 4.29 the relative dielectric constant is:

$$\varepsilon_r(\omega) = 1 - \frac{\omega_p^2}{\omega^2} \tag{4.30}$$

When ω is lower than ω_P, $-(\omega_P/\omega)$ is dominating ε_r and it is negative indeed [100].

$$(j\omega C')^{-1} = [j\omega(c' + c)]^{-1} \approx (j\omega c')^{-1} = (j\omega\varepsilon_r c_0)^{-1} \tag{4.31}$$

where c_0 represents vacuum capacitance in the unit of Farad and c is the normal capacitor of the insulating polymer, which can be dropped compared with c’. c’ is the capacitor as a result of the negative dielectric constant. When substituting 4.30 into 4.31,

$$(\mathrm{j}\omega\varepsilon_r\mathrm{c}_0)^{-1} \approx -(\mathrm{j}\omega c_0\frac{\omega_\mathrm{p}^2}{\omega^2})^{-1} = \mathrm{j}\omega(\mathrm{c}_0\omega_\mathrm{p}^2)^{-1} = \mathrm{j}\omega\mathrm{L} \qquad (4.32)$$

Finally, an “inductor” is created from the negative dielectric constant capacitor caused by static electricity in 4.32 and 4.33. It is obvious that the inductor value is only a function of plasma frequency

$$L \approx \frac{1}{c(\omega_p)^2} \qquad (4.33)$$

This unusual capacitor must be located within the part of the sample containing static charge near the surface bulk. The capacitor with negative dielectric constant has to be aligned parallel with the rest of the sample, which is not influenced by static charge. The overall picture becomes the one in figure 4.10:

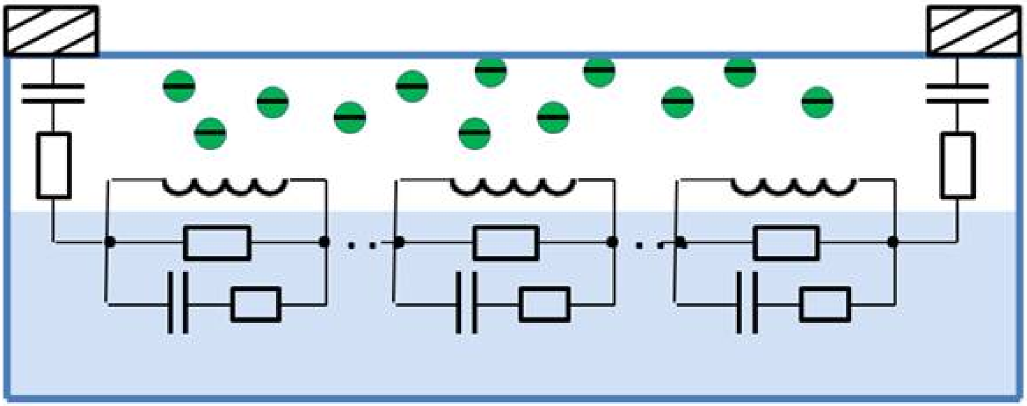

Figure 4. 10 An overall picture of the charged sample photoconductor

Between two metal electrodes coated on far ends of the photoconductor, many slices of the sample are formed in line within the surface bulk. Within each slice, the top part with static charge forms an “inductor” by the negative dielectric constant. The top part is connected in parallel with the bottom part, which still acts as a normal capacitor. Together they form “L”-R-C loops with various resonant frequencies and the resistors in parallel with them are those regular ones found in equivalent circuits of ordinary dielectrics. Due to the resonance nature of the series circuit, each slice is “excited” while reaching its resonance frequency, therefore producing a spiral for the overall impedance. It is clear from figure 4.2 that each “L”-R-C loop only responses in a very narrow frequency range and otherwise becomes “invisible” on Nyquist plot. In particular, those slices near the electrodes have lower static charge concentrations due to the presence of metal, therefore involving larger resistance and larger inductance. They are corresponded to the outer most circles of the spiral with lower resonance frequencies. The opposite is true for those far away from the electrodes, namely the middle section between two electrodes. They are related to the inner part of the spiral with lower higher resonance frequencies.

The resulting negative dielectric constant may also be explored by treating the whole sample as one capacitor.

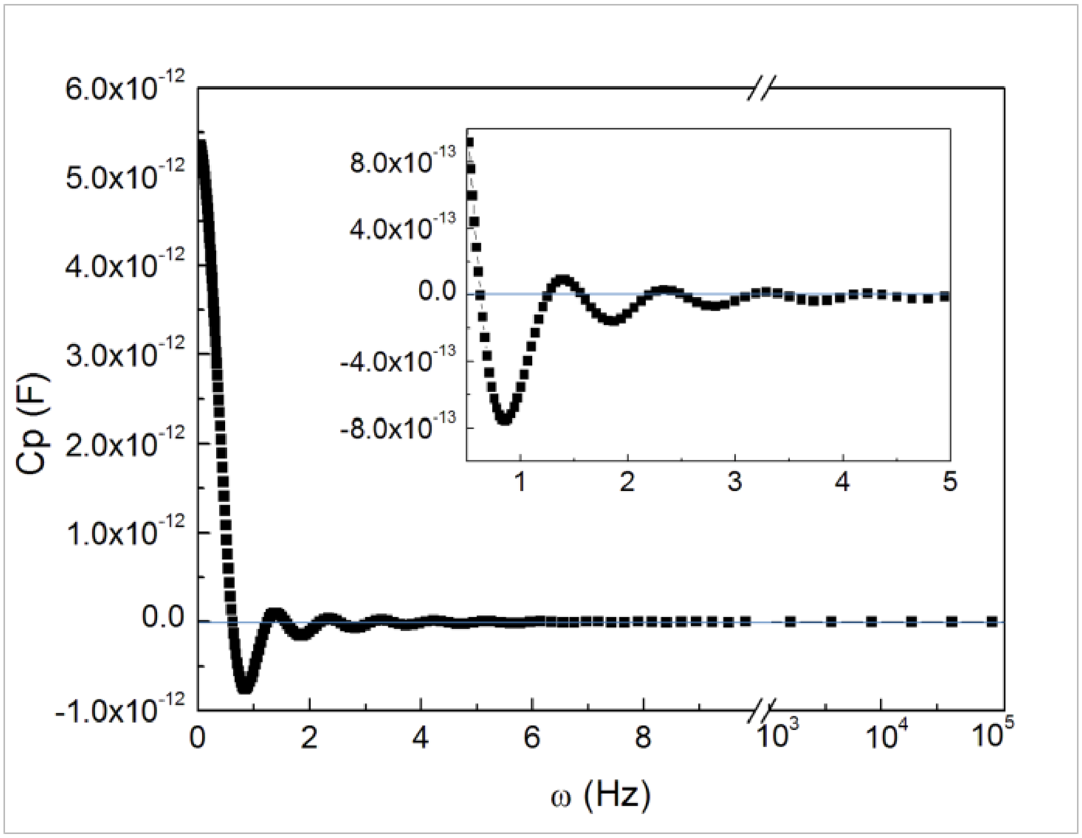

Figure 4. 11 Negative dielectric constant by treating the entire sample as a capacitor

As shown in the figure 4.11, the overall capacitance of the photoconductor is plotted in frequency domain and it is simply the projection of the values on imaginary axis in figure 4.2 against frequency. The overall capacitance oscillates and diminishes with an increasing angular frequency where the negative value only appears at certain frequency intervals. The positive and negative intervals are the reflections of the semicircles above and below the real axis in figure 4.2 respectively. They oscillating nature of overall capacitance is essentially caused by the resonance behavior of various “L”-R-C connected in series, as a result of static charge [100]. However, the exact values of the negative dielectric constants cannot be calculated by the ratio of the overall capacitance versus that of geometrical capacitor. It is simply because the overall behavior involves many such “L”-R-C loops connected in series. The unevenly distributed static charge directly results in unevenly distributed “inductors”, representing many “L”-R-C loops. Nevertheless it provides a qualitative overview of the overall sample response.

It is observed from figure 4.2 and figure 4.11 that at megahertz range, imaginary impedance are still showing diminishing oscillations. The negative dielectric constant appears from <1Hz to 1 MHz. Since the plasma frequency ω_p must be larger than ω, for the negative dielectric constant to occur, we may safely judge that ω_p must be larger than 1 MHz, but not much higher. By substituting all known constants into equation 4.26, it is estimated that the average charge density is around 10^4 cm^{-3}, for the region representing the outmost semi-circle.

Moreover, the variation of the static charge density is expected to affect the overall results through the change of the plasma frequencies. For example, samples with less amount of static charging would involve lower static charge density, thus smaller plasma frequencies, and higher L values and lower resonant frequencies. However, they would also give larger resistance, which may result in too weak a current to be detected. In the meantime, the negative static charges are expected to locate near the positive charges on the polymer structures [101]. This relationship can be seen in 4.33 by combining equation (4.28) and (4.33). The value for inductor is inversely proportional to the charge density.

$$L \approx \frac{m_e \varepsilon_0}{cNe^2} \tag{4.34}$$

Their lifetime is intimately related to the thermal agitation and other conduction mechanisms. Additionally, the static charges diminish faster in humid air as the water molecules make the air more conductive. For example, a longer lifetime may be obtained in a low temperature and dry environment.

4.8. Explanation of NDC in photoconductor caused by static electricity

In a two-metal-plates model similar to that in figure 2.9, once the electric field D caused by free charge is applied onto the surface of the dielectric material, dipoles that were randomly orientated starts to reorient themselves and are gradually aligned so that the total polarization field P starts to increase. The process of reorientation takes time and that time measures the relaxation of the dielectric material.

After the polarized charge density P has reached its maximum, the difference between surface free charge density D and polarized charge density P reaches its minimum and it is called the total charge density $\varepsilon_0 E$. The relationship between D, $\varepsilon_0 E$ and P, expressed in equation (2.9) is not only valid in magnitude, but also they are in the same direction, as illustrated in figure 4.12.

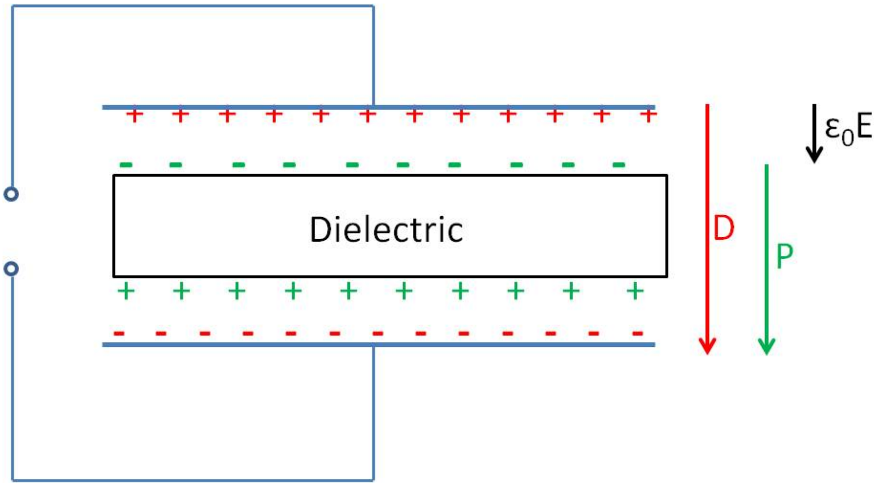

Figure 4. 12 Two-metal-plates model that shows D, P and E for regular dielectric material

The driving force and the only premise for dipole alignment is the total charge density $\varepsilon_0 E$ that caused an electric field. On the other hand, the recovery action within dipoles is the reversed effect that prevents the opposite ends of the dipoles from moving away too far from each other or getting perfectly aligned. After applying the external electric field, permanent dipoles are aligned along the electric field. When the field is removed, the recovery action, driven by entropy will make the dipoles go back to their original state: randomly oriented within the dielectric material. The situation is the same for induced dipoles. The recovery action brings the separated centers of positive charge and negative charge back to their positions when there is no electric field. The recovery action can be modeled by linking a spring to a small object in figure 4.13. The force F is used to simulate the total charge field $\varepsilon_0 E$ and the spring is used to mimic the action of the recovery.

Figure 4. 13 Recovery model that simulates dipole moment alignment

The moment the total electric field $\varepsilon_0 E$ reaches $1/\varepsilon_r$ times of that the field caused by the free charge density D, the driving force for alignment of dipoles comes to an end. In other words, the recovery action in dipoles is identical in magnitude to the attraction caused by the total field $\varepsilon_0 E$, albeit in reversed direction: a dynamic equilibrium is established within the dielectric material.

This is the situation for regular dielectric material where a recovery model is adopted to describe the force to keep the positive ends and negative ends from getting too far apart or getting completely aligned with the external field. However, the situation is slightly different from that in systems where free electrons instead of dipoles are found. The recovery model cannot be used in the presence of free electrons only. In Drude model for plasma, the electron-electron interaction is ignored during the application of external field and the only field that causes the electronic polarization is the total field $\varepsilon_0 E$ (often electromagnetic wave in sinusoidal form).

In our system where negative dielectric constant is realized by free static charge within the surface bulk of the dielectric material, the total field $\varepsilon_0 E$ is similar to that in plasma.

The analysis of negative dielectric constant under DC field can be treated within a period of an AC field with extremely low frequency. The cycle of the external AC field is so long that the free electron response can adequately reach the equilibrium state and the rate of change in external AC field is close to zero when discussing the flow of free electrons in the photoconductor.

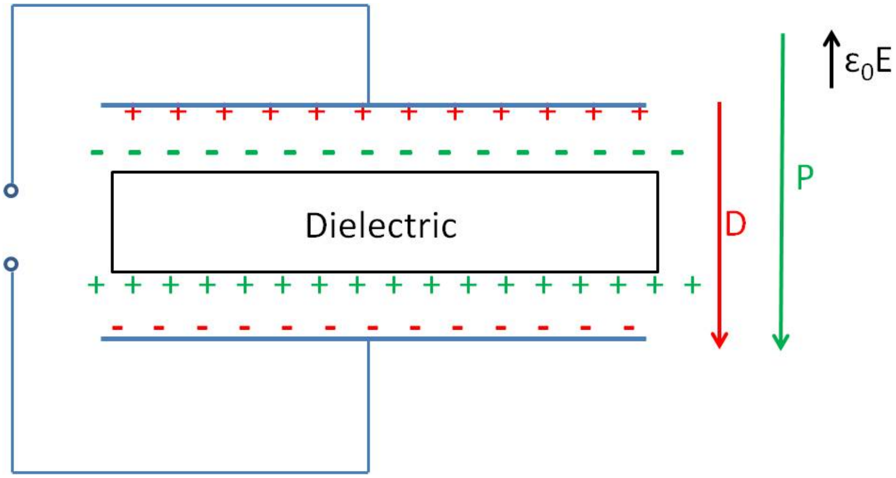

Figure 4. 14 Two-metal-plates model that shows D, P and E for negative dielectric material

In this particular case, the driving force for the growing of the polarized field is still the total field $\varepsilon_0 E$. Once the external field D is applied, the polarized field P starts to grow so that it gradually approaches the magnitude of the external field D. With the absence of recovery action, although the driving force $\varepsilon_0 E$ is getting smaller and smaller, the growth of polarized field P will continue as a result of inertia, even when P is equal to the external field D. As in figure 4.14, the polarized field P keeps growing sluggishly so that the total electric field $\varepsilon_0 E$ starts to reverse its direction and the negative dielectric constant begins to show its "negative" essence commencing this moment. The polarized field P grows to the ultimate value: that the total field $\varepsilon_0 E$, in magnitude, is $1/\varepsilon_r$ times as big as the field D. This is similar to that in a regular dielectric material, only a total field $\varepsilon_0 E$ with reversed direction is found.

In all, the value of the dielectric constant changes as a function of time and its value is schematically illustrated in figure 4.15.

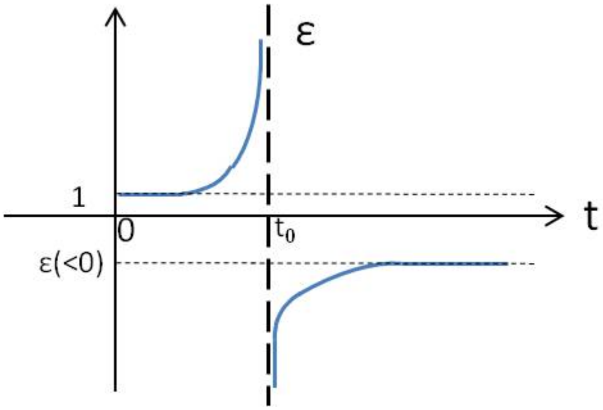

Figure 4. 15 Dielectric constant as a function of time during polarization

At time t=0, when the field D caused by free charge is just applied with no polarization occurring, the dielectric constant is 1. It increases rapidly and mathematically goes to infinity when the magnitude of polarized charge density P approaches the free charge density D. At the exact moment $t=t_0$, when P is identical to D, the value of the dielectric constant is not defined. Similarly, when the polarized charge density P continues to grow and deviates from the free charge density D, the value of dielectric constant goes from negative infinity to an asymptotic line. The value of the asymptotic line exhibits the negative essence of the dielectric constant. In this particular case, the plain fact that the induced polarized field P exceeding the value of its premise, the external field D, seems to have violated the conservation of energy. As a matter of fact, the external field is supplied by external source and extra energy has been provided to the system constantly.

By adopting Drude model [102] to explain negative dielectric constant manifested by static electricity, the highest values of the distributed inductors seem to be invalid when considering equation (4.28). It is obvious that the vacuum dielectric constant ε_0 and electron charge e are constants and an extremely low charge density still couldn't adequately describe the measured low plasma frequencies. In this case, we image that the effective mass of electron is significantly magnified by its hopping motion. Static electrons in the surface bulk are not truly free. Their motion is influence by the total field $\varepsilon_0 E$ and could only move from one site to another through hopping. Hopping is a thermally activated process that has to overcome energy barriers. Their motion is much more difficult than that in metal or plasma: a gas of free electrons and ions. We may in this case conclude that the motion of static charge in a dielectric material gives rise to magnified effective mass of free electrons. The plasma frequencies are measured values and the ratio of charge density over effective mass of electron (N/m_e) can be calculated and treated as a whole. Due to the distributed nature, it seems difficult now to discuss charge density N and effective electron mass m_e separately.

5. Summary and Conclusion

5.1. Corona charge can cause dielectric constant to shift to negative

After Corona exposure, the unwanted surface conduction parallel to surface direction was found in the photoconductor, used as the charge transport layer in laser printers. The unfavorable behavior can cause image blurring thus result in rapid replacement of drums. Due to the nature of the dielectric material, high time constant and high resistance prevents the usual AC impedance analysis from investigating the origin of the unwanted surface conduction. We instead introduced step-function as the perturbation signal for impedance analysis and Fourier transformed the response signal. Consequently, physically impossible inductors were found in the Nyquist plot of the current transients for the samples treated with Corona charging. The thesis provided an experimental means to characterize the unwanted surface conduction using step-function impedance analysis.

5.2. Possible solutions to the long standing problem

The long standing problem of inductive behavior during impedance analysis could be dated back to the 70s and they were found in many research areas. Researchers have provided various explanations ranging from surface adsorption to water hydration, based on their specific systems. The theories provided by these researchers cannot universally explain the observed inductive behavior. More specifically, no quantitative analysis has been proposed, relating the details of microstructure to the inductance observed.

We related the Drude model in plasma to the photoconductor exposed to high voltage Corona charging. Aided with side evidence, we conclude that static charges “planted” in the top bulk of the photoconductor are the cause of physically impossible inductor.

The explanation will likely be expanded to other research areas where the long-standing problem of the mysterious inductor are also found, by considering charge carrier in those system with applied external electric field.

Additional to that, the understanding of negative dielectric constant of a simple dielectric material at low frequency may provide a possible revolution in electronics and photonics, where large inductors coils may be replaced by dielectric materials.

On a broader view, if negative dielectric constant can be realized at low even zero frequency, electrons would be attracted to each other instead of repulsion. This unordinary change would provide new opportunities in physics and electronics, such as high temperature superconductivity.

Reference:

[1] Mort, J. Xerography - a Study in Innovation and Economic Competitiveness. *Phys. Today* **47**, 32-38, (1994)

[2] Von Auer, L. and Trede, M. The dynamics of brand equity: a hedonic regression approach to the laser printer market. *J. Oper. Res. Soc.* **63**, 1351-1362, (2012).

[3] Thourson, T. L. Xerographic development processes: A review. *IEEE Trans. Electron. Dev.* **19**, 495-511, (1972).

[4] Duke, C. B., Noolandi, J. and Thieret, T. The surface science of Xerography. *Surf. Sci.* **500**, 1005-1023, (2002).

[5] Tabti, B., Dascalescu, L., Plopeanu, M., Antoniu, A. and Mekideche, M. Factors that influence the Corona charging of fibrous dielectric materials. *J. Electrostat.* **67**, 193-197, (2009).

[6] Louft, R. O., Hor, A. M., Hsiao, C. K., Baranyi, G. and Kazmaier, P. Organic photoconductive materials. *Pure Appl. Chem.* **60**, 1047-1054, (1988)

[7] Weiss, D. S. and Abkowitz, M. Advances in organic photoconductor technology. *Chem. Rev.* **110**, 479-526, (2010).

[8] Pai, D. M. and Springett, B. E. Physics of electrophotography. *Rev. Mod. Phys.* **65**, 163-211, (1993)

[9] Borsenberger, P. M. and Weiss, D. S. Organic Photoreceptors for Xerography, (Marcel Dekker: New York, 1998).

[10] Cole, K. S. and Baker, R. F. Longitudinal impedance of the squid giant axion. *J. Gen. Physiol.* **6**, 771-788, (1941).

[11] Erne, B. H. and Vanmaekelbergh, D. T. The low-frequency impedance of anodically dissolving semiconductor and metal electrodes - A common origin? *J. Electrochem.Soc.* **144**, 3385-3392, (1997).

[12] Rouquettesanchez, S. and Picard, G. Electrochemical Oxidation of a Metal Involving 2 Successive Charge-Transfer Steps with Adsorbed Intermediate Species .1. Theoretical

Expressions for the Steady-State Current Potential Curves. *Electrochim. Acta.* **38**, 487-493, (1993).

[13] Vanmaekelbergh, D. and Erne, B. H. Coupled partial ion-transfer steps in the anodic dissolution of metals. *J. Electrochem.Soc.***146**, 2488-2494, (1999).

[14] Baril, G. and Pebere, N. The corrosion of pure magnesium in aerated and deaerated sodium sulphate solutions. *Corros. Sci.* **43**, 471-484, (2001).

[15] Song, G. L. and Xu, Z. Q. Crystal orientation and electrochemical corrosion of polycrystalline Mg. *Corros. Sci.* **63**, 100-112, (2012).

[16] Chen, W. C., Wen, T. C., Hu, C. C. and Gopalan, A. Identification of inductive behavior for polyaniline via electrochemical impedance spectroscopy. *Electrochim. Acta*.**47**, 1305-1315, (2002).

[17] Chen, W. C., Wen, T. C. and Gopalan, A. Negative capacitance for polyaniline: an analysis via electrochemical impedance spectroscopy. *Synth. Met.* **128**, 179-189, (2002).

[18] Schneider, I. A., Bayer, M. H., Wokaun, A. and Scherer, G. G. Impedance response of the proton exchange membrane in polymer electrolyte fuel cells. *J. Electrochem.Soc.***155**, B783-B792, (2008).

[19] Nanda, P., Maity, S., Pandey, N., Ray, R., Thakur, A. K. and Tarafdar, S. Conductivity enhancement in polymer electrolytes on gamma irradiation. *Radiat. Phys. Chem.* **80**, 22-27, (2011).

[20] Roy, S. K. and Orazem, M. E. Error analysis of the impedance response of PEM fuel cells. *J. Electrochem.Soc.***154**, B883-B891, (2007).

[21] Le Canut, J. M., Latham, R., Merida, W. and Harrington, D. A. Impedance study of membrane dehydration and compression in proton exchange membrane fuel cells. *J. Power Sources*. **192**, 457-466, (2009).

[22] Schaffert, R. M. and Oughton, C. D. Xerography: a new principle of photography and graphic reproduction. *J. Opt. Soc. Am.* **38**, 991-998, (1948).

[23] Law, K. Y. Organic photoconductive materials – recent trends and developments. *Chem. Rev.* **93**, 449-486, (1993).

[24] Schaffert, R. M. A new high-sensitivity organic photoconductor for electrophotography. *IBM J. Res. Dev.* **15**, 75-59, (1971).

[25] Vahtra, U. and Wolter, R. F. Electrophotographic process in a high-speed printer. *IBM J. Res. Dev.* **22**, 34-39, (1978).

[26] Borsenberger, P. M. Mey, W. and Chowdry, A. Hole Transport in Binary Solid-Solutions of Triphenylamine and Bisphenol-a-Polycarbonate. *J. Appl. Phys.* **49**, 273-279, (1978).

[27] Pai, D. M. and Yanus, J. F. Layered photoconductors in electrophotography. *Photogr. Sci. Eng.* **27**, 14-19, (1983).

[28] Murayama, T. The design of high performance organic photoconductors. IS&T's NIP 17: International Conference on Digital Printing Technologies, 557-560, (2001).

[29] Whitten, P. G. and Brown, H. R. Polymer entanglement density and its influence on interfacial friction. *Phys. Rev. E.* **76**, 026101-025108, (2007).

[30] Kasap, S. and Capper, P. Handbook of electronic and photonic materials. (Springer: New York, 2007).

[31] Molaire, M. F. A semi-empirical model for dip coating: thickness and thickness uniformity control. IS&T's NIP 21: International Conference on Digital Printing Technologies, Final Program and Proceedings. 17-19, (2005).

[32] Oshikawa, Y., Utsunomiya, K., Takahashi, Y., Yoshida, S., Kita, E., Tsuda, K., Terai, J., Tanmaki, S., Kato, K. and Ishikawa, T. Ricoh SD-Development Technology and Pre-mix System for Image Quality. IS&T’s NIP 24: International Conference on Digital Printing Technologies, Technical Program and Proceedings. 329-332, (2008).

[33] Maruyama, Y. Charge-carrier mobilities in organic molecular-solids. *Mol. Cryst. Liq. Cryst.* **171**, 287-303, (1989).

[34] Shirota, Y. and Kageyama, H. Charge carrier transporting molecular materials and their applications in devices. *Chem. Rev.* **107**, 953-1010, (2007).

[35] Pai, D. M., Yanus, J. F. and Stolka, M. Trap-controlled hopping transport. *J. Phys. Chem.* **88**, 4714-4717, (1984).

[36] Stolka, M., Yanus, J. F. and Pai, D. M. Hole transport in solid-solutions of a diamine in polycarbonate. *J. Phys. Chem.* **88**, 4707-4714, (1984).

[37] Abkowitz, M. A. Studies of injection and transport in polymeric media: the connection to key issues in electrophotographic technology. *Synth. Met.* **141**, 29-37, (2004).

[38] Bassler, H. Localized states and electronic transport in single component organic-solids with diagonal disorder. *Phys. Status. Solidi. B.* **107**, 9-54, (1981).

[39] Abkowitz, M. A., Bassler, H. and Stolka, M. Common features in the transport behavior of diverse glassy solids-exploring the role of disorder. *Philos. Mag. B.* **63**, 201-220, (1991).

[40] Gill. W. D. Drift mobilities in amorphous charge-transfer complexes of trinitrofluorenone and poly-n-vinylcarbazole. *J. Appl. Phys.* **43**, 5033-5040, (1972).

[41] Abkowitz, M. A., Facci, J. S., Limburg, W. W. and yanus, J. F. Electronic Transport in a Model Tetraphenylbenzidine Main-Chain Polymer - Direct Comparison of Time-of-Flight Hole Drift Mobility and Electrochemical Determinations of Hole Diffusion. *Phys. Rev. B.* **46**, 6705-6717, (1992).

[42] Abkowitz, M. A. and Stolka, M. Electronic transport in sigma conjugated polymers. *Polym. Prepr.***31**, 254-255, (1990).

[43] Miller, R. D., Rabolt, J. R., Sooriyakumaran, R., Fickes, G. N., Farmer, B. L. and Kuzmany, H. Soluble polysilane derivatives: chemistry and spectroscopy. *Polym. Prepr.* **28**, 422-427, (1987).

[44] Hertel, D., Bassler, H., Scherf, U. and Horhold, H. H. Charge carrier transport in conjugated polymers. *J. Chem. Phys.* **110**, 9214-9222, (1999).

[45] Schein, L. B. Comparison of charge transport models in molecularly doped polymers. *Philos. Mag. B.* **65**, 795-810, (1992).

[46] Bassler, H. Nondispersive and Dispersive Transport in Random Organic Photoconductors. *Mol. Cryst. Liq. Cryst.* **252**, 11-21, (1994).

[47] Borsenberger, P. M., Magin, E. H., Vanderauweraer, M. and Deschryver, F. C. The role of disorder on charge-transport in molecularly doped polymers and related materials. Phys. Status Solidi. A. **140**, 9-47, (1993).

[48] Novikov, S. V. and Vannikov, A. V. Cluster structure in the distribution of the electrostatic potential in a lattice of randomly oriented dipoles. *J. Phys. Chem.* **99**, 14573-14576, (1995).

[49] Novikov, S. V., Dunla, D. H., Kenkre, V. M., Parris, P. E. and Vannikov, A. V. Essential role of correlations in governing charge transport in disordered organic materials. *Phys. Rev. Lett.* **81**, 4472-4475, (1998).

[50] Dunlap, D. H. Explanation for the root-e-dependent motilities of charge-transport in molecularly doped polymers. *Phys. Rev. B.* **52**, 939-954, (1995).

[51] Dunlap, D. H., Parris, P. E. and Kenkre, V. M. Charge-dipole model for the universal field dependence of motilities in molecularly doped polymers. *Phys. Rev. Lett.* **77**, 542-545, (1996).

[52] Young, R. H., Kung, T. M., Sinicropi, J. A., Rule, N. G., Fitzgerald, J. J. Eilers, J. E. Chen, C. H. and Boaz, N. W. Effect of group and net dipole moments on electron transport in molecularly doped polymers. *J. Phys. Chem.* **100**, 17923-17930, (1996).

[53] Young, R. H. and Fitzgerald, J. J. Effect of polar additives on charge-transport in a molecularly doped polymer - evaluation of disorder models. *J. Chem. Phys.* **102**, 9380-9391, (1995).

[54] Schein, L. B. and Tyutnev, A. The contribution of energetic disorder to charge transport in molecularly doped polymers. *J. Phys. Chem. C.* **112**, 7295-7308, (2008).

[55] Schein, L. B., Saenko, V., Pozhidaev, E. D., Tyutnev, A. and Weiss, D. S. Transient conductivity measurements in a molecular doped polymer over wide dynamic ranges. *J. Phys. Chem. C.* **113**, 1067-1073, (2009).

[56] Abkowitz, M. A. Electronic transport in polymers. *Philos. Mag. B.* **65**, 817-829, (1992).

[57] Schmidlin, F. W. Theory of trap-controlled transient photoconduction. *Phys. Rev. B.* **16**, 2362-2385, (1997).

[58] Abkowitz, M., Facci, J. S. and Stolka, M. Time-resolved space charge-limited injection in a trap-free glassy polymer. *Chem. Phys.* **177**, 783-792, (1993).

[59] Haridoss, S., Perlman, M. M. and Carlone, C. Vibrationally excited diatomic-molecules as charge injectors during Corona charging of polymer-films. *J. Appl. Phys.* **53**, 6106-6114, (1982).

[60] Shahin, M. M. Mass spectrometric studies of Corona discharges in air at atmospheric pressures. *J. Chem. Phys.* **45**, 2600-2605, (1966).

[61] Goldman, A. and Sigmond, R. S. Corona corrosion of aluminum in air. *J. Electrochem. Soc.* **132**, 2842-2853, (1985).

[62] Kawamoto, H. Modeling of ozone emission by a corotron used in electrophotography. *J. Imaging Sci. Technol.* **39**, 439-441, (1995).

[63] Kawamoto, H. Modeling of ozone formation by a contact charger roller. *J. Imaging Sci. Technol.* **39**, 267-271, (1995).

[64] Jiang, S., Huang, J. C. and Hoshino, Y. The effect of relative humidity on Corona discharge. IS&T's NIP23: International Conference on Digital Printing Technologies, Technical Programs and Proceedings. 56-60, (2007).

[65] Chen, I., Mort, J., Machonkin, M. A. and Larson, J. R. Degradation of electrographic images due to the surface lateral conduction. *J. Imaging Sci. Technol.* **40**, 431-435, (1996).

[66] Kobayashi, T., Saito, T., Aratani, S., Suzuki, S. and Iwayanagi, T. A mechanism for resolution decrease in organic photoconductors. *J. Imaging Sci. Technol.* **39**, 485-489, (1995).

[67] Yarmchuk, E. J. and Keefe, G. E. High-resolution surface-charge measurement on an organic photoconductor. *J. Appl. Phys.* **66**, 5435-5439, (1989).

[68] Yarmchuk, E. J. and Keefe, G. E. Motion of surface-charge on layered organic photoconductor. *J. Imaging Sci.* **35**, 231-234, (1991).

[69] Tokarski, Z., Ahn, Y. J., Gaidelis, V., Maldzius, R., Lozovksi, T. and Sidaravicius, J. Incremental charging method to elucidate the role of (+) trapped charges near the OPC surface in electrostatic image defect formation. IS&T's NIP 23: International Conference on Digital Printing Technologies, Technical Programs and Proceedings. 643-648, (2007).

[70] Endo, K., Miyaoka, S. and Katsuya, Y. IS&T’s NIP 20: International Conference on Advances in Non-Impact Printing Technologies Proceedings. 279-283, (1994).

[71] Kochelev, K. K., Tameev, A. R., Kocheleva, G. A., Kozlov, A. A., Kocheleva, O. K., Golovin, V. E. and Vannikov, A. V. IS&T’s NIP 14: International Conference on Digital Printing Technologies Proceedings. 524-530, (1998).

[72] Daintith, J. Biographical Encyclopedia of Scientists, (CRC Press: New York, 2009)

[73] McCrum, N. G., Read, B. E., and Williams, G. Anelastic and Dielectric Effect in Polymeric Solids. (Dover Publications: New York, 1967)

[74] Macdonald, J. R. Impedance spectroscopy. *Ann. Biomed. Eng.* **20**, 289-305, (1992).

[75] Cole, K. S. and Cole, R. H. Dispersion and absorption in dielectrics I. Alternating current characteristics. *J. Chem. Phys.* **9**, 341-351, (1941).

[76] Bonmassar, G., Iwaki, S., Goldmakher, G., Angelone, L. M., Belliveau, J. W. and Lev, M. H. On the Measurement of Electrical Impedance Spectroscopy (EIS) of the Human Head. *Int. J. Bioelectromagn.* **1**, 32-46, (2010).

[77] Metherall, P., Barber, D. C., Smallwood, R. H. and Brown, B. H. Three-dimensional electrical impedance tomography. *Nature* **380**, 509-512, (1996).

[78] Barsoukov, E. and Macdonald, J. R. Impedance spectroscopy theory, experiment, and application. 2nd ed (John Wiley & Sons: New Jersey, 2005)

[79] Tokarski, Z. and Ahn, Y, J. Charging characteristics of fatigued photoconductors. *J. Imaging. Soc. Jpn.* **47**, 494-500, (2008)

[80] Balcou, Y. The problem of calculating the fast-fourier transform of a step-like sampled function. *IEEE Trans. Instrum. Meas.* **28**, 97-99, (1979).

[81] Keddam, M., Lizee, J. F., Pallotta, C. and Takenouti, H. Electrochemical behavior of passive iron in aid-medium. 1. Impedance approach. *J. Eletrochem. Soc.* **131**, 2016-2024, (1984)

[82] Epelboin, I., Gabrielli, C., Keddam, M. and Tanenouti, H. A model of the anodic behaviour of iron in sulphuric acid medium. *Electrochim. Acta* **20**, 913-916, (1975).

[83] Gohr, H. Impedance modelling of porous electrode. *Electrochemical Applications* **1**, 2-3,(1997)

[84] Muller, J. T., Urban, P. M. and Holderich, W. F. Impedance studies on direct methanol fuel cell anodes. *J. Power Sources* **84**, 157-160, (1999).

[85] Liu, Y. C., Qiu, X. P., Zhu, W. T. and Wu, G. S. Impedance studies on mesocarbon microbeads supported Pt-Ru catalytic anode. *J. Power Sources* **114**, 10-14, (2003).

[86] Bechet, B., Epelboin, I. and Keddam, M. New data from impedance measurements concerning anodic dissolution of iron in acidic sulfuric media. *J. Electroanal. Chem.* **76**, 129-134. (1977).

[87] Bessone, J. B., Salinas, D. R., Mayer, C. E., Ebert, M. and Lorenz, W. J. An EIS study of Aluminum barrier-type oxide-films formed in different media. *Electrochim. Acta* **37**, 2283-2290, (1992).

[88] Gray, F. M. Solid polymer electrolytes. (VGH publisher Inc.: New York, 1991)

[89] Neyertz, S., Brown, D. and Thomas, J. O. Molecular dynamics simulation of crystalline poly(ethylene oxide). *J. Chem. Phys.* **101**, 10064-10068, (1994).

[90] Thomson, J., Lightfoot, P. and Bruce, P. G. Structure of polymer electrolytes: the crystal structure of poly(ethylene oxide). *Solid State Ionics* **85**, 203-208, (1996).

[91] Gonzalez, A. M. and Alemany, C. Determination of the frequency dependence of characteristic constants in lossy piezoelectric materials. *J. Phys. D-Appl. Phys.* **29**, 2476-2482, (1996)

[92] Fox. M. Optical properties of solids. (Oxford University Press: New York, 2001)

[93] Connor, J. W., Hastie, R. J., Wilson, H. R. and Miller, R. L. Magnetohydrodynamic stability of tokamak edge plasmas. *Phys.Plasmas* **5**, 2687-2700, (1998).

[94] Xiao, S. M., Drachev, V. P., Kildishev, A. V., Ni, X. J., Chettiar, U. K., Yuan, H. K. and Shalaev, V. M. Loss-free and active optical negative-index metamaterials. *Nature* **466**, 735-738, (2010)

[95] Ramakrishna, S. A. Physics of negative refractive index materials. *Rep. Prog. Phys.* **68**, 449-521, (2005).

[96] Smith, D. R., Padilla, W. J., Vier, D. C., Nemat-Nasser, S. C. and Schultz, S. Composite medium with simultaneously negative permeability and permittivity. *Phys. Rev. Lett.* **84**, 4184-4187, (2000).

[97] Li, B., Sui, G. and Zhong, W. H. Single Negative Metamaterials in Unstructured Polymer Nanocomposites Toward Selectable and Controllable Negative Permittivity. *Adv. Mat.* **21**, 4176-4180, (2009)

[98] Wang, C. C., Liu, G. Z., He, M. and Lu, H. B. Low-frequency negative capacitance in La0.8Sr0.2MnO3/Nb-doped SrTiO3 heterojunction. *Appl. Phys. Lett.* **92**, 52905-53909, (2008)

[99] Rahman, A. and Sanyal, M. K. Negative capacitance in Wigner crystal forming polymer nanowires. *Appl. Phys. Lett.* **94**, 242102-242104, (2009),

[100] Yan, H., Zhao, C., Wang, K., Deng, L., Ma, M. and Xu, G. Negative dielectric constant manifested by electricity. *Appl. Phys. Lett.* **102**, 062904 (2013)

[101] Zenkiewicz, M., Richert, J., Ryllewski, P. and Moraczewski, K. Some effects of Corona plasma treatment of Polylactide/Montmorillonite Nanocomposite. *Plasma Process Polym.* **6**. S387-S390 (2009).

[102] Ashcroft, N. W. and Mermin, N. D. Solid state physics. (Saunders College Publishing: Fort Worth, 1076)